UC Santa Barbara

UC Santa Barbara Electronic Theses and Dissertations

Title

Structural and Metamorphic Controls on Gold Mineralization in the Rochford District: A Comparison to the Homestake Mine, Black Hills, South Dakota

Permalink

https://escholarship.org/uc/item/21r987gq

Author

Quigley, Brenna Jane

Publication Date

2015

Peer reviewed|Thesis/dissertation

UNIVERSITY OF CALIFORNIA

Santa Barbara

Structural and Metamorphic Controls on Gold Mineralization in the Rochford District:

A Comparison to the Homestake Mine, Black Hills, South Dakota

A thesis submitted in partial satisfaction of the

requirements for the degree Master of Science

in Geological Science

by

Brenna Jane Quigley

Committee in charge:

Professor Phillip Gans, Chair

Professor Bradley Hacker

Professor John Cottle

December, 2015

The thesis of Brenna Jane Quigley is approved.

_____

Bradley Hacker

_____

John Cottle

_____

Phillip Gans, Committee Chair

December, 2015

ACKNOWLEDGEMENTS

ABSTRACT

Structural and Metamorphic Controls on Gold Mineralization in the Rochford District:

A Comparison to the Homestake Mine, Black Hills, South Dakota

by

Brenna Jane Quigley

The Rochford District of the Black Hills, South Dakota was heavily prospected for gold in the late 19th Century, and more recent prospecting has identified many areas with anomalous gold values (Great Lakes Exploration, unpublished data; Bayley, 1972), including some samples exceeding 20 ppm Au. The Rochford District is only 30 kilometers south of the Homestake Mine, one of the largest gold producers in North American history. Gold mineralization at the Homestake Mine is intimately related to a complex Proterozoic deformational and metamorphic history that has affected the entire Black Hills Region, and shares many similarities with the Rochford District. Despite the similarities to Homestake, and compelling evidence for gold mineralization, the Rochford District has remained largely unexplored. This study integrates geologic mapping, structural measurements, and petrographic analyses with an extensive new gold assay database in order to identify the major controls on gold mineralization in the Rochford District.

Both the Rochford District and Homestake Mine contain early F1 folds and an S1 fabric that has been transposed by a later S2 fabric. This pervasive, NNW-trending, S2

foliation is associated with tight to isoclinal F2 folds. F2 folds display dramatic thickening in the hinge regions, which increases the volume of iron formation available to host mineralization in discrete, predictable locations. A late, S3 crenulation cleavage only observed in the Rochford District is associated with strong pressure solution and is believed to represent a major fluid migration event.

The gold is concentrated in the Homestake and Rochford iron formations, which act as chemical traps for gold and sulfides. The greenschist to amphibolite transition seems to represent the most favorable combination of host rock mineralogy and permeability for gold mineralization at the Homestake Mine and within the Rochford District. Gold mineralization in the Rochford District is texturally and chemically similar to that at Homestake, but the relationship between ore-type and gold grade is different, suggesting a similar source for the gold, but different mineralization mechanisms. Textural relationships between sulfides and metamorphic minerals suggest two distinct pulses of mineralization. The first is potentially synchronous with the gold mineralization event at Homestake. The second pulse is potentially associated with the late, S3 crenulation and pressure solution that remobilized and enriched the mineralization in the Rochford Formation. The close similarities between the Homestake Mine and the Rochford District in host rock composition, structural style, metamorphic grade, and gold mineralization suggest that the Rochford District has the potential to contain a world-class gold deposit. Exploration efforts should focus on areas of thickened F2 fold hinges of Rochford Formation within the greenschist to amphibolite transition zone.

TABLE OF CONTENTS

LIST OF FIGURES

I. INTRODUCTION

The Rochford Mining District of the Black Hills, South Dakota has potential for gold mineralization, and shares many structural and mineralogic similarities to the Homestake Mine of Lead, South Dakota. The Homestake Mine is hosted by banded iron formation, and is one of the largest hydrothermal gold deposits on Earth, (Goldfarb et al., 2005). The Rochford iron-formation of the Rochford District, less than 30 kilometers south of Lead (Fig. 1), is nearly identical to the gold-bearing Homestake Formation, and has yielded gold assay values comparable to ore at the Homestake Mine (Fig. 26).

The Rochford Mining District consists of approximately 180 km^2 of heavily vegetated, steep terrain in northwestern Pennington County, of the Black Hills, South Dakota at approximately 1500-1800 meters above sea level (Fig. 2). The area underwent significant mining and prospecting for gold, probably between the years 1881-1902 (Bayley, 1972). There is evidence for production from eight small mines throughout the district including the Golden West and Black Eagle mines mentioned in this report. What is known about each of these deposits has been summarized by Bayely (1972). Early prospecting in the Rochford District was focused on the silicate to carbonate facies iron formations, as at the Homestake Mine. Despite the similarities between the two mining districts, the Rochford District has been largely unexplored (Bayley, 1972), and the complex structural and metamorphic history of this District is poorly understood.

The Homestake Mine and Rochford District are both within the Proterozoic core of the Black Hills. The Proterozoic rocks of the Black Hills are affected by a polydeformational history associated with the Trans-Hudson Orogeny, beginning about 1775 Ma (Dahl et al., 2005). This orogenic event created map-scale structures and metamorphic rock units that

host the gold at the Homestake Mine. Gold ore at Homestake was mainly produced from the

metamorphosed Homestake iron-formation, which acts as a chemical trap for gold and

sulfides. The iron formation that is transitional from greenschist to amphibolite facies

contains the highest grades of gold mineralization throughout the Homestake Mine. The

mineralization event at Homestake occurred after both major deformation events (D1 and

D2), and has been related to early, intrusion-related hydrothermal activity that occurred prior

to the emplacement of the Harney Peak Granite (HPG) in the southern Black Hills (1715 $\pm$

10 Ma, Dahl et al., 2005; Frei et al., 2009; Morelli et al., 2010).
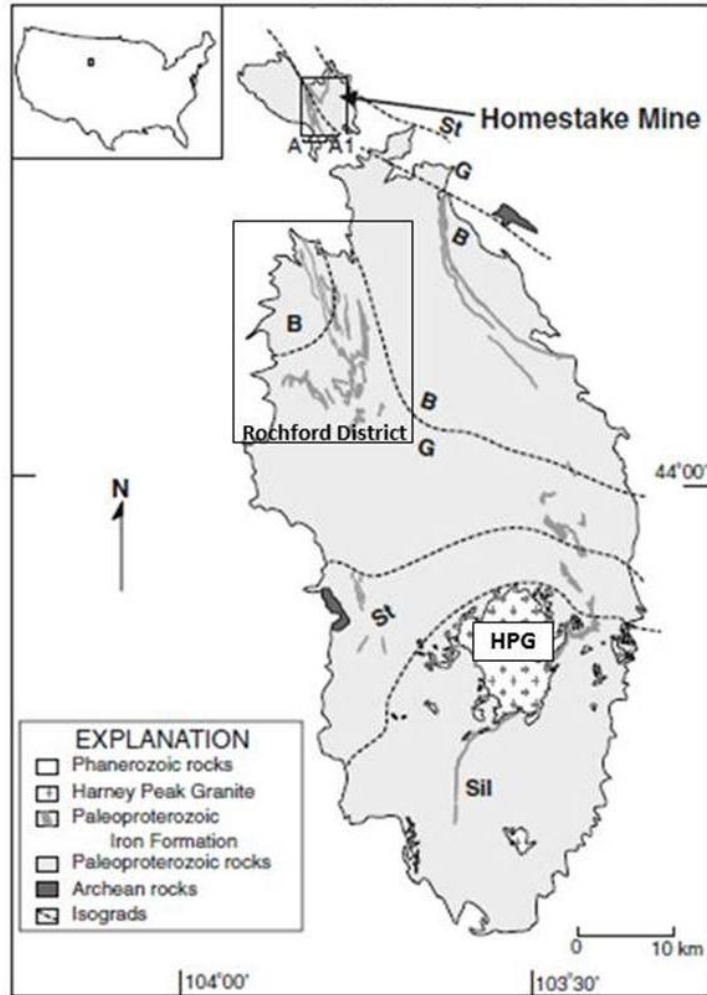
Figure 1: Simplified geologic map highlighting the Proterozoic rocks of the Black Hills. Outline of the shaded region represents the Proterozoic-Paleozoic unconformity. Locations significant to this study include the Rochford District, the Homestake mine, and the Harney Peak Granite (HPG). Also shown are positions of the biotite (B), garnet (G), Staurolite (St), and Sillimanite (Sil) isograds (from Morelli et al., 2011).

The Rochford District has a similar structural and metamorphic history to Homestake, as well as a similar stratigraphic succession. Bayley (1972) conducted detailed geologic mapping of the Rochford District at 1:24,000, and concluded that the Rochford and Homestake iron-formations are stratigraphically distinct, but nearly identical in composition. Due to the broad similarities between these two districts, and the significance of the Homestake Mine as a major gold producer, the obvious question arises: "Just how similar are the two districts, and what is the potential for a Homestake-class gold deposit in the

3

Rochford District?" To answer that question, this study employed mapping, structural analyses, and petrographic studies throughout the Rochford District in order to document the structural style, metamorphic and deformational history, and their controls on gold mineralization. Important outcomes of this study include characterization of gold mineralization in existing mines and prospects, the identification and delineation of the transition from greenschist to amphibolite facies rocks within the district, and a clearer picture of how map-scale structures control the distribution of map units throughout the district, and at depth. As a whole this study provides a comprehensive framework of the structures, metamorphic conditions, and gold mineralization of the Rochford District as a direct comparison to Homestake, and presents a new mineralization model for the Rochford District that has important implications for future exploration efforts.

II. BACKGROUND

The dramatic topographic relief of the Black Hills was created by a domal uplift associated with the last stages of the Laramide orogeny (Darton and Paige, 1925). Erosion following the uplift exposed a 13,000 km^2 dome of steeply dipping Proterozoic metamorphic rocks, surrounded by shallowly dipping, unmetamorphosed Paleozoic sedimentary rocks (Darton and Paige, 1925). The angular unconformity between these two units represents a time gap of over a billion years (Caddey et al., 1991). Proterozoic rocks were intensely deformed by the Trans-Hudson orogeny (at 1800-1600 Ma) and then intruded by the Harney Peak Granite (1715 Ma, Dahl et al., 2005) prior to the Laramide uplift. The complex poly-deformational and poly-metamorphic Proterozoic history of the Black Hills is intimately related to the distribution of gold throughout the region, particularly at the Homestake Mine.

2.1 Regional Proterozoic Geology

The Homestake and Rochford Formations are two distinct, Superior-type banded iron formations (BIF). The depositional age for the Homestake Formation is ~2010-1975 Ma (Dahl et al., 2008; Redden et al., 1990; Frei et al., 2009), and for the Rochford Formation is ≤1886 ± 7 Ma (Dahl et al., 2008). These iron formations and the surrounding successions of graphitic shales and basaltic lavas and tuffs were deposited in two distinct intercratonic rift basins. The earlier (Homestake) basin is associated with the Kenorland/Superia breakup and the younger (Rochford) with back-arc basins associated with early Trans-Hudson convergence (Frei et al., 2009). The deposition of these iron formations is attributed to an increase in mantle plume activity (Isley and Abbot, 1999), which likely caused both an increase in magmatism and hydrothermal activity, providing a source for the iron (Frei et al., 2009). The Homestake and Rochford formations were later metamorphosed to grunerite schists during the Trans-Hudson Orogeny (1800-1600 Ma).

Age constraints and thermotectonic relationships have only recently been documented for the polyphase deformation of the Black Hills (Redden et al., 1990; Dahl et al., 2005; Morelli et al., 2010). The first deformation event (D1) is evidenced by NE-trending isoclinal folds, and is attributed to arc accretion during the early stages of the Trans-Hudson orogeny at 1775 ± 10 Ma (Dahl et al., 2005). Evidence for this event has been largely obliterated by later deformational and metamorphic events. The second deformation event (D2) is defined by more-prominent, map-scale, isoclinal, NNW-trending folds and a ubiquitous NNW-trending cleavage (S2). D2 is believed to be the result of EW contraction between the Wyoming and Superior plates at 1750 ± 10 Ma (Dahl et al., 2005). Peak metamorphic mineral assemblages are commonly associated with this deformation, attaining maximum pressures of 5 kbar at Homestake, and decreasing to 3 kbar southward at Harney

5

Peak (Kath and Redden, 1990; Nabelel et al., 2006). The approximate trace of F1 and F2 fold axes and how they control the distribution of rock units in the Rochford district is illustrated in Figure 2.

Younger deformation events have been described in a few locations, including a west-trending fabric that re-folds F2 folds (Redden et al., 1990; Noble, 1949) and ductile shearing of D1 and D2 fabrics (Redden et al., 1990, Morelli et al., 2010; Caddey et al., 1991). The Harney Peak Granite was emplaced in the southern Black Hills at 1715 ± 10 Ma (Dahl et al., 2005), and produced a well-defined contact metamorphic aureole with temperatures up to 700°C, and warped earlier fabrics (Nabelel, 2006). Finally, a localized, steep, NE-trending spaced cleavage overprints all of these fabrics, and is particularly prominent in the Rochford District. This fabric will be referred to as S3 throughout this study, though has been referred to as S4 or S5 in other studies (Redden et al., 1990; Morelli et al., 2010). Redden et al. (1990) noted that this fabric deforms sillimanite in the contact aureole of the HPG, and therefore interprets it to be post-1715 Ma. They also associate this late S3 crenulation with an isotopic reequilibration event at 1543 ± 43 Ma, but do not attribute it to a specific tectonic event (Redden et al., 1990). Although these locally developed, NE-trending crenulation cleavages in the Black Hills have been broadly correlated (Redden et al., 1990), it is possible that they formed at different times.
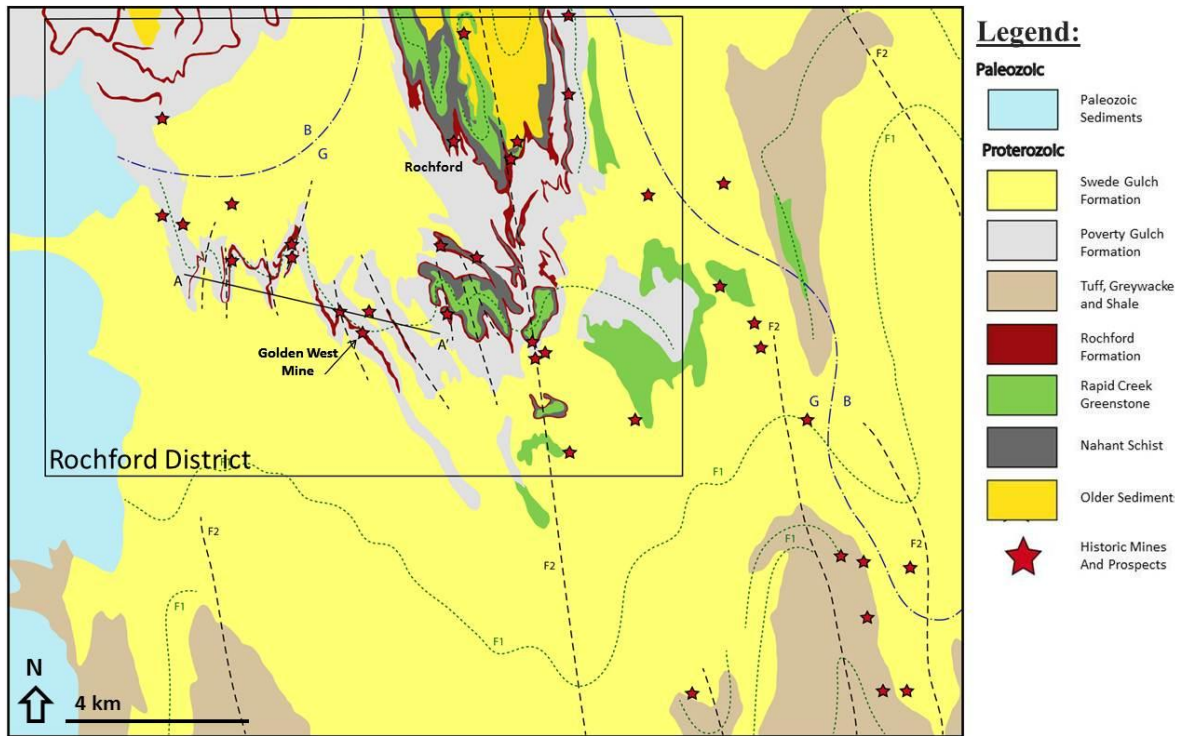
Figure 2: Simplified geologic map of the Rochford district and surrounding areas showing major rock distributions, fold axes, locations of historic mines, line of cross-section A-A', and the position of the isograd between biotite stable to biotite + garnet stable rocks. Note the relationship between historic mines, F2 fold axes, and the Rochford Formation. The Rochford anticlinorium is located in the central portion of the map and continues to the north. See Appendix A for larger version of this image with sample locations and structural orientation data. Map compiled from Bayley (1972), Redden and Dewitt (2008), Martin et al. (2004), and new data.

2.2 Gold Mineralization at the Homestake Mine

The Homestake Mine is located in the northern Black Hills, within the Whitewood Mining District, in the town of Lead, South Dakota. The Homestake Mine operated from 1878-2002, and produced over 40 million ounces of gold. The average gold grade in 1988 was 8.36 g/t Au, but is known to vary over distances of just a few meters (Caddey et al., 1991). Until its closure, the Homestake Mine was known as the largest and deepest gold mine in North America (Goldfarb et al., 2002).

Caddey et al. (1990) describe in detail the gold mineralization at Homestake, and determined that the mineralization is stratabound to the Homestake iron formation, which acted as a chemical trap for gold and sulfides. The gold-bearing Homestake Formation was intensely deformed during the earlier D2 deformation event, and thickened hinges of the F2

7

folds apparently acted as structural traps for the gold (Caddey et al., 1990). The Homestake Mine straddles the transition zone between greenschist and amphibolite facies rocks, and many of the highest gold concentrations are associated with this transition. This transition zone is defined in the Homestake Formation by the coexistence of siderite and grunerite. At higher metamorphic grades the Homestake Formation underwent volume loss due to devolitilization reactions, which apparently inhibited its ability to trap gold and sulfides (Caddey et al., 1991).

Two forms of gold-sulfide ore have been described at Homestake: 1) replacement ore, which is stratabound and often stratiform, and 2) "shear"-ore that is spatially associated with ductile-brittle shears, but does not preserve the original fabrics. Replacement ore consists of pyrrhotite with minor gold and arsenopyrite, whereas shear-ore has high concentrations of gold and arsenopyrite (Caddey et al., 1991; Fig. 3). Replacement-ore likely represents in-situ replacement of pre-existing compositional layers by sulfides via an intergranular hydrothermal fluid (Fig. 3A). Shear-ore likely represents hydrothermal deposition of sulfides associated with fracturing or shearing of the rock, and in-filling with a free fluid phase (Fig. 3B). Three types of shears have been described within the Homestake Mine: 1) ductile shears, 2) ductile-brittle shears most commonly associated with the gold-ore, and 3) semi-brittle kink shears that cut across the other shears and postdate gold mineralization (Caddey et al., 1991).
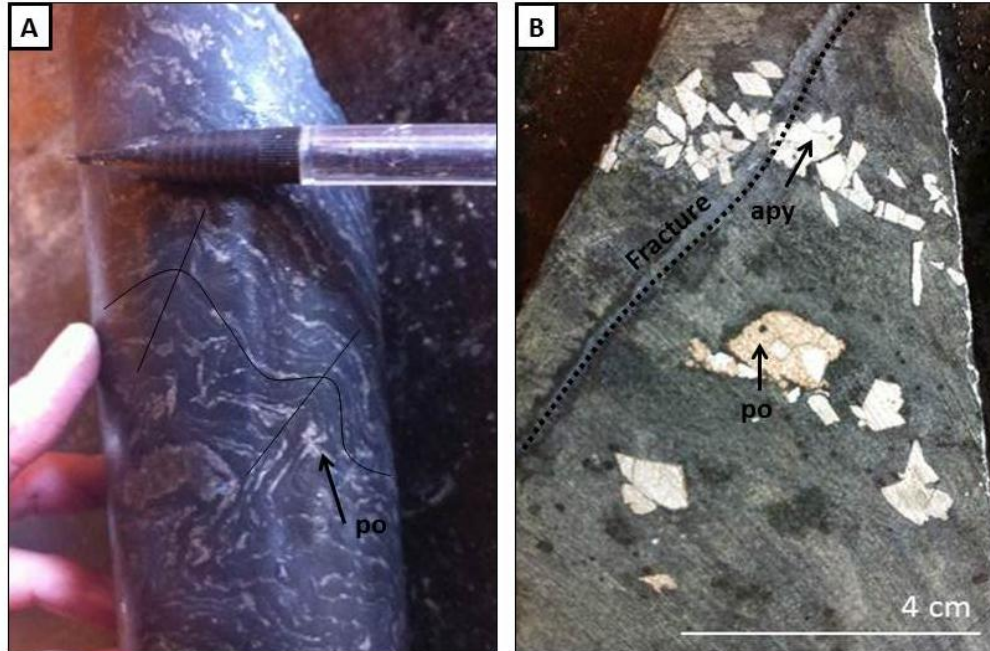
Figure 3: Drill core showing ore textures at the Homestake mine **Figure 3A:** Replacement-ore textures are stratiform and stratabound. Sulfides, pyrrhotite (po) with minor arsenopyrite (apy), preserve depositional and metamorphic fabrics (specific fabrics not identified for this sample). **Figure 3B:** Shear-ore textures have largely obliterated the original fabrics and sulfides are associated with a small fracture. Mineralization is dominantly arsenopyrite and gold, with minor pyrrhotite. Samples courtesy of the Sanford Core Repository.

The source of gold at Homestake has been a topic of debate for many years. Gold mineralization has been dated as 1736 ± 8 Ma by rhenium-osmium dating of arsenopyrite associated with the gold mineralization (Morelli et al., 2010). This postdates the 1750 ± 10 Ma D2 deformation (Dahl et al., 2005), and precedes the onset of Harney Peak Granite magmatism. The source of gold was initially thought to be directly related to the emplacement of the Harney Peak Granite due to the abundance of granitoid bodies of similar age near the Homestake Mine (Caddey et al., 1990; Frei et al., 2009). However, initial $^{187}Os/^{188}Os$ isotopes of auriferous arsenopyrite mineralization from Homestake are unradiogenic. This suggests that the source of the fluids was a primitive melt, likely associated with the earliest hydrothermal stages of Harney Peak Granite emplacement, but not sourced from the granites themselves (Morelli et al., 2010).

For additional details of gold mineralization at the Homestake Mine the reader is directed to papers by Caddey et al. (1991), Noble (1950), and Noble and Harder (1948). In the following sections, the general stratigraphic, structural, and metamorphic controls on gold mineralization in the Rochford District will be described based on new data collected in this study, and compared to the better known gold mineralization at Homestake.

III. METHODS

This study combined several different methods to investigate the structure, stratigraphy, metamorphism, and mineralization in the Rochford District. Methods include systematic sampling for gold assay, geologic mapping and structural data collection at regional to outcrop scales, detailed petrography, scanning electron microscopy (SEM), electron microprobe analyses, and whole rock major and trace element geochemistry.

3.1 Assay Sampling

Assay samples were collected throughout the field area to assess what rock types and structural features are most associated with anomalous gold values. Rocks were mainly sampled if there was at least some evidence for potential mineralization (i.e. rusty, altered, or presence of visible sulfides). Because the Rochford Formation is generally rusty and was suspected to contain gold, it was sampled more generously than other rock types. Reference samples were taken of all representative rock types in addition to the samples with evidence for mineralization. Gold analyses were performed by Minerals Processing Corporation's ISO/IEC 17025 certified analytical laboratory in Carney, Michigan. Samples were crushed and a 250 gram split was pulverized to 80% minus a 200 mesh (0.074 mm). Thirty grams of the pulverized sample were fire assayed for gold utilizing a gravimetric finish.

3.2 Mapping and Structural Investigation

Several areas were mapped to understand the distribution of rock types, particularly the Rochford Formation, at regional to outcrop-scales. Orientations of compositional layering, foliations, lineations, and fold axes were systematically measured throughout the Rochford District and surrounding areas. Identification of metamorphic assemblages in the field helped constrain the locations of various mineral-in isograds and the greenschist to amphibolite transition. Due to the fine-grained nature of these rocks, samples for thin section were often required for mineral identification. The area surrounding the Golden West open pit mine (Golden West Area, Fig. 9 and 13) provides particularly good exposures of both structures and mineralized rock. A 1:300 scale map was made of the 60x25 meter open pit mine (Fig. 13A), in addition to careful mapping of the surrounding area (Fig. 13). Geologic maps were compared with assay data to examine correlations between rock types, structures, metamorphic grades, and gold concentrations. All new mapping and structural data was compiled along with several other maps of various scales (Bayley, 1972; Redden and Dewitt, 2008; and Martin et al., 2004) in order to construct a comprehensive geologic map of the Rochford District and surrounding areas (Fig. 2).

3.3 Detailed Microscopy

Most rock types in the study area are extremely fine grained, and required detailed microscopy to fully characterize metamorphic assemblages, textures, and microstructures. SEM and microprobe analyses helped elucidate textural relationships and measure elemental compositions of gold, sulfides, and silicate minerals. Locations of all samples mentioned in this study can be found in Appendix A.

3.4 Whole-Rock Geochemistry

Early SEM images suggested that several samples from the Rochford District may contain anomalous concentrations of rare earth elements (REEs). In order to determine the concentrations of REEs in these rocks, representative samples of the main stratigraphic units (Swede Gulch and Poverty Gulch phyllites, as well as mineralized and unmineralized Rochford Formation) were selected for whole rock major and trace element geochemistry. No anomalous REE concentrations were found, but the data has been included here to potentially support future geochemical studies (Appendix C). Samples were powdered, fluxed with lithium tetraborate, and fused at 1000°C before being re-powdered and re-fused to ensure complete homogenization. The resulting glass bead was polished and sent to Cal Poly Pomona in Pomona, California for whole-rock major element measurement via x-ray fluorescence (XRF) spectrometry. Whole-rock trace elements were measured for each sample by cutting 2-3 mm chips from the final glass beads and analyzing them with laser-ablation quadrupole inductively coupled mass spectrometry (LA-Q-ICPMS) at UCSB.

IV. STRATIGRAPHY OF THE ROCHFORD DISTRICT

The rocks of the Rochford District consist of metamorphosed sedimentary and volcanic rocks, deposited in a back-arc basin associated with the earliest stages of the Trans-Hudson Orogeny (Frei et al., 2009). They consist mainly of fine-grained, graphitic, pelitic to semi-pelitic shales and siltstones. The Rochford and Montana Mine Formations are silicic to calcic banded iron-formations (Bayley, 1972). Because the Montana Mine Formation was not a focus of this study, it is not described in detail. Both the phyllites and iron-formations locally contain chert layers. Other rock types include more quartz-rich siltstones and sandstones, and basaltic lavas and tuffs. These rocks were metamorphosed during the Trans-

Hudson Orogeny to greenschist to amphibolite facies phyllites, schists, and greenstones. Rock descriptions below supplement the original descriptions by Bayley (1972) with new petrographic data.

4.1 Rochford Stratigraphy and Correlation to Homestake

The succession of sedimentary units in Lead is strikingly similar to that in the Rochford District, which initially caused some confusion as to their correlation and relative ages (Bayley, 1972). For example, the Rochford Formation was correlated with the Homestake formation, and the Rochford Anticlinorium was interpreted as a synform. Bayley (1972) noted that despite the similarities between the Rochford and Homestake iron-formations and the successions of rock units that contain them, the two formations are stratigraphically distinct. This is based on the identification of a major unconformity between the older meta-sediments in the Rochford District (roughly correlated with the Ellison and Homestake Formations at the Homestake Mine) and the Flag Rock Group, containing the Rochford Formation (Fig. 4). The map distribution of rock units is complex in this area as a consequence of polyphase deformation structures.
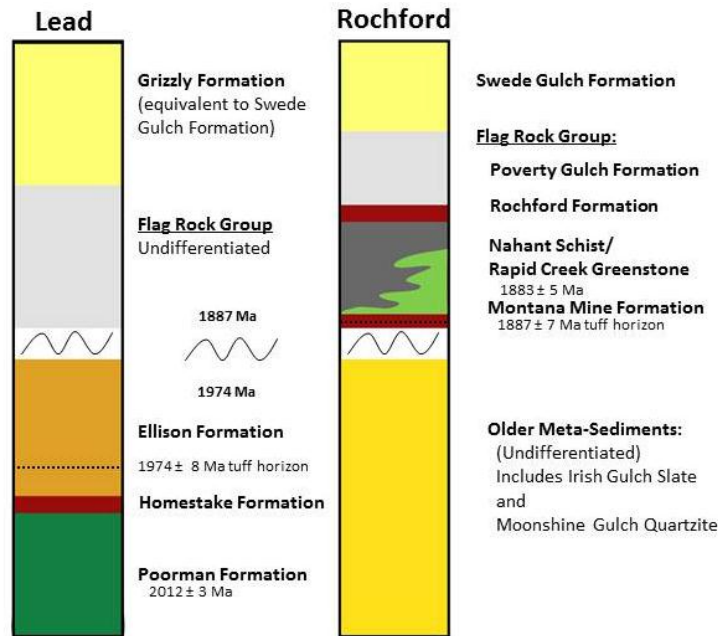
Figure 4: Stratigraphic columns of the Lead (Homestake) and Rochford areas, highlighting the correlation of the younger units, and the unconformity separating the Homestake and Rochford Formations (after Frei et al., 2009; for more detail on age constraints see Hark, 2008; Redden et al., 1990; and Dahl et al., 2008)

4.2 Rock Descriptions:

Older Meta-Sediments (Ellison Formation at Homestake):

The oldest rock units in the Rochford District are only exposed in the northeastern part of the study area, in the core of the Rochford Anticlinorium (Fig. 2), and were not a major focus of this investigation. These units are broadly correlative with the Ellison and Homestake Formations in the Lead area, and are separated from the overlying Flag Rock Group described below by a major unconformity (Fig. 4). They include the Moonshine Gulch Quartzite, a dark, distinctly bedded quartzite with interbedded slate, and the Irish Gulch Slate, a very dark, phyllite to fine-grained schist with no distinct compositional layering.

14

<u>Flag Rock Group:</u>

Rapid Creek Greenstone

The Rapid Creek Greenstone consists of basaltic lavas, pillow lavas, and volcaniclastic tuffs that have been metamorphosed to hard, dense greenstone. The Rapid Creek Greenstone is either interbedded with, or underlies the Nahant Schist (Bayley, 1972). In outcrop, the greenstone is identified by its dark green color, more massive structure, and steep slopes. Carbonate veins are commonly found throughout the greenstone. Layering within the greenstone is typically on the order of 10-50 centimeters. The best exposures of the greenstone are along Rapid Creek, in the SE corner the Rochford District**.**

Nahant Schist

The Nahant Schist is a monotonous graphitic slate or schist that is closely related to the Rapid Creek Greenstone. Bayley (1972) noted that the Nahant Schist and Rapid Creek Greenstone were likely deposited contemporaneously, in a deep marine setting, as the two units are often interbedded. The Nahant Schist is distinguished from the Poverty Gulch and Swede Gulch Formations by lacking clear compositional layering. This unit tends to be poorly exposed, forming topographic lows and heavily vegetated slopes.

Rochford Formation

The Rochford Formation (and the lithologically similar Montana Mine Formation, not discussed here) is a metamorphosed, mixed silicate-carbonate-sulfide facies iron formation, which now consists of grunerite schist with thinly interbedded quartzite (metamorphosed chert). The contacts with the underlying Nahant Schist and overlying Poverty Gulch Slate are conformable and gradational. At lower

metamorphic grades the Rochford Formation is a poorly exposed, fine-grained unit composed of siderite, biotite, and quartz. At higher grades the iron formation is easily distinguished from other map units by the presence of coarse (mm to cm scale) grunerite rosettes (Fig. 5). The iron formation often contains layers of graphitic slate or phyllite, particularly near the contact with the Poverty Gulch Slate. The Rochford Formation varies dramatically in thickness from 7 to 70 meters, likely due to heterogeneous strain, boudinage, and local thickening in the hinges of folds. Though the unit does not crop out well, hundreds of prospecting pits in the area generally follow the trend of the Rochford Formation, providing many exposures and allowing detailed mapping of the overall trend of the unit (Bayley, 1972; this study). The deformed Rochford Formation creates a thin, folded, sinuous trend throughout the field area, and is best observed within the town of Rochford and near the Golden West mine.
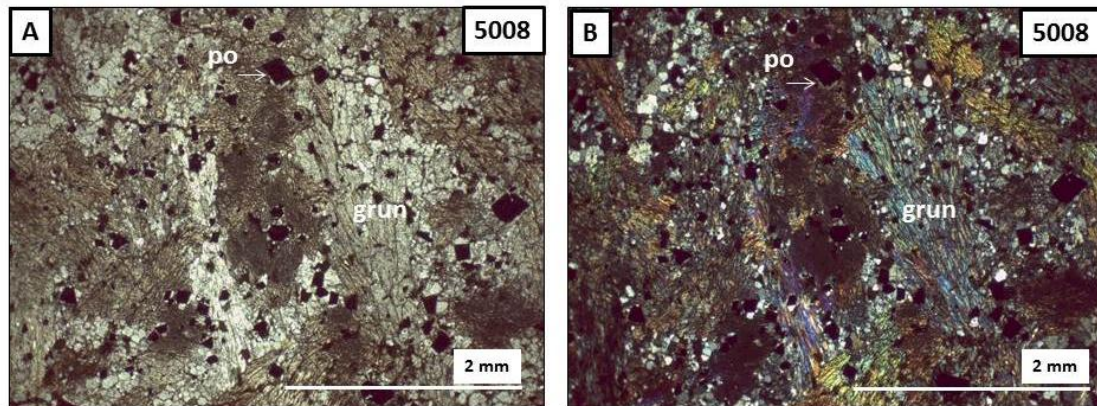
Figure 5: Photomicrographs of the Rochford Formation from the Golden West open pit in the Rochford District in plane polarized light (5A) and cross polarized light (5B). Note the large grunerite rosettes and euhedral disseminated sulfides (opaques).

Poverty Gulch Formation

The Poverty Gulch "Slate" is a graphitic phyllite or even fine-grained schist, which lies conformably on top of the Rochford Formation. It is brown to grey, with 1-10 mm compositional laminations and layers, and often has abundant 1 mm garnets (Fig. 6A and 7A). The Poverty Gulch Formation consists primarily of biotite ± muscovite, quartz, and graphite, and closely resembles the Swede Gulch formation, even in thin-section. On average, the Poverty Gulch Formation is more graphitic than the Swede Gulch, and finer-grained (Fig. 7). The Poverty Gulch Formation is also more likely to have only a single mica (biotite or muscovite) as the dominant mineral. The contact between the Poverty Gulch Formation and the Swede Gulch Formation appears to be conformable, but is poorly exposed. Large, discontinuous, resistant quartzite ridges in the lower part of the Swede Gulch Formation help to delineate the contact. The pelites of the Poverty Gulch and Swede Gulch Formations provide the best evidence for mesoscopic folding and cleavage development, and most structural data was collected from these two units, particularly along roadside outcrops. The Poverty Gulch Formation is best observed near the Golden West mine, and in the NW corner of the mapping area (Fig. 2).
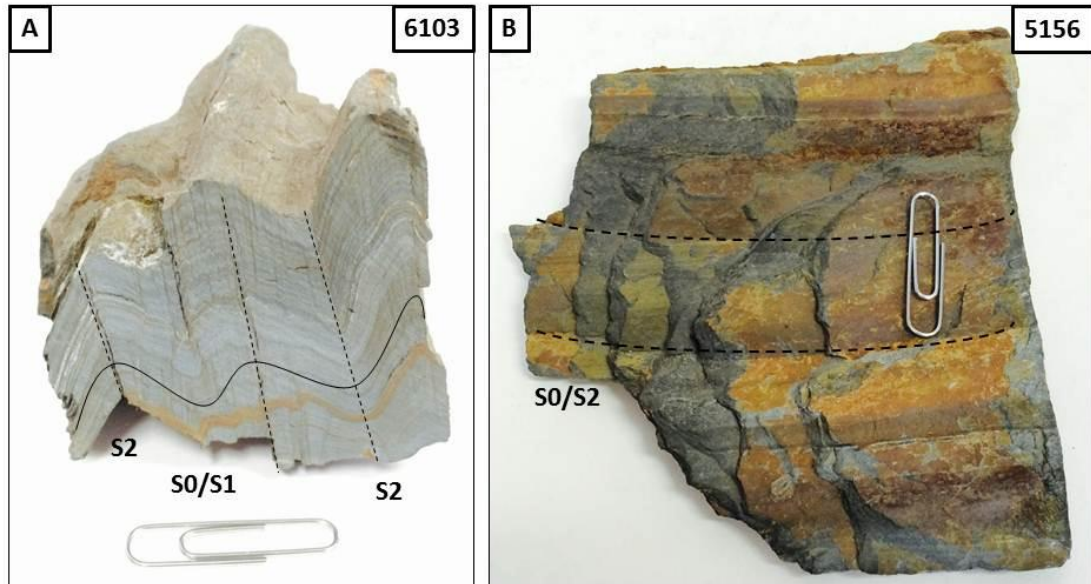
Figure 6: Hand samples of Poverty Gulch Formation (**6A**) and Swede Gulch Formation (**6B**). Note the thin laminations in 6A compared to the thicker compositional layering in 6B. This sample of the Poverty Gulch Formation also shows compositional layering (S0) parallel to S1, and S2 is a disjunctive crenulation cleavage. The Swede Gulch sample displays S0 parallel to S2, with S1 having been rotated into parallel with S2. Four centimeter paperclip for scale.

Swede Gulch Formation

        The Swede Gulch Formation is one of the most wide-spread units in the Black Hills, and is thought to be equivalent to the Grizzly Formation near Homestake (Dodge, 1942; Noble and Harder, 1948). The lower Swede Gulch is a graphitic phyllite or fine-grained schist, very similar to the Poverty Gulch Formation, but is typically coarser grained and less graphitic (Fig. 6B and 7B). The lower Swede Gulch also contains large quartzite (metamorphosed chert) lenses (up to 5x30 meter long outcrops). These abundant, ridge-forming ferruginous quartzite lenses consist entirely of recrystallized, sugary-textured quartz, and small amounts of iron oxides, primarily hematite. The lower portion of the Swede Gulch Formation often contains small garnets, typically 1-3 mm in diameter. The upper part of the Swede Gulch is easily distinguished from the other phyllites as a distinctive greywacke with graded

18

beds. The Swede Gulch Formation is well exposed along roadside outcrops throughout the field area, particularly along South Rochford Road.
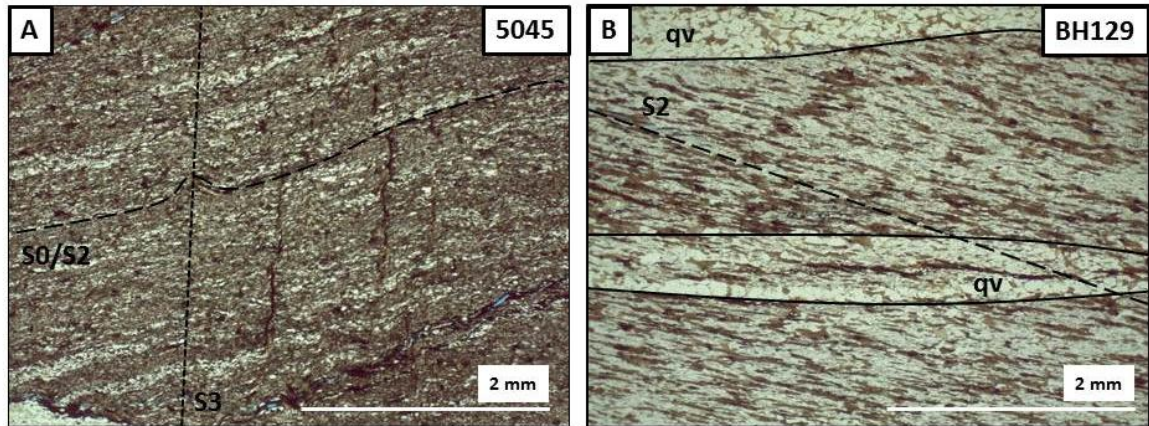
Figure 7: Photomicrographs of the Poverty Gulch Formation (7A) and the Swede Gulch Formation (7B) in plane polarized light. Both mineral assemblages consist of biotite, quartz, and graphite, but note the higher concentration of opaque minerals and slightly finer grain size of the Povery Gulch Slate (7A). 7A shows compositional layering (S0) parallel to S2, and crenulated by S3. 7B shows S2 at an oblique angle to early (pre-S2) quartz veins (qv).

V. STRUCTURAL GEOLOGY OF THE ROCHFORD DISTRICT

The structural history of the Rochford District is complex, involving polyphase folding and cleavage development, transposition of older fabrics by younger fabrics, and poly metamorphism, including both dynamothermal and static events. This section focuses on the geometry and character of micro-scale to map-scale structures and fabrics, but will inevitably allude to aspects of the metamorphic history. A more complete description of the conditions and history of metamorphism in the Rochford district are presented in Section 6.

5.1 Structural Overview

Folds are the dominant map-scale structures in the Rochford District, and several different folding events have resulted in a complex distribution of map units. The most parsimonious explanation of the map pattern involves an early F1 folding event, which produced EW trending, tight to isoclinal folds that were later re-folded by the F2 folding

event with approximately NS trending fold axes (Fig. 2). Direct structural evidence for the F1 folding event is rare, as the fabrics associated with this deformation have generally been transposed and rotated parallel to the S2 foliations. S1 foliations have only been measured directly in the NW portion of the field area. The oldest units are found in the core of F1 anticlines such as in the northeast portion of the map, whereas the youngest units (such as the Swede Gulch Formation) coincide with F1 synclines. The F2 fold hinges are more apparent on the map from the sinuous trace of the Rochford Formation (Fig.2), and were contemporaneous with development of a NNW trending foliation (S2) throughout the Rochford District. The S2 foliation consistently strikes to the NNW and dips steeply to the ENE throughout the field area, with some variation in the southern and northwestern areas (Fig. 2 and 9). The S2 foliation typically dips between 60 degrees to vertical, and occasionally steeply to the WSW (Fig. 8).

A third deformation event is expressed by an S3 cleavage and localized warping of earlier fabrics. This distinctive, spaced crenulation cleavage is often at a high angle to S2, strikes consistently to the NE and dips approximately 50 degrees to the SE (Fig. 8). The D3 event does not influence map unit distributions, but is responsible for the slight variations in the orientations of the other fabrics (Fig. 8 and 9).
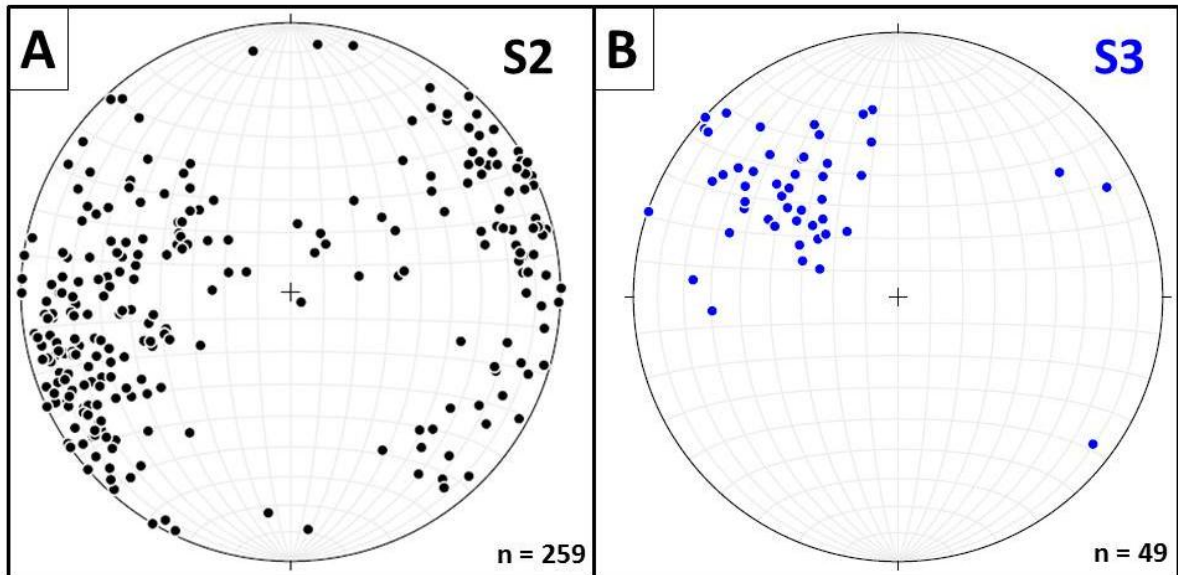
Figure 8: Lower hemisphere projections of poles to cleavages for all structural measurements of S2 and S3 fabrics throughout the Rochford District and surrounding areas. **8A:** Pervasive S2 foliation and **8B:** the S3 crenulation cleavage. The S2 foliation generally strikes to the NNW and dips steeply to the NE, with some variation throughout the field area. S3 measurements are tightly clustered and dip approximately 40 degrees to the SE.

Map-scale trends of S2 and S3 fabrics relative to the rock units in the Rochford District are illustrated in Figure 9, with the general NNW trend of the S2 foliation, and consistent NE trending S3 crenulation. The S2 foliation defines a broad fan, from NE trending in the NW to NNW in the east. In addition to changing orientation, the nature of each fabric also changes in the northwestern portion of the mapping area. These changes seem to correspond to the garnet-in isograd and a weaker D2 event (see below).
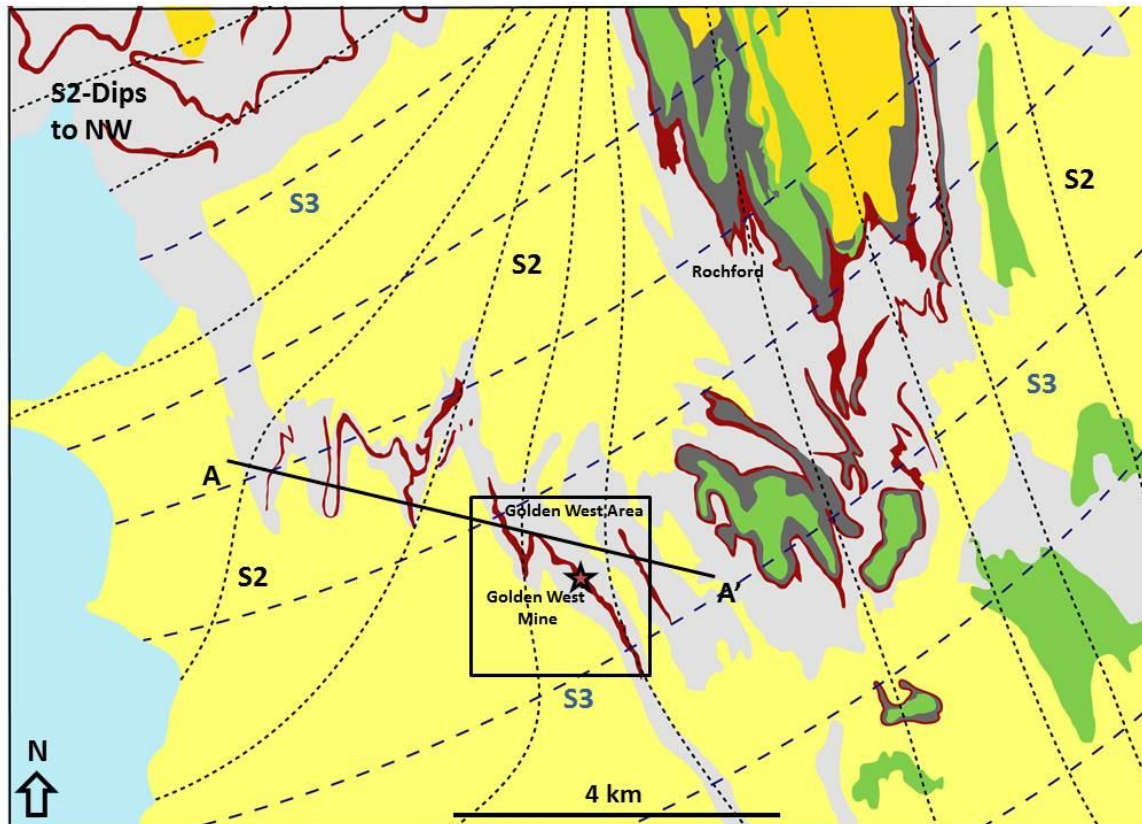
Figure 9: Structural map of the Rochford District from Figure 2, showing the trends of the S2 and S3 fabrics throughout the Rochford District. See Appendix A for structural orientation data. S2 generally strikes to the NNW, except in the NW corner of the map where it strikes to the SW and dips to the NW. S3 consistently sweeps across the map pattern, and is not observed in the NW corner. Map units modified from Bayley (1972).

5.2 Mesoscopic Structures

The Rochford and surrounding formations are tightly folded at a mesoscopic scale by F2 folds throughout the map area. Virtually all mesoscopic folds observed in outcrop are tight to isoclinal with apical angles of 5 to 30 degrees, and display impressive thickening in the hinge regions that approach Class 2 (similar) fold morphologies (Fig. 10). Hinges can be angular (Fig. 10A) to sub-rounded (Fig. 10B).
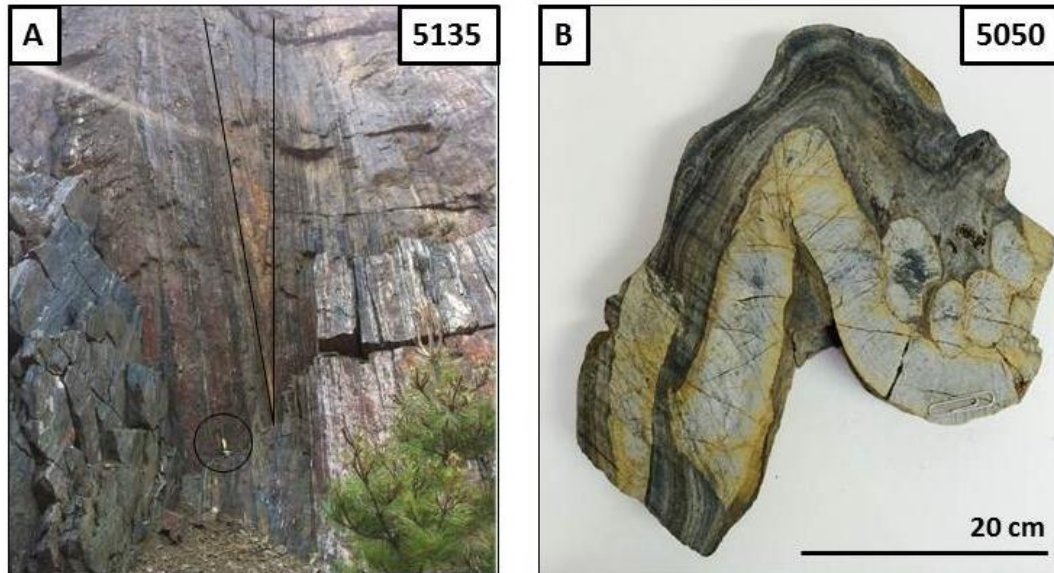
Figure 10: F2 folds in the Rochford Formation. **9A:** Tight, isoclinally folded Rochford Formtion in the town of Rochford (Fig. 2 and 9). Hammer for scale. **9B:** folded chert layer within the Rochford Formation near the Golden West mine. Note how the chert has been boudinaged, rounded, and thickened in the hinges of the fold.

Figure 11: Upright, tight, F2 folds in the Golden West open pit (Fig. 9), cut by two sets of sub-horizontal fractures, with minor amounts of offset juxtaposing antiformal and synformal closures across from each other. Also note the location of sample 5008 (Fig. 12).

23

The Golden West open pit mine provides excellent exposures to measure and observe F2 folds. Throughout the pit, meter-scale, tight, angular F2 folds are cut by sub-horizontal fractures with minor amounts of offset (Fig. 11). The axes of these F2 folds are systematically deflected about an axis parallel to the S3 crenulation (Fig. 12 and 13A). This pattern is illustrated as deflecting the map units in the Golden West Area (Fig. 12), and can also be seen microscopically as F3 micro-folds (Fig. 13B). The plunges of the F2 folds measured in the Golden West open pit vary widely, from horizontal to near vertical, and to the NW or SE (Fig. 13A). This is likely due to variations in the orientation of compositional layering following F1 folding.
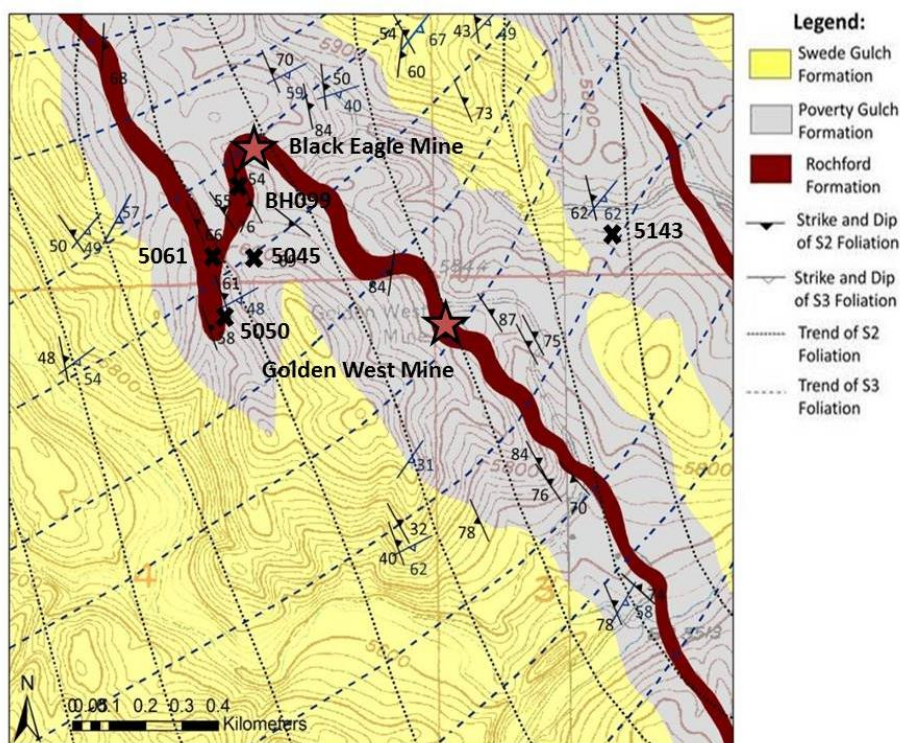
Figure 12: Detailed map of the area surrounding the Golden West mine (from Fig. 9), showing the locations of the Golden West and Black Eagle mines, sample locations, strike and dips of S2 and S3 foliations, and form lines for the general trend of the S2 and S3 fabrics. Note how the S3 crenulation deflects the S2 foliation on the map scale.

24
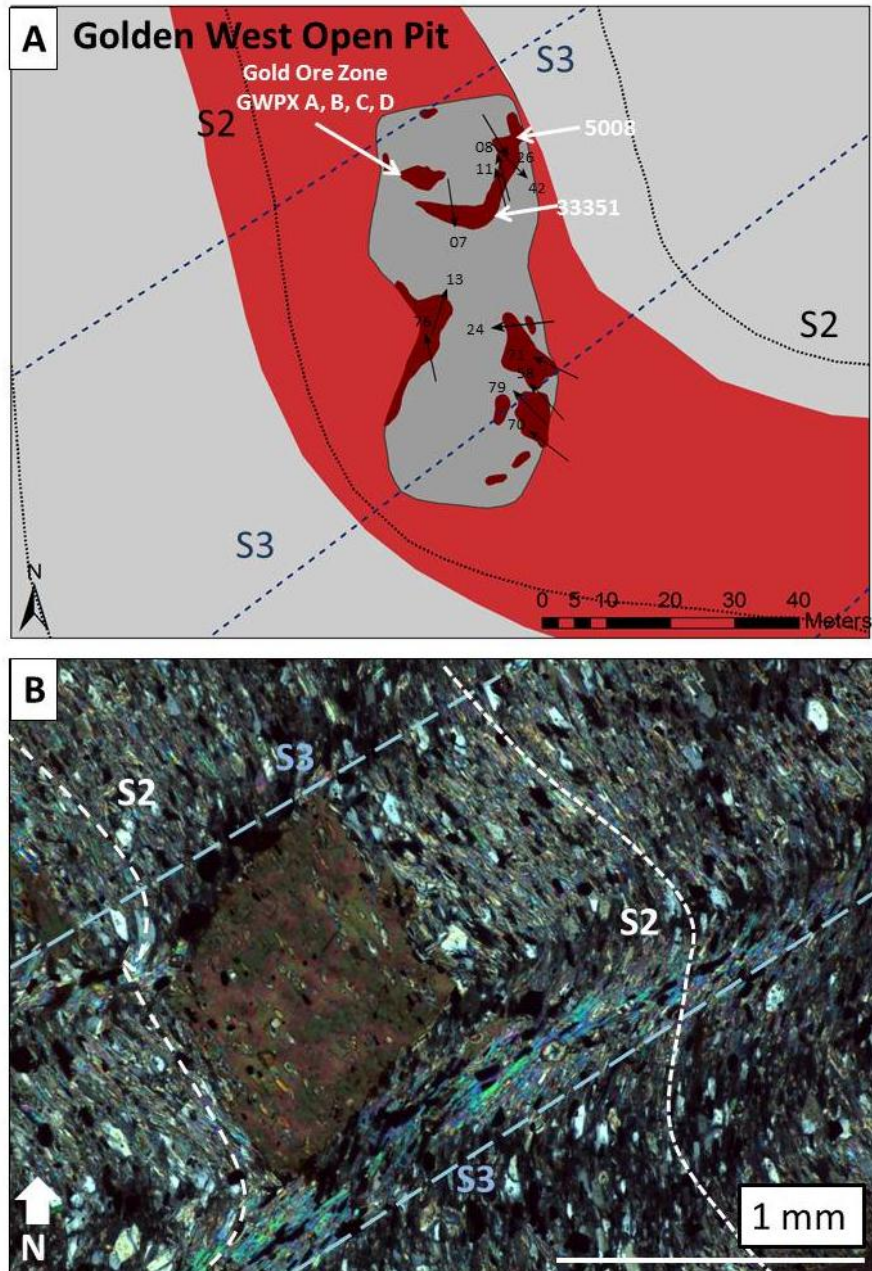
Figure 13: D2 and D3 structures at the Golden West mine. **13A:** Detailed map of the Golden West open pit with sample locations. General trend of the Rochford Fomation is red, with outcrops in dark red. Grey is the Poverty Gulch Formation. Arrows indicate trend and plunge of F2 folds, and illustrate how outcrop-scale F2 folds have been deflected by the S3 crenulation. **13B:** Oriented photomicrograph showing the deflection of the S2 foliation (white) by the S3 crenulation (blue).

Although these fabrics remain fairly consistent throughout most of the Rochford District and Black Hills, the fabric character and geometric relationships change in the northwestern corner and far eastern edge of the field area near the garnet-in isograd (Fig. 2). Outcrop scale folds in the northwestern corner of the mapping area are fairly open, and the fabric associated with these folds is a spaced crenulation (Fig. 14), much like the S3 fabric elsewhere. However, these folds have a different orientation (with axial surfaces dipping to the NE), and there is no evidence for an early, transposed S1 fabric. Based on the lower metamorphic grade associated with the D2 deformation event in this area, these folds have been interpreted as F2 folds.
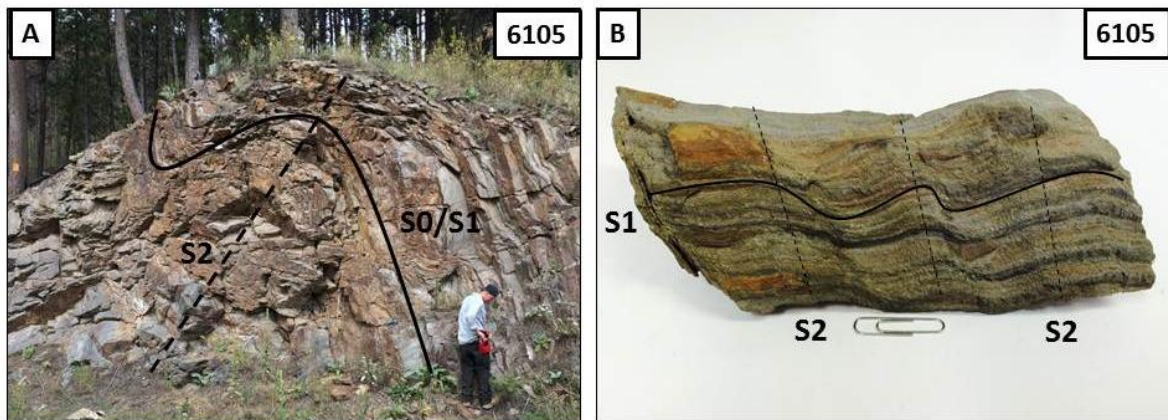
Figure 14: Gentle F2 folds from the northwest corner of the field area (Fig. 2) in outcrop (14A, oblique view) and hand sample (14B). These folds have been interpreted as F2 folds associated with weaker D2 deformation. There is no evidence for the S3 crenulation is this location.

5.3 Microstructures and Petrographic Observations

Evidence for the early D1 deformation is rarely preserved, and is only observed microscopically. Direct evidence for the S1 foliation is most compelling as inclusion trails within porphyroblasts, such as garnet (Fig. 15A). Occasionally, the S2 foliation obliquely transects the limbs and axial surfaces of F1 folds (Fig. 15B). These types of petrographic

observations provide strong evidence for an early D1 event, even though in most areas the S1 fabric is largely obliterated or transposed by the subsequent deformation events.
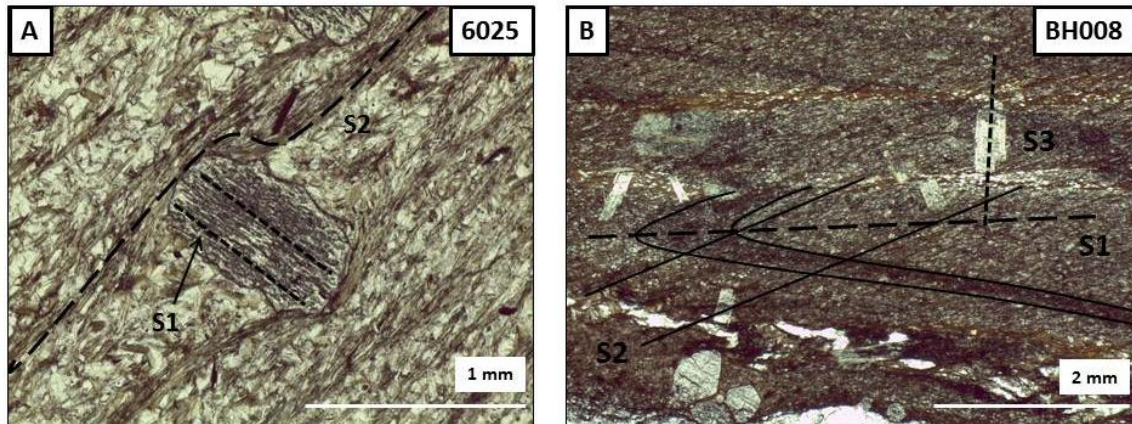
Figure 15: Evidence for the D1 Deformation Event. 15A: Early S1 foliation preserved as inclusion trails within garnets, not parallel to the disjunctive S2 cleavage. 15B: Pervasive S2 foliation is not axial planar to the folding of compositional layering (S0). Late, aligned, chloritoid grains are interpreted to grow during the D3 deformation event. Plane polarized light.

In the majority of the field area, the S2 foliation is recognized in thin section as a pervasive alignment of micaceous minerals (Fig. 13B). This foliation is commonly sub-parallel to compositional layering (S0/S1), but can be at a moderate to high angle in the hinge regions of F2 folds, or where D1 folds were not isoclinal. The spaced S3 crenulation is at a high angle to the S2 foliation and deflects and/or folds the earlier foliation (Fig. 13B). Microlithons are typically less than 3 mm wide, and contain micro-folds with open to nearly isoclinal, rounded hinges. The S3 crenulation is defined by spaced, but well-aligned mica grains, and often displays evidence for pressure solution. Occasionally, the S3 fabric is weakly developed, and is indicated only by sparse, biotite and/or chloritoid grains that grow across the S2 foliation.

Rock composition also impacts how the fabrics are expressed, even from one compositional layer to another. The S3 crenulation can change from broad micro-folding in more micaceous layers, to an intense pressure solution in the more quartz-rich layer. The

27

volume loss and heterogeneous strain associated with this pressure solution is sufficiently large to deflect the S3 cleavage and give an apparent sense of shear across the compositional boundary (Fig. 16A). All rock types throughout the Rochford District display evidence for pressure solution and volume loss associated with the S3 cleavage development (Fig. 16B), suggesting that the D3 deformation event may have been accompanied by extensive fluid migration.
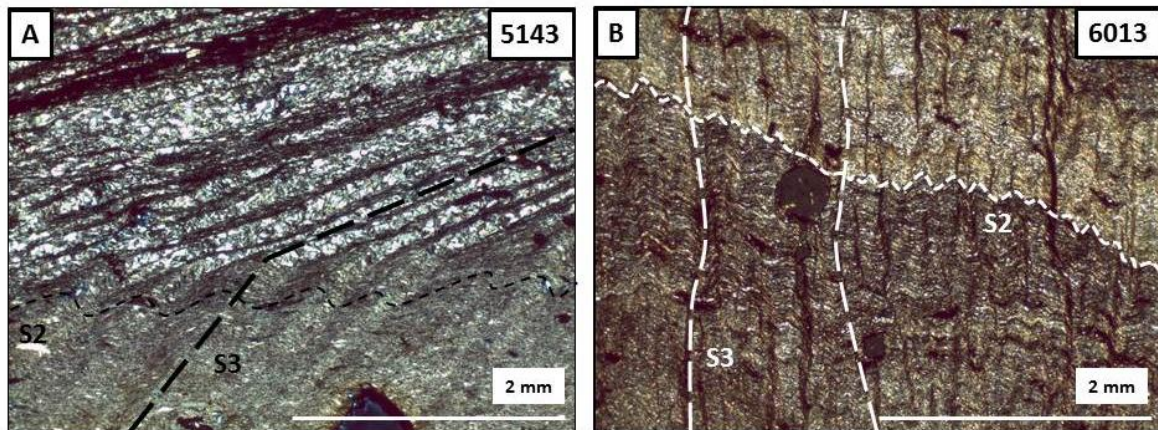
Figure 16: S3 crenulation cleavage and pressure solution. **16A:** Influence of rock composition and the expression of the S3 cleavage. Note the gentle crenulation in the more micaceous layers and strong pressure solution in the more quartz-rich layers, giving the illusion of a sense of shear (plane polarized light). **16B:** Well developed S3 pressure solution, likely recording significant volume loss (cross polarized light).

5.4 Interpretation and Discussion of Structural Data

The evidence for at least three deformation events (D1, D2, and D3) described above had previously only been inferred in the Rochford District based on map unit distributions and their similarities to relationships described in the Homestake Mine. This study has documented that the orientation and structural style of these fabrics changes across the Rochford District and that these changes are spatially related to the location of the garnet-in isograd (Fig. 9). This change is interpreted to be a result of the relative weakness of the D2 deformation event in this location. The S2 fabric is also at an unusual orientation in this area, dipping to the NE as opposed to dipping to the NW as in the majority of the field area. It is

unclear why the orientation of the S2 fabric is different, but is likely related to the change in deformation style. Similar changes in structural style can be observed near the garnet-in isograd in the eastern portion of the field area, but are not as clearly documented.

This study also highlights the widespread character of the S3 crenulation and associated pressure solution throughout the Rochford District. This deformation event has largely been overlooked in previous studies, and has been attributed to a later, unrelated and unspecified deformation not associated with the Trans-Hudson Orogeny or emplacement of the Harney Peak Granite (Redden et al., 1990; Caddey et al., 1991; Dahl et al., 2005). The amount of volume loss implied by the pressure solution suggests voluminous fluid migration, and likely resulted in a large volume of quartz veins emplaced at structurally higher levels.
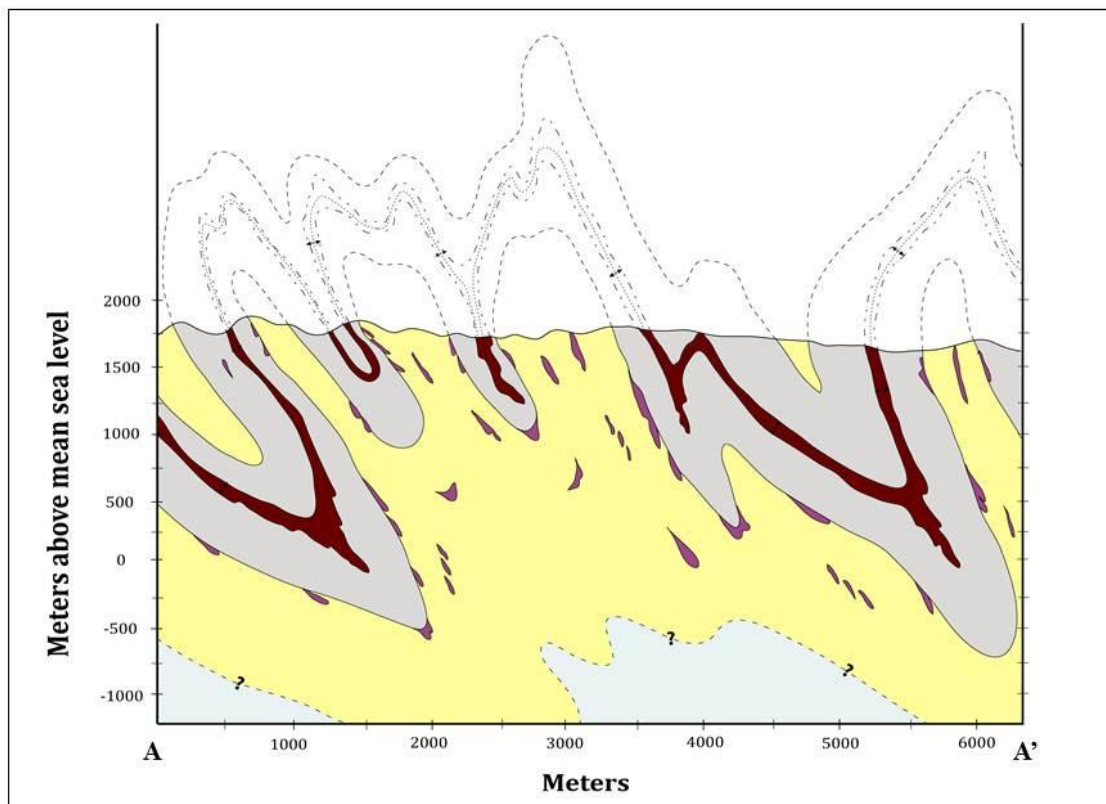
Figure 17: Cross section of A-A' (Fig. 2 and 9) with view to the north. Note that the Rochford Formation (red) is always at least doubled in thickness from early F1 folding and has then been re-folded by D2 deformation. This significantly thickens the Rochford Formation in the hinges of F2 folds. The purple unit within the Swede Gulch represents the quartzite layers that have been boudinaged due to D2 deformation (see Fig. 10B).

29

An additional goal of this study was to use map pattern distributions of rock types combined with new outcrop and microstructural observations to construct a realistic cross section of the district (Fig. 17). Note that due to the early F1 folding event, the Rochford Formation in this cross-section is nearly always doubled in thickness, as it defines the core of an F1 fold. The northeastern portion of the field area, not shown in this cross section, shows a deeper section into the F1 folds, where units older than the Rochford are present in the core of the same anticline (Fig. 2). These F1 folds have then been refolded by the map-scale F2 folds, and the thickened hinges of the F2 folds thicken the Rochford Formation to an even greater degree. These folds have been interpreted as plunging approximately 45 degrees to the North, based on the majority of measured mesoscopic fold axes, with the hinges of the Rochford Formation projected from the north (Fig. 9 and 15). This cross section is believed to be a reasonable interpretation of the three-dimensional extent of these rock units, and broadly resembles the cross sections that have been made of the Homestake Mine (Fig. 18). The cross section of the Rochford District undoubtedly simplifies the extent of the F2 folding, as there are likely many additional parasitic F2 folds, such as those seen in outcrop but are not easily traceable.
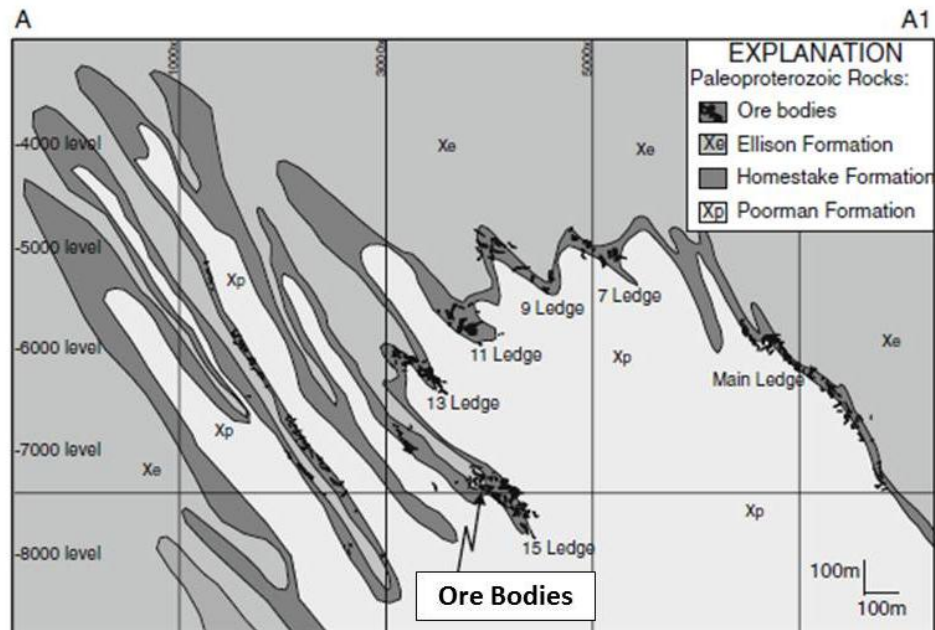
Figure 18: East-West cross-section looking north through the Homestake mine, showing the subsurface geometries of the Homestake Formation and locations of ore bodies, based on extensive drilling and underground workings (from Morelli et al., 2010). See Figure 1 for section location.

VI. METAMORPHIC HISTORY

The metamorphic history of the Rochford District is closely tied to the deformational history. The metamorphic grade of metasedimentary rocks in the Rochford area varies from low-greenschist facies slates and phyllites to mid-to-upper amphibolite facies phyllites and schists. One goal of this study was to better document the greenschist to amphibolite facies transition in pelitic rocks and in the Rochford Formation. Understanding the conditions of metamorphism is critical for understanding the mineralogic and structural controls in place prior to mineralization.

6.1 Prograde Metamorphism

The most important constraints on peak metamorphic conditions are the changes in mineral assemblages, particularly within the Rochford Formation, and the presence and

timing of garnet growth. The mineral assemblage of greenschist facies pelites consists of chlorite, white mica, quartz, and graphite. Amphibolite facies pelites typically consist of biotite, quartz, ± muscovite ± chloritoid ± garnet. Pelites from greenschist and amphibolite facies are similar in grain size. The mineral assemblages from lower-greenschist facies to lower-amphibolite facies Rochford Formation differ dramatically. Lower amphibolite-facies Rochford Formation consists of grunerite, quartz, biotite, stilpnomelane, and opaque minerals (primarily sulfides, although some iron oxides are still present) (Fig. 19B). Greenschist facies Rochford Formation consists primarily of siderite, quartz, biotite, ± stilpnomelane, and the opaque minerals are iron oxides with no sulfides (Fig. 19A). Due to poor exposure, lower grade Rochford Formation was sampled minimally in this study. However, based on the few samples collected, as well as the absence of historic mines and prospects, the lower grade Rochford Formation seems to contain little or no gold mineralization.

Quantitative assessments of peak metamorphic conditions are difficult to make in the Rochford Formation due to its unusual bulk composition. Although grunerite is a metamorphic amphibole, its stability field relative to typical amphibolite temperatures is not well known. At Homestake, the coexistence of grunerite and siderite was used to identify the greenschist to amphibolite facies transition (Caddey et al., 1990). However, in this study, siderite was rarely observed in hand sample or thin section, and only a few samples analyzed with the SEM were able to confirm the presence of co-existing grunerite and siderite.
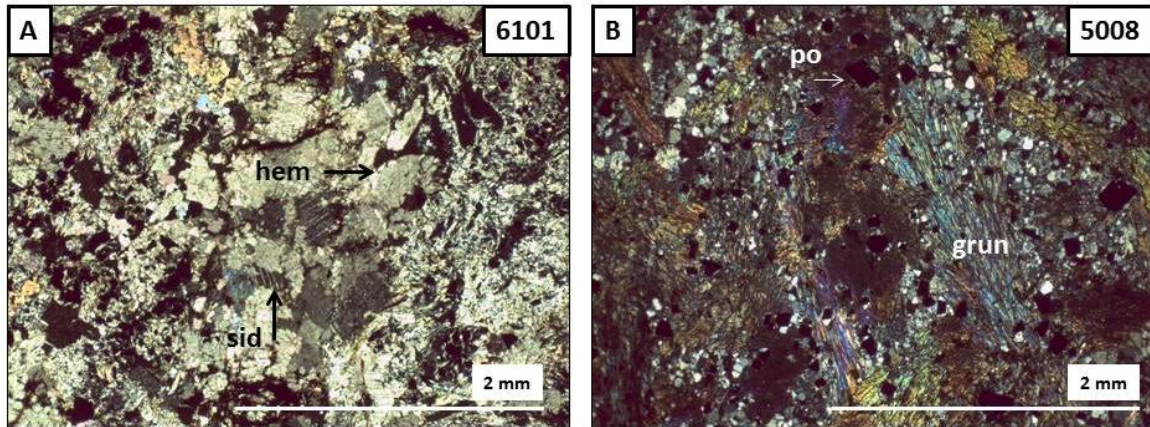
Figure 19: Variations in mineral assemblages of greenschist facies Rochford Formation consisting of siderite, white mica, quartz, and iron oxides (19A), and amphibolite facies Rochford Formation consisting of grunerite, quartz, and sulfides (19B). Cross polarized light.

The first appearance of stable garnet in phyllites as well as the Rochford Formation is the most obvious indicator for elevated metamorphic grades. Reconnaissance mapping and sampling was carried out in order to identify the distributions of garnet-stable and garnet-absent rocks in order to identify the location of the greenschist to amphibolite transition zone. Petrographic analyses were used to characterize and document the different types of garnets. Garnets vary in inclusion patterns and chemical zoning. The garnets in the Rochford District show a wide variation of inclusion patterns, including A) pinwheel zoning, B) linear inclusion trails C) inclusion free cores, D) graphite-inclusion-rich cores, and finally E) inclusion-free garnets (Fig. 20). At least three distinct garnet types have been identified based on the combination of common inclusion patterns and chemical zoning (Fig. 21). A-type garnets are typically subhedral to anhedral, have straight, linear inclusion trails interpreted to indicate post-kinematic garnet growth, and show no internal prograde zoning, but may have a slight Mn-rich rim (Fig. 21A). B-type garnets are rare, also tend to be subhedral to anhedral, have curved inclusion trails implying syn-kinematic garnet growth, and show strong prograde zoning (Fig. 21B). Finally, C-type garnets are euhedral and overgrow all other fabrics in the rock, often have minimal inclusions, and show moderate

33

prograde zoning (Fig. 21C). Each garnet type is interpreted to have grown during a separate
metamorphic event, suggesting that rocks of the Rochford District reached upper greenschist
to lower amphibolite facies temperatures several times during the metamorphic history of the
Rochford District.
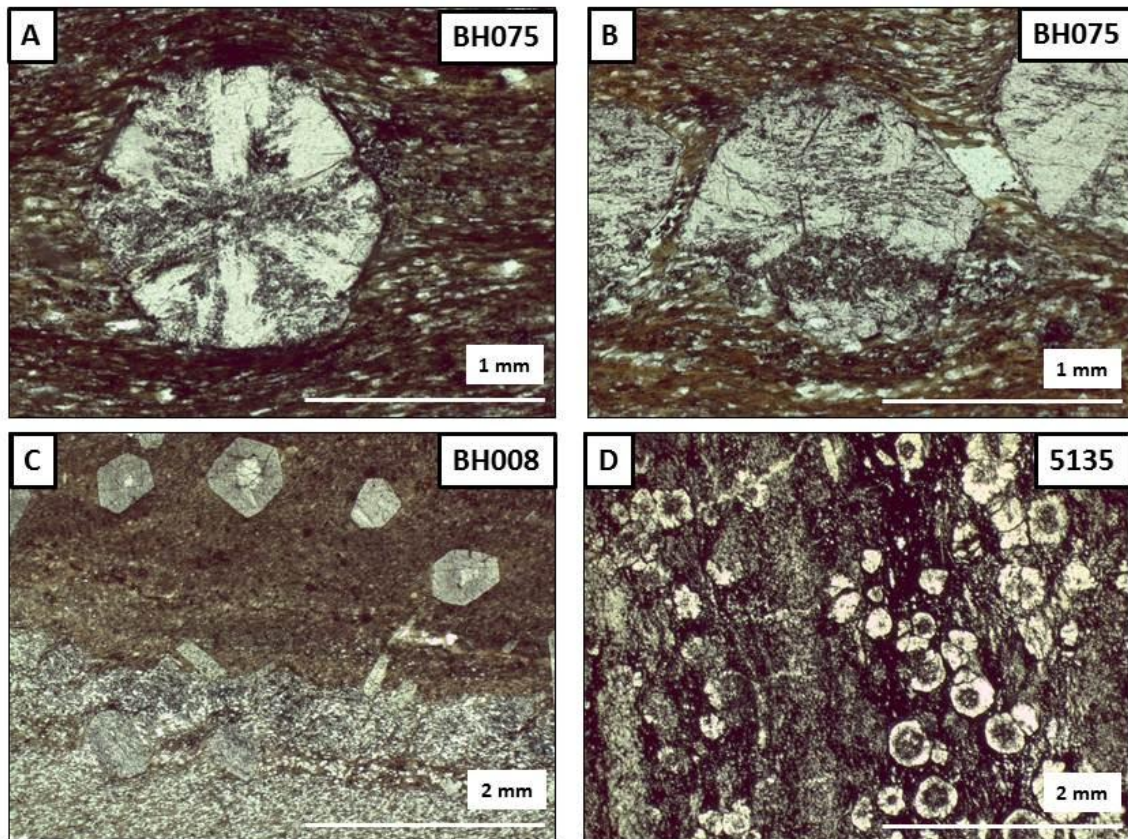
Figure 20: Examples illustrating the variety of inclusion patterns in garnets from phyllites in
the Rochford District. **20A:** segmented, pinwheel zoning **20B:** curved inclusion trails **20C:**
inclusion-free cores **20D:** graphitic inclusion-rich cores. The variation in inclusion patterns
suggests episodic garnet growth. Plane polarized light.
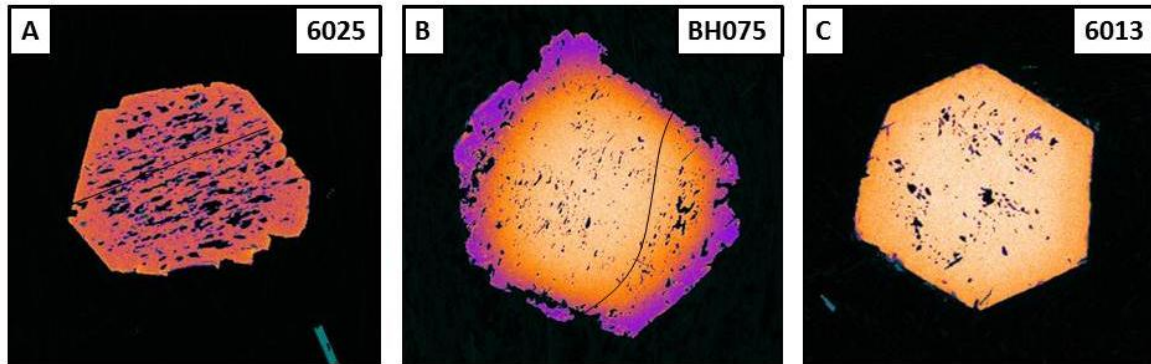
Figure 21: Mn composition maps of the three garnet-types described within the Rochford District. Warm colors (oranges and white) indicate high Mn compositions, cooler colors indicate lower Mn compositions. **21A:** Type-A garnet, with linear inclusion trails and no compositional zoning **21B:** Type-B garnet with curved inclusion trails and strong prograde zoning **21C:** Type-C, euhedral garnet that overgrows all other foliations in the rock with moderate prograde zoning. All garnets are approximately 1 mm in diameter.

Garnets within the Rochford Formation rarely match the A, B, and C-types identified in the surrounding phyllites. They are typically anhedral, in large mats and/or layers, and display various degrees of prograde zoning. Rare C-type garnets within the Rochford Formation contain grunerite inclusions, indicating that these garnets grew after the initial formation of grunerite, again suggesting multiple metamorphic events (Fig. 22). The unusual bulk composition of the Rochford Formation makes it difficult to use the presence of garnet as an indicator for amphibolite facies metamorphism, because the temperature at which garnet becomes stable is not known for this particular bulk composition.
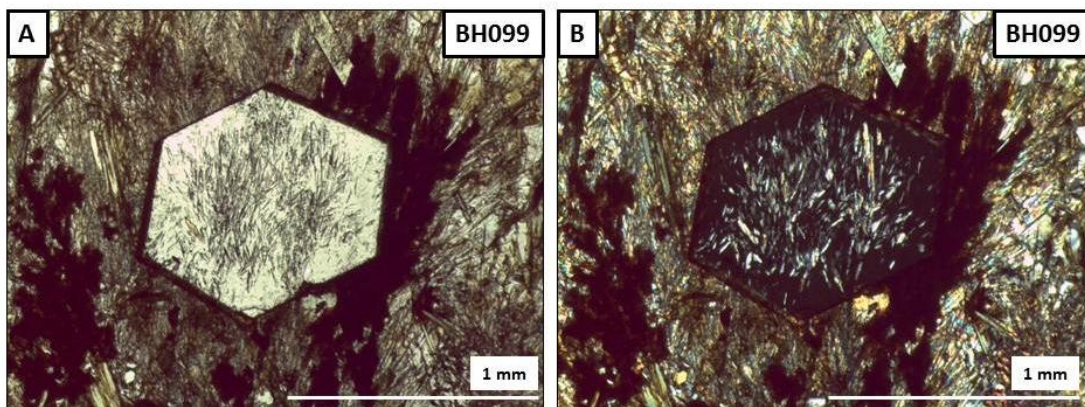
Figure 22: C-type garnet (Fig. 21) in the Rochford Formation in plane polarized light (22A) and cross polarized light (22B). Note the inclusions of grunerite, suggesting that these garnets must have grown after the prograde formation of grunerite. Also note the late chloritoid grain directly above the garnet.

35

Several samples of garnets from phyllites and the Rochford Formation were analyzed for their compositions and to make compositional maps for chemical zoning (Fig. 21). The sample size in this study is far too low to draw any firm conclusions about spatial variations in peak metamorphic conditions for the Rochford District as a whole, but compositional data for garnet and biotite has been included in this study as perhaps a starting point for future investigations (Appendix B). Overall, the garnet compositions in both the Rochford Formation and the surrounding phyllites are high in both iron and manganese, but extremely low in magnesium; with Mg #'s as low as 0.03 and lower. Such low Mg #'s severely limits the utility of these measurements for the garnet-biotite Fe-Mg exchange thermometer (Ferry and Spear, 1978).

6.2 Retrograde Metamorphism

Evidence for retrograde metamorphic events is limited to a few areas, usually near the garnet-in isograd. Evidence includes Mn-rich garnet rims (Fig. 21A), garnet and albite porphyroblast breakdown, and new mineral growth (primarily biotite and chloritoid) that cross-cut local fabrics.
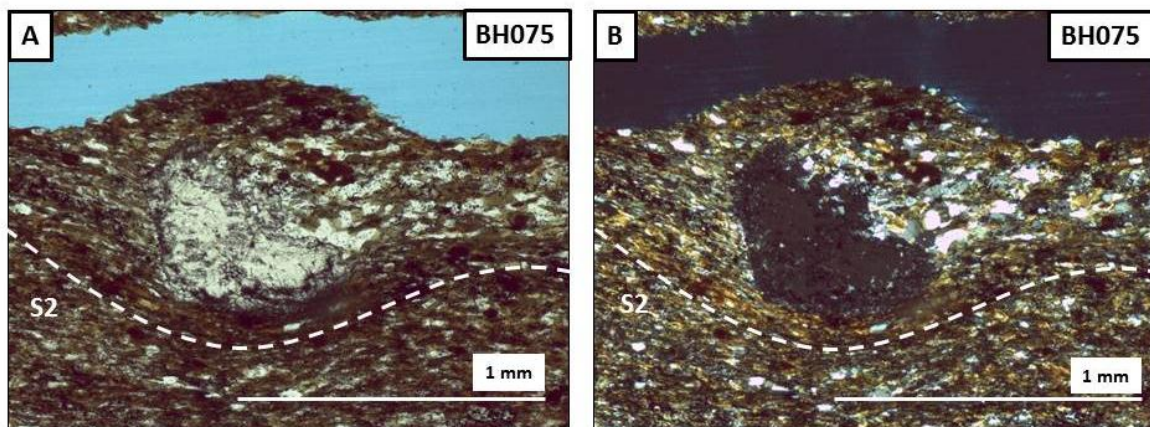
Figure 23: Retrograde garnet breakdown into biotite+quartz, syn-kinematic with the pervasive S2 foliation in plane polarized light (23A) and cross polarized light (23B).

Evidence for garnet retrogression is particularly convincing in the NW corner of the study area (Fig. 2). Garnet breaks down most commonly to biotite + quartz (Fig. 23). However, garnets that were once rich in graphite-inclusions can break down to biotite + quartz + graphite (Fig. 24C and D), and some relict garnet grains contain almost entirely graphite + quartz (Fig. 24B). The composition of the surrounding rock controls the composition of the resulting porphyroclast, as evidenced when a grain straddles a compositional boundary and portions of the relict grain from within a darker compositional layer are richer in graphite relative to the portions in a lighter compositional layer (Fig. 24C). This retrograde breakdown of garnet appears to have been syn-kinematic with the development of the surrounding foliation (S2), and only rarely shows evidence for grain rotation (Fig. 24). Occasionally other relict grains can also be observed, again almost exclusively in the NW portion of the field area. These grains are now mostly sericite + quartz, and are thought to have originally been albite porphyroblasts.
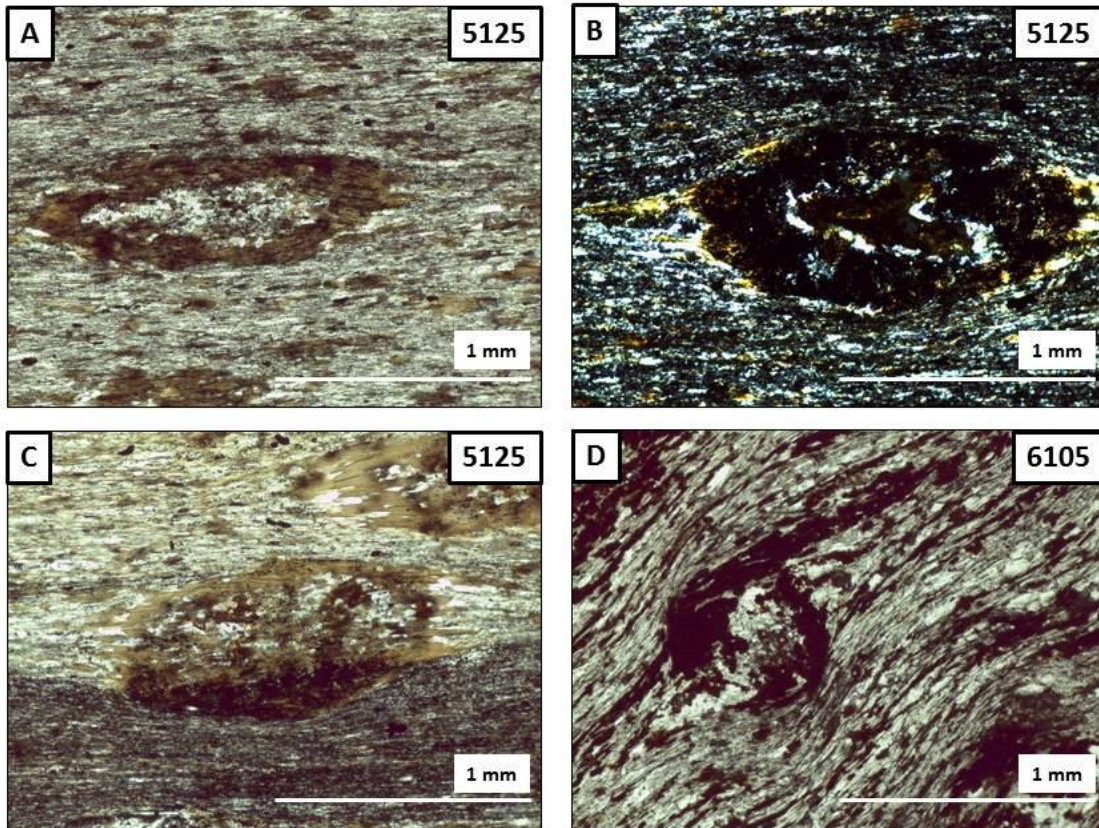
Figure 24: Variations in the compositions of retrograde garnet relicts. Retrogradation was synkinematic with the dominant foliation (S2) in all examples. **24A:** quartz core with biotite rim. **24B:** graphite and minor quartz **24C:** relict grain is graphite-rich in the darker compositional layer. **24D:** rotated relict garnet porphyroblast. Plane polarized light.

Finally, evidence for new mineral growth is also associated with retrograde metamorphic conditions. Large biotite and chloritoid grains commonly grow in preferred orientations across the dominant foliation(s) within the rocks (Fig. 15B). This is often interpreted as either static growth following a deformation event, or as a distinct, late, lower grade metamorphic event.

6.3 Interpretation and Discussion of Metamorphic History

Metamorphic history has a direct connection to the gold mineralization at the Homestake Mine, and is therefore an important comparison to make with the Rochford District. The greenschist to amphibolite transition zone is identified by the first appearance of garnet stable rocks throughout the Rochford District, as well as by the co-existence of

38

grunerite and siderite in the Rochford Formation. The formation of grunerite is understood to

be a result of the prograde reaction of siderite and quartz illustrated in the following

equation: (Klein, 1978).

$$1)\ FeCO_3\ + 8SiO_2 + H_2O \rightarrow Fe_7Si_8O_{22}(OH)_2 + 7CO_2$$
$$(siderite + quartz + H_2O \rightarrow\ grunerite + CO_2)$$
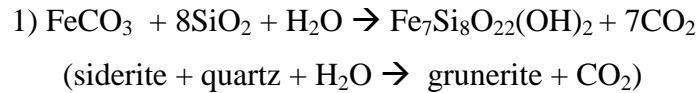
The temperature of the formation of grunerite is not well calibrated experimentally,

however, field observations have shown a clear relationship between grunerite stability and

garnet stability, (Klein, 1978). Thus, the coexistence of grunerite and siderite was used to

identify the greenschist to amphibolite transition zone within the Homestake Formation

throughout the Homestake Mine (Caddey et al., 1990).

Most sampling of the Rochford Formation in this study focused on the area

surrounding the Golden West mine. Based on the mineral assemblages described above, this

area is well within the amphibolite facies, due to the abundance of garnet and grunerite, and

the lack of obvious siderite. Fine-grained siderite has been identified within ore grade rocks

by SEM at the Golden West mine (Fig. 27), suggesting that this area may be close to but

slightly above the greenschist to amphibolite transition zone. Not all samples could be

analyzed with the SEM, so the transition zone was not consistently identified based on the

co-existence of grunerite and siderite for the rest of the field area. This study focused instead

on constraining the location of the garnet-in isograd.

The three types of garnets mentioned (above) are interpreted to represent at least

three distinct periods of garnet growth. A-type garnets are interpreted to have grown

statically following the D1 deformation event, due to their linear inclusion trails, and their

lack of chemical zoning is attributed to thermal relaxation caused by subsequent

metamorphic events. Warped inclusion trails and strain shadows imply B-type garnets grew

syn-kinematically with the D2 deformation event. C-type garnets are believed to have grown

statically following the D2 and D3 deformation events. The complex inclusion patterns

found in many garnets make it difficult to assign every garnet with one particular "type", but

provide further evidence that garnet growth happened episodically, where inclusion-rich or

inclusion-poor cores represent a change in the conditions under which the garnets were

growing. This is consistent with the observations made of garnets in the southern Black Hills

by Dahl et al. (2005), who also noted episodic garnet growth, as well as at least two distinct

episodes of garnet breakdown.

Garnet compositions did not vary significantly within each sample, which suggests

that garnet composition was controlled by the bulk composition of the rock. Of the measured

garnet compositions, all garnets were rich in both iron and manganese, and remarkably low

in magnesium and calcium. Garnets with high manganese compositions are stable at

temperatures well below the greenschist to amphibolite transition (Miyashiro, 1973; Hsu,

1980). Caddey et al. (1990) noted that small (<1 mm), pink, Mn-rich garnets found within

and around the Homestake Mine were not used to map the garnet-in isograd, because of their

lower temperature stability compared to garnets of a more iron-rich composition. This

approach was followed in this study. The transition zone was mapped based largely on the

first appearance of garnet-stable samples and samples displaying the co-existence (not

necessarily equilibrium) of garnet and chloritoid (Powell and Holland, 1990; Powell et al.,

1998). Retrograded garnet grains (biotite, quartz, opaques) are mainly observed in the

northwestern corner and towards the eastern edge of the field area, near the garnet-in

isograds. Because the retrogradation of these garnets is apparently syn-kinematic with the S2

foliations, it suggests that the D2 deformation event in these locations was of lower

temperature than the D1 deformation. This finding conflicts with many of the metamorphic

studies of the Black Hills, which consistently associate the D2 event with peak metamorphic conditions (Morelli et al., 2010; Dahl et al., 2005; Redden et al, 1990).
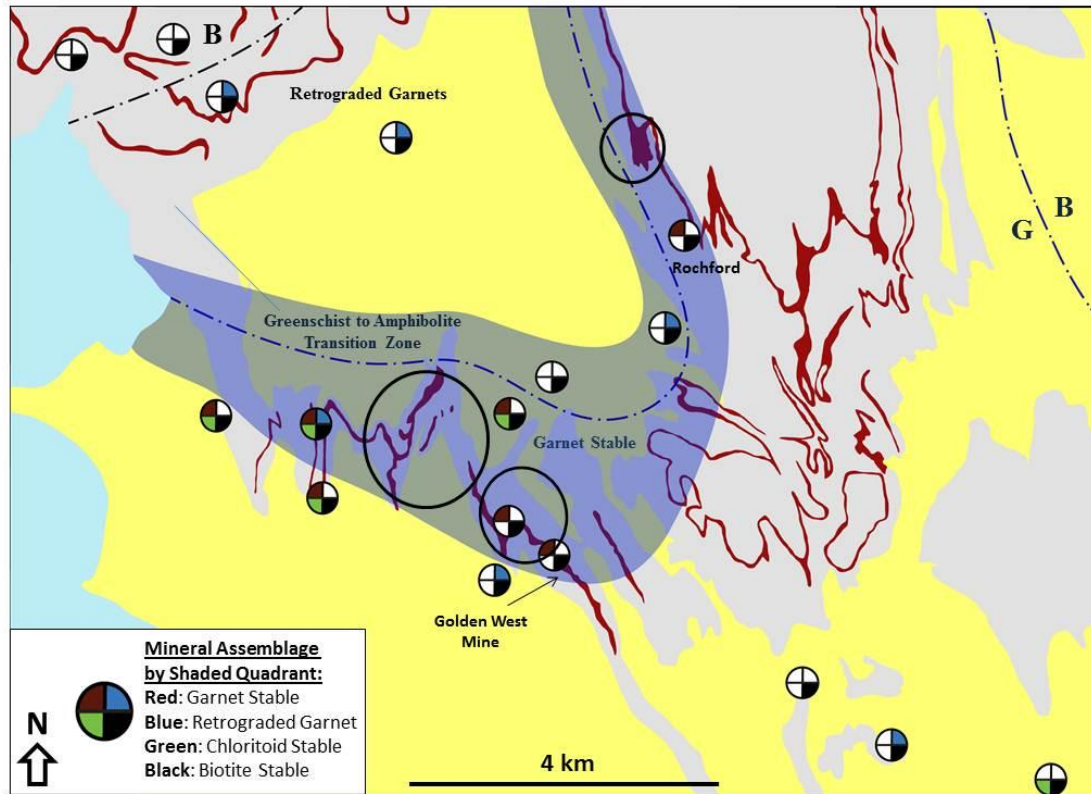
Figure 25: The post-D2 greenschist to amphibolite transition zone in the Rochford District (from Fig. 2). Colored circles represent the presence of diagnostic mineral assemblages used to define the approximate boundary of the transition zone. Because D2 deformation is occasionally associated with retrogression, this transition zone does not reflect peak metamorphic assemblages, but the state of metamorphism prior to gold mineralization. Black circles highlight areas that are 1) within the transition zone 2) contain Rochford Formation and 3) are influenced by F2 folding, and therefore are most likely to contain Homestake-style gold mineralization.

Using all of the field and petrographic observations described above, it is possible to broadly delineate the approximate transition from greenschist to amphibolite facies in the Rochford District (Fig. 25). Because the D2 deformation event was responsible for retrogression in at least some areas, and that the mineralization at Homestake likely favored rocks that were within the transition from greenschist to amphibolite facies at the time of mineralization, this transition zone was mapped based on post-D2 metamorphic conditions. The morphology of the transition zone parallels the general pattern of the Rochford

anticlinorium, and follows the inner boundary between the Swede Gulch and Poverty Gulch Formations (Fig. 25). This suggests that the isograd was folded by the D2 event, providing further evidence that peak metamorphic assemblages in the Rochford District are associated with the D1 deformation.

VII. GOLD MINERALIZATION

The presence of gold in the Rochford District is known from historic mines and mining records, published studies (Bayley, 1972), and a large new assay database (this study). A primary focus of this study is to better characterize the distribution of gold and the mineralization styles, and to examine the relationship between the mineralization and the stratigraphic, structural, and metamorphic relations described above. Another focus of this study is to compare the controls and character of mineralization to those described for the Homestake Mine.

7.1 Assay Data and Mineralogic Controls
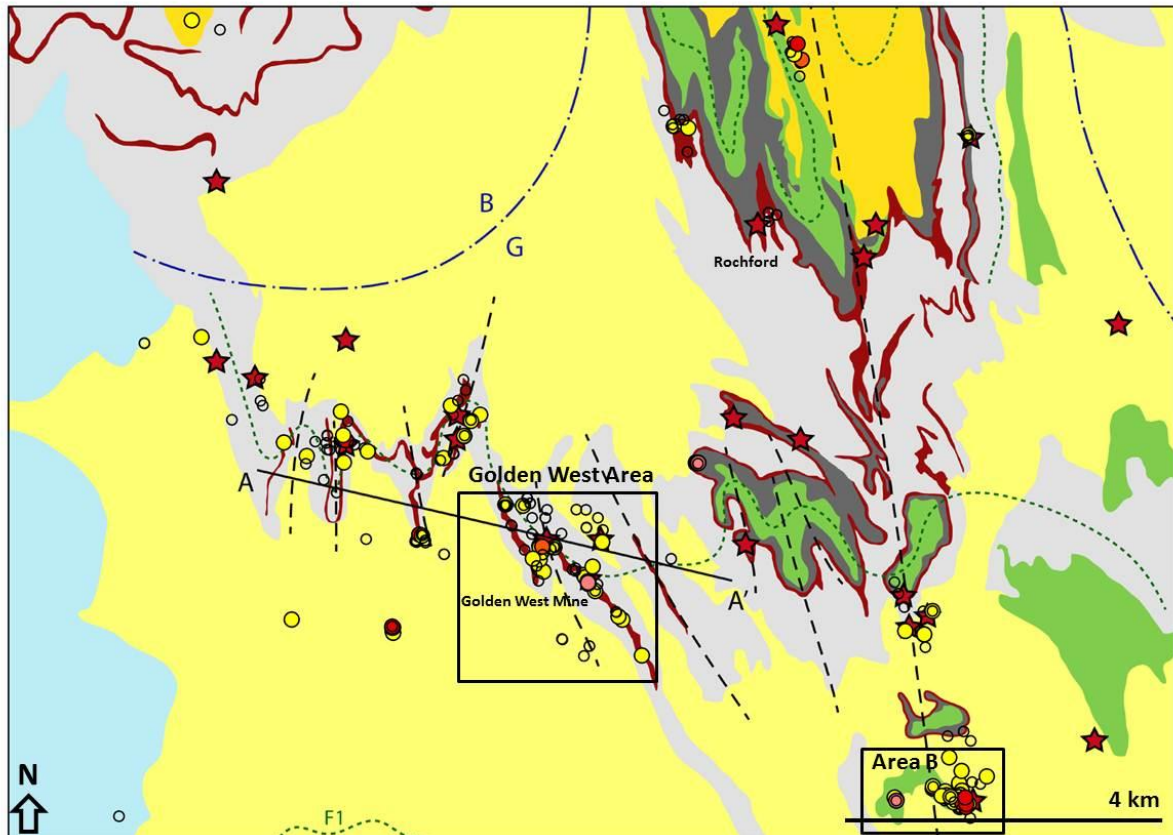
Figure 26: Simplified geologic map of the Rochford District (from Fig. 2), with locations of historic mines and prospects (stars) and gold assay values (circles). Unfilled circles: 0-0.1 ppm Au, yellow: 0.1-0.5 ppm Au, orange: 0.5-1.0 ppm Au, red: 1-5 ppm Au, pink: >5 ppm Au. The Golden West Mine and surrounding area has been highlighted, as has Area B, the location of non-Homestake-style mineralization. Note the relationship between anomalous gold values and the Rochford Formation (red).

A total of 389 samples of various rock types throughout the Rochford District were assayed, and 138 of them were found to have highly anomalous concentrations of gold (here defined as > 0.10 ppm Au). Of all the anomalous samples, 40 were > 1 ppm and 13 were >5 ppm, with local values as high as 21 and 35 ppm. Of these 138 anomalous samples, 62 (or 45%) were found to be samples of the Rochford Formation (Fig. 26 and Table 1). Within the Golden West Area (Fig. 26), 33 of 42 anomalous samples, or 78.6%, were of the Rochford Formation. One location (Area B in Fig. 26) was found to have a different mineralization style from the rest of the Rochford District. Mineralization in this area is restricted to sub-vertical faults with several meters of offset, which have been in-filled with quartz and

carbonate vein material. This area does not contain any outcrops of Rochford Formation, so

is not considered to contain Homestake-style mineralization. Excluding this area, for all rock

types within the Rochford District, less than 7% of anomalous samples come from a rock

unit that is more than 50 meters away from the Rochford Formation (Table 2). There are

extensive exposures of Rochford Formation in the NW quadrant of the field area (Fig. 2 and

26), but here the formation is below the stability of grunerite. In this area, the Rochford

Formation is not commonly associated with anomalous amounts of gold or sulfides (Fig.

19).

Table 1: Assay Data for All Samples						
	All Samples					
Rock Unit	Rochford	Phyllite	Quartzite	Quartz Veins	Other	Total
Total Number of Samples	180	55	23	90	41	389
Total Number of Anomalous Samples	62	12	10	38	16	138
Percent Anomalous Samples Within Rock Unit (#A in rock unit/ total # of rock unit)*100	34.44%	21.81%	43.48%	42.22%	39.02%	n/a
Percent of All Anomalous Samples (#A of rock unit/ total #A Samples)*100	44.93%	8.70%	7.24%	27.53%	11.60%	100%

Table 1: Assay values from all samples taken in the Rochford District. The number of anomalous samples is given as well as the percentages of anomalous samples per rock type, and the percentage of anomalous samples of each rock type out of all anomalous samples. Anomalous samples are most likely to be found within the Rochford Formation.

Table 2: Anomalous Assay Data From Golden West and Surrounding Areas													
Rock Unit	Phyllite			Quartzite			Quartz Veins			Other			Rochford	
	Outside 50m	Within 50m	Total	Outside 50m	Within 50m	Total	Outside 50m	Within 50m	Total	Outside 50m	Within 50m	Total		Including Samples Within 50m
# Anomalous Samples	6	4	10	4	6	10	5	2	7	4	3	7	62	77
0.1-0.5 ppm Au	6	3	9	3	1	4	5	1	6	2	1	3	38	44
0.5-1.0 ppm Au	1	0	1	0	1	1	0	0	0	1	0	1	6	7
1-5 ppm Au	0	1	0	1	1	2	0	1	1	1	1	2	11	15
>5 ppm Au	0	0	0	0	3	3	0	0	0	0	1	1	7	11
Percent Anomalous (#A/Total #A)*100	6.25%	4.17%	10.40%	4.17%	6.25%	10.41%	5.21%	2.09%	7.29%	4.17%	3.13%	7.29%	64.58%	80.21%

Table 2: Number of anomalous samples (excluding Area B in Fig. 26) per rock type, with total number of anomalous samples designated by proximity to the Rochford Formation (outside or within 50 meters of the Rochford Formation). 80% of anomalous samples are found within 50 meters of the Rochford Formation.

7.2 Gold Ore at the Golden West Mine

The open pit at the abandoned Golden West mine contains several exposures of sulfide-rich, high-grade gold ore. Several samples were collected of both mineralized and barren Rochford Formation in order to document the style(s) of mineralization and compare to that at the Homestake Mine. Gold values change rapidly over distances of a few meters. Ore-grade Rochford Formation is characterized by the presence of abundant sulfides, primarily pyrrhotite and arsenopyrite. However, a thin lens of massive pyrrhotite is barren, despite being adjacent to high gold grades. Just above the massive pyrrhotite, the Rochford Formation has disseminated, euhedral to subhedral crystals of arsenopyrite, and contains approximately 1 ppm Au (Fig. 5); below the massive pyrrhotite the Rochford Formation contains grunerite rosettes that have been partially replaced by pyrrhotite, and contains small amounts of siderite and chloritoid. This horizon yielded assays between 10 and 18 ppm Au (Fig. 27A).

Elevated gold concentrations within the Rochford Formation (> 1 ppm) were measured throughout the pit, and visible gold was identified in one sample and confirmed using an SEM. The gold in this sample occurs in small blebs 10-50 μm in diameter and

occurs either within or adjacent to arsenopyrite grains, similarly to the gold described at Homestake (Figure 27B; Caddey et al., 1991; Morelli et al., 2010). Microprobe analyses indicate the gold flecks also contain small amounts of silver with an Au:Ag ratio of 6.8:1, similar to the reported 5:1 Au:Ag ratio at Homestake (Gustafson, 1933).
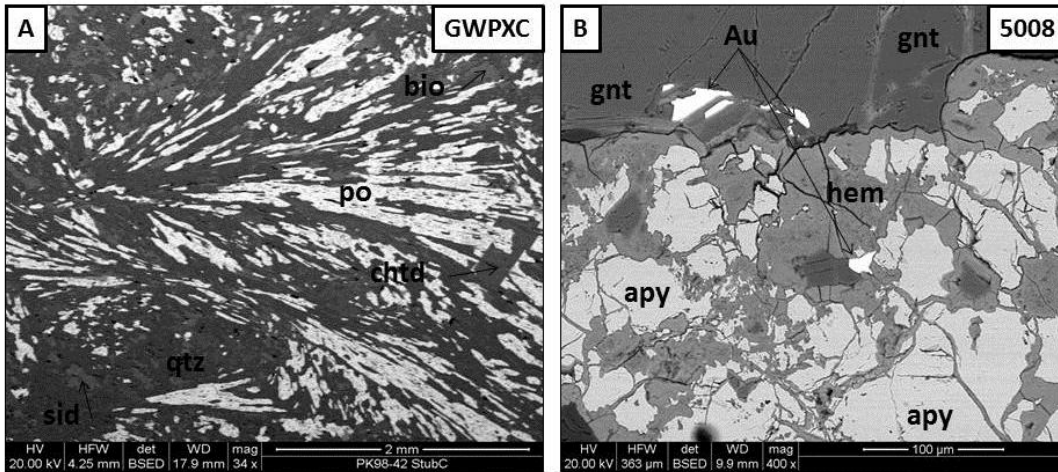
Figure 27: Mineralization textures at the Golden West mine. SEM BSE images of two mineralized samples from the Golden West pit (Fig. 12). **27A:** Pyrrhotite directly replaces grunerite rosettes in a sample with over 17 ppm Au. Also note the chloritoid (chtd) potentially growing contemporaneously with the pyrrhotite, and the presence of siderite (sid). **27B:** Native gold within or adjacent to grains of arsenopyrite (apy) that have been weathered to hematite (hem).

7.3 Mineralization Style and Comparison to the Homestake Mine

This study has determined that the gold mineralization in the Rochford Formation resembles what has been described at the Homestake Mine. A plausible chemical reaction that allows an iron-formation to act as a chemical trap involves the oxidation of sulfur (S^{-2}) to pyrite (S^{-1}), which drives the precipitation of gold from auriferous fluids. The following reactions illustrate this process for both pyrite (1) and pyrrhotite (2) (Phyllips, Groves, and Martyn, 1984).

$$(1)\ FeO(silicate) + HAu(HS)_2 + 1/4\ O = FeS_2 + 3/2\ H_2O + Au$$

$$(2)\ 2Fe_3O_4 + 3HAu(HS)_2 = 6\ FeS + 9/2\ H_2O + 7/4\ O_2 + 3Au$$

46
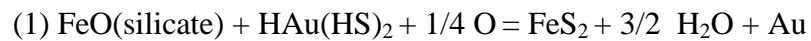
Similar to the Homestake Formation, the Rochford Formation contains iron silicates and iron oxides, and is thus capable of acting as a chemical trap for gold and sulfides.

The assay data from this study indicate that anomalously high gold concentrations are favored in the Rochford Formation compared to other rock types. However, anomalous gold is not restricted to the Rochford Formation. It is also difficult to distinguish mineralized Rochford Formation from unmineralized Rochford Formation due to highly weathered and oxidized outcrops.

At the Homestake Mine, the greenschist to amphibolite transition zone is an important controlling factor for high grade gold distribution. A plausible explanation is that the prograde formation of grunerite is required for gold deposition, but that the higher grade iron formations have undergone too much volume loss and lack the requisite porosity and permeability. Thus, the greenschist to amphibolite transition zone may represent the most favorable combination of host rock mineralogy and permeability for gold mineralization— both at the Homestake Mine and in the Rochford District.

The mineralization at both the Homestake Mine and the Rochford District is dominated by pyrrhotite and arsenopyrite, where gold is texturally related to arsenopyrite. The types of ore within the Golden West open pit are comparable to the types of ore associated with the Homestake Mine. However, the ore textures most similar to the "replacement-type" ore at Homestake consistently contain some of the highest gold values obtained in this study (Fig. 27A), and the massive sulfide lenses most similar to the "shear"-type ore at Homestake are completely barren in the Golden West pit.

The textural relationships between sulfides and metamorphic minerals help to constrain the timing of the mineralization in the Rochford District. Chloritoid appears to have overgrown, and been overgrown by, pyrrhotite, indicating the mineralization event may

47

have been synchronous with the lower temperature S3 crenulation cleavage often associated

with chloritoid growth (Fig. 27A). In another sample, pyrrhotite, which likely

pseudomorphed grunerite, is replaced by fresh siderite (Fig. 28A). This relationship suggests

that there was retrograde siderite growth following a mineralization event. Pyrite can also be

observed replacing pyrrhotite suggesting at least two pulses of sulfide mineralization (Fig.

28B). Together, these observations suggest that there were two mineralizing events in the

Rochford District, and that one of these events may have been synchronous with the

retrograde growth of chloritoid and siderite, which has been attributed to the late, S3

crenulation in the rest of the field area.
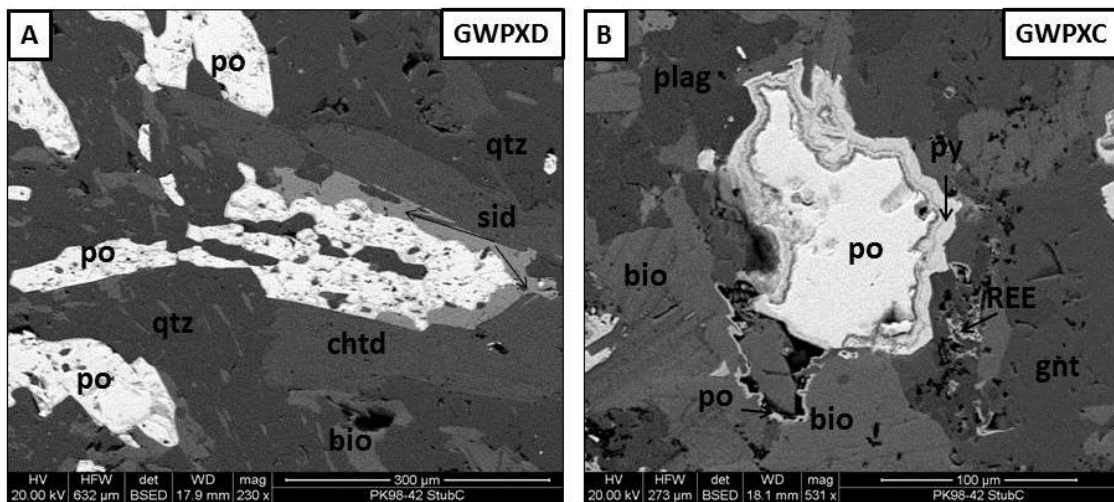
Figure 28: Timing of mineralization at the Golden West mine. SEM BSE images of two mineralized samples from the Golden West pit. **28A:** Retrograde siderite (sid) replaces pyrrhotite (po), which likely pseudomorphed grunerite during an earlier mineralization event. **28B:** Pyrite (py) replaces pyrrhotite (po), indicating there were likely two separate pulses of mineralization at the Golden West mine.

7.4 Discussion of Structural Controls on Mineralization

The most plausible model for gold mineralization at both Homestake and the

Rochford District invokes the metamorphosed Homestake and Rochford Formations acting

as chemical traps that trigger the precipitation of gold and sulfides from an auriferous,

hydrothermal fluid. The size of any potential ore body will be limited to the total

48

volume/thickness of the metamorphosed iron formation in any one place. Thus, it makes sense that the largest ore bodies at Homestake occur in the thickened hinge regions of map-scale F2 folds, as these provide the largest concentrated volume of favorable host rock. For the same reasons, the most attractive exploration targets in the Rochford District are hinge regions of map scale folds of the Rochford Formation. The heterogeneous strain associated with F2 folding may have also caused local shearing, resulting in open spaces in which free fluid phases could infill during mineralization. These open spaces allowed for the deposition of "shear" ore at the Homestake Mine, and are likely responsible for the lenses of massive sulfides at the Golden West mine in the Rochford District.

Another potentially important control on gold mineralization is the development of the S3 crenulation cleavage and pressure solution. This fabric records extensive volume loss and fluid migration, and is commonly associated with growth of late biotite and chloritoid. The spatial association of late chloritoid and sulfide mineralization in the Golden West mine suggests a contemporaneous relationship between these two events. It seems reasonable that the same event responsible for regional-scale dissolution and fluid migration might have been responsible for mobilizing gold and re-depositing it in favorable structural and stratigraphic traps. Thus, I suggest that the S3 fabric is likely synchronous with one of the mineralization events in the Rochford District because 1) it records the migration of large volumes of fluids and solutes, and 2) it provides a network of fluid migration pathways.

The interpretation that the S3 foliation is synchronous with a gold mineralizing event may be in conflict with other observations about the regional geology of the Black Hills. For example, Morelli (2010) has dated the mineralization event at Homestake to just prior to the emplacement of the Harney Peak Granite, but Redden et al. (1990) noted that the S3 crenulation in the vicinity of the Harney Peak Granite crenulates sillimanite formed in the

49

metamorphic aureole, suggesting that the S3 fabric is younger than the granite. If the S3

foliation is responsible for gold mineralization at Rochford, it must either be a younger

mineralizing event than at Homestake, and/or a separate event from that observed near the

Harney Peak Granite. One possibility, supported by petrographic observations described

above, is that there were two mineralizing events in the Rochford District (Fig. 28B), with

the first event synchronous with Homestake, and the younger event representing gold that

was remobilized during the D3 deformation event. The mineralization at Homestake is often

linked to the hydrothermal fluids associated with the earliest stages of the emplacement of

the Harney Peak Granite, and the area surrounding the mine contains several large granitoid

bodies. If this mineralization event affected the Rochford District, it would have likely been

a weaker event due to the lack of granitoid bodies, and the second mineralization event may

have helped to enrich mineralization in the Rochford District.

7.5 Summary: Gold Mineralization Model for the Rochford District

This study has examined several factors that likely controlled gold mineralization in

the Rochford District. In order to act as an effective chemical trap, the Rochford Formation

apparently had to have been metamorphosed to the transition between greenschist and

amphibolite facies. This allows for grunerite growth, which acts as a chemical trap for gold

and sulfides, without resulting in so much volume loss that permeability was degraded. The

folding of the Rochford Formation is required to increase the volume of potential host rock.

Finally, widespread fluid flow, perhaps in multiple events is required to mobilize gold in

auriferous, sulfide-rich hydrothermal fluids from deep sources and introduce the gold to

favorable structural and stratigraphic traps. The first mineralization event may have been

synchronous with the event responsible for the mineralization at Homestake, and the second

event is likely synchronous with the pressure solution and fluid migration documented by the

S3 crenulation cleavage. Primary targets for continued exploration are the thickened F2 fold hinges of Rochford Formation near or within the greenschist to amphibolite transition zones, perhaps particularly in areas that possess a strong, late (S3) crenulation/pressure solution cleavage (Fig. 25).

VIII. CONCLUSIONS

This study documents the structures, metamorphic assemblages, and gold mineralization in the Rochford District in order to understand the controls on gold mineralization and how they compare to the Homestake Mine. Three distinct deformation events have been documented in the Rochford District. D1 consists of tight EW folds, and a penetrative foliation, S1, that has been transposed by the later, S2 fabric. D2 makes up the dominant NNW-trending, penetrative foliation, and is responsible for tight to isoclinal F2 folds. In most locations D2 completely transposes D1, except in the NW corner of the field area (Fig. 2 and 9) where a weaker zone of D2 deformation can be observed. In this area, F2 folds are broad and open, the S2 fabric is a spaced crenulation, and the penetrative foliation is interpreted as S1. D3 is expressed as a late, spaced, crenulation cleavage, often associated with pressure solution and implies a significant amount of volume loss and fluid mobilization.

Prograde metamorphism occurred during both D1 and D2 deformation events, with several generations of garnet growth followed by continued static growth. The greenschist to amphibolite transition represents the most favorable combination of host rock mineralogy and permeability for gold mineralization. This transition zone was identified in the Rochford District by the coexistence of grunerite and siderite in the Rochford Formation and by the first appearance of garnet stable rocks in pelites (Fig. 25). The northwestern corner of the

51

field area contains relict garnet porphyroblasts that were retrograded during D2, which suggests that this area represents a zone of weaker deformation and lower metamorphic temperature than observed elsewhere in the Black Hills.

Gold in the Rochford District is concentrated in the Rochford Formation because the iron formation acted as a chemical trap for gold and sulfides, as at the Homestake Mine. Multiple folding events with thickening in the hinge regions increased the volume of Rochford Formation available to host gold mineralization (Fig. 17). Mineralization in the Rochford District likely occurred in two pulses, the first, a weak hydrothermal event contemporaneous with the gold mineralization at Homestake and temporally related to the earliest stages of the emplacement of the Harney Peak Granite. The second pulse is recorded by the S3 cleavage as a pressure solution that remobilized and enriched gold deposits throughout the Rochford District. This general model for mineralization in the Rochford District is similar to the mineralization model at Homestake, but highlights the unique structural setting of the Rochford District. Future exploration efforts should focus on the thickened F2 fold hinges of Rochford Formation within the greenschist to amphibolite transition zone throughout the Rochford District, particularly in areas with a well-developed S3 crenulation.

References:

1. Bayley, RW (1972). A preliminary report on the geology and gold deposits of the Rochford district, Black Hills, South Dakota: *United States Geological Survey Bulletin*. Vol. 1332-A, 24.

2. Caddey, SW, Bachman, RL, Campbell, TJ, Reid, RR, and Otto, RP (1991). The Homestake gold mine, an early Proterozoic iron-formation hosted gold deposit, Lawrence County, South Dakota. *United States Geological Survey Bulletin* 1857-J, 67.

3. Dahl, PS, Terry, MP, Jercinovic, MJ, Williams, ML, Hamilton, MA, Foland, KA, Clement, SM, Friberg, LM (2005). Electron probe (Ultrachron) microchronometry of metamorphic monazite: unraveling the timing of polyphase thermotectonism in the easternmost Wyoming Craton (Black Hills, South Dakota). *American Mineralogist*. Vol. 90, 1712-1728.

4. Dahl, P.S,. Foland, K.A., 2008. Concentric slow cooling of a low P high T terrane: Evidence for 1600-1300 Ma mica dates in the 1780-1700 Ma Black Hills orogeny, South Dakota, USA. American Mineralogist. Vol. 93, 1215-1229.

5. Darton, NH, and Paige, S (1925). Description of the central Black Hills, South Dakota: U.S. Geological Survey Geol. Atal, Folio 219.

6. Deer, W.A., Howie, R.A., Zussman, J., 1997. *Rock Forming Minerals: Double-Chain Silicates*. Geological Society, Vol. 2B, Ed. 2.

7. Dodge, T.A., 1942. Amphibolites of the Lead area, northern Black Hills, South Dakota. *Geological Society of America Bulletin*. Vol. 53, 561-584.

8. Ferry, J.M. and Spear, F.S., 1978. Experimental calibration of the partitioning of Fe and Mg between biotite and garnet. *Contributions to Mineralogy and Petrology*. Vol. 66, 113-117.

9. Frei, R, Dahl, PS, Frandsson MM, Jensen, LA, Hansen, TR, Terry, MP, Frei, KM (2009). Lead-isotope and trace element geochemistry of Paleoproterozoic metasedimentary rocks in the Lead and Rochford basins (Black Hills, South Dakota, USA): implications for genetic models, mineralization ages, and sources of leads in the Homestake gold deposit. *Precambrian Research*. Vol. 172, 1-24.

10. Goldfarb, RJ, Baker, T, Dube, B, Groves DI, Hart CJR, Gosselin P (2005). Distribution, character, and genesis of gold deposits in metamorphic terranes. In: Hedenquist JW, Thompson JFH, Goldfarb RJ, Richards JP (eds) *Economic Geology:* 100th Anniversary Volume, Society of Economic Geology, 407-451.

11. Hark, J.S., Frei, R., Whitehouse, M.J., Dahl, P.S., 2008. New evidence for 2.01 Ga rifting of the easternmost Wyoming crating (Black Hills, SD): implications for

breakup of a supercraton (Superia). Geologic Society of America Abstracts with Programs 40 (6), 145-217.

12. Hsu, 1980. Hydration and phase relations of grossular-spessartine garnets of $pH_2O=2kb$. *Contributions to Mineralogy and Petrology*. Vol. 71, Issue 4, 407-415.

13. Isley, A.E., Abbot, D.H., 1999. Plume related mafic volcanism and the deposition of banded iron formation. *Journal of Geophysical Research*-Solid Earth 104. 15461-15477.

14. Kath, RL, and Redden, JA (1990). Petrogenesis of the Homestake iron formation, Lead, South Dakota; assemblages of metamorphism. In: Paterson Colin, J, Lisenbee Alvis, L. (Eds.), Metallogeny of gold in the Black Hills, South Dakota: guidebook prepared for Society of Economic Geologists field conference. Guidebook series, pp.112-118.

15. Klein, C., 1978. Regional metamorphism of Proterozoic iron-formation, Labrador Trough, Canada. *American Mineralogy*. Vol. 63, 898-912.

16. Miyashiro, A., 1973. *Metamorphism and Metamorphic Belts*. George, Allen, and Undwin.

17. Morelli. RM, Bell, CC, Creaser, RA, Simonetti, A. Constraints on the genesis of gold mineralization at the Homestake Gold Deposit, Black Hills, South Dakota from rhenium-osmium sulfide geochronology (2010) *Miner Deposita.* Vol. 45, 461-480.

18. Nabelel, PI, Labotka, TC, Helms, T, and Wilke, M (2006). Fluid-mediated polymetamorphism related to Proterozoic collision of Archean Wyoming-Superior provinces in the Black Hills, South Dakota. *American Mineralogist.* Vol. 91, 1473-2187.

19. Noble, J.A., Harder, J.O., Slaughter, A.L., 1949. Structure of a part of the northern black hills and the Homestake Mine, Lead, South Dakota. *Geological Society of America Bulletin*. Vol. 60, 321-362.

20. Noble, J.A., 1950. Ore mineralization in the Homestake gold mine, Lead, South Dakota. *Geological Society of America Bulletin*. Vol. 61, 221-252.

21. Noble, J.A., and Harder, J.O., 1948. Stratigraphy and metamorphism in a part of the northern Black Hills and the Homestake Mine, Lead, South Dakota. *Geological Society of America Bulletin*. Vol. 59, 941-975.

22. Phyllips, G.N., Groves, D.I., and Martyn, J.E. 1984. An epigenetic origin for Archean banded iron-formation-hosted gold deposits. Scientific Communications. *Economic Geology*. Vol. 79, 162-171.

23. Powell, R., and Holland, T., 1990. Calculated mineral equilibria in the pelite system, KFMASH K2O-FeO-MgO-Al2O3-SiO2-H2O. *American Mineralogy*. Vol. 75, 367-380.

24. Powell, R., Holland, T., Worley, B., 1998. Calculating phase diagrams involving solid solutions via non-linear equations, with examples using Thermocalc. *Journal of Metamorphic Geology*. Vol. 16, 577-588.

25. Redden, J.A. and DeWitt, E. (2008). Maps showing geology, structure, and geophysics of the Central Black Hills, South Dakota. South Dakota School of Mines and Technology Foundation. Scientific Investigations Map 2777. Sheet 1 of 2.

26. Redden, JA, Peterman, ZE, Zartman, RE, DeWitt, E (1990). U-Th-Pb zircon and monazite ages and preliminary interpretation of the tectonic development of Precambrian rocks in the Black Hills. In: Lewry, JF, Stauffer, MR (eds) The early proterozoic Trans-Hudson Orogen of North America. Geological Association of Canada Special Paper 37, pp 229-251.

27. Rye, DM, Doe, BR, Delevaux, MH (1974). Homestake gold mine, South Dakota II. Lead isotopes, mineralization ages, and source of lead in ores of the northern Black Hills. *Economic Geology*. Vol. 69, 814-822.

28. Spear, F.S., and Peacock, S.M., (1989). Metamorphic Pressure-Temperature-Time Paths. American Geophysical Union. Short Course in Geology: Vol. 7.

Appendix A: Supplementary Maps of the Rochford District and Surrounding Areas

(Fig. 2) with Sample Locations and Structural Data
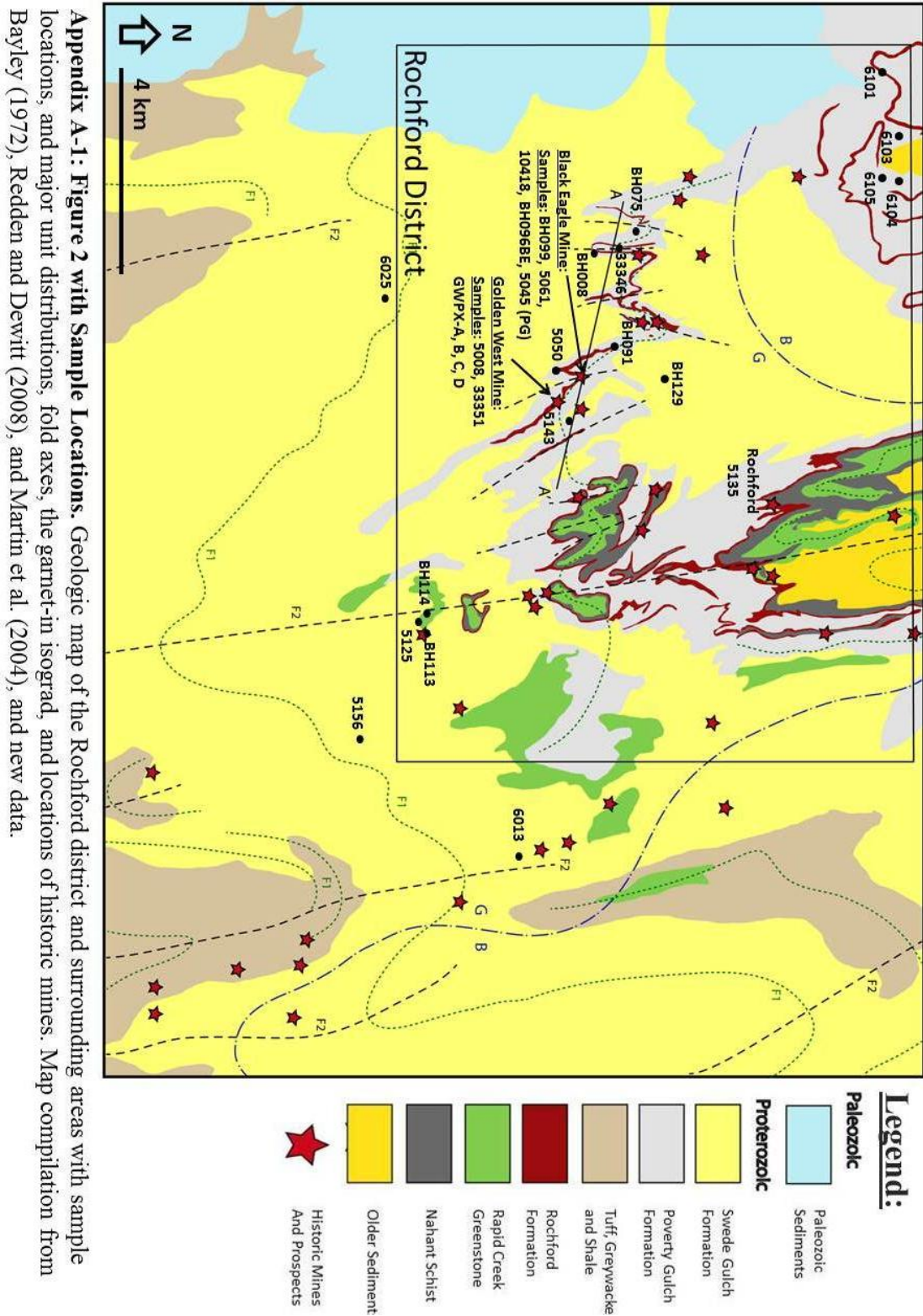
Appendix A-1: Figure 2 with Sample Locations. Geologic map of the Rochford district and surrounding areas with sample locations, and major unit distributions, fold axes, the garnet-in isograd, and locations of historic mines. Map compilation from Bayley (1972), Redden and Dewitt (2008), and Martin et al. (2004), and new data.
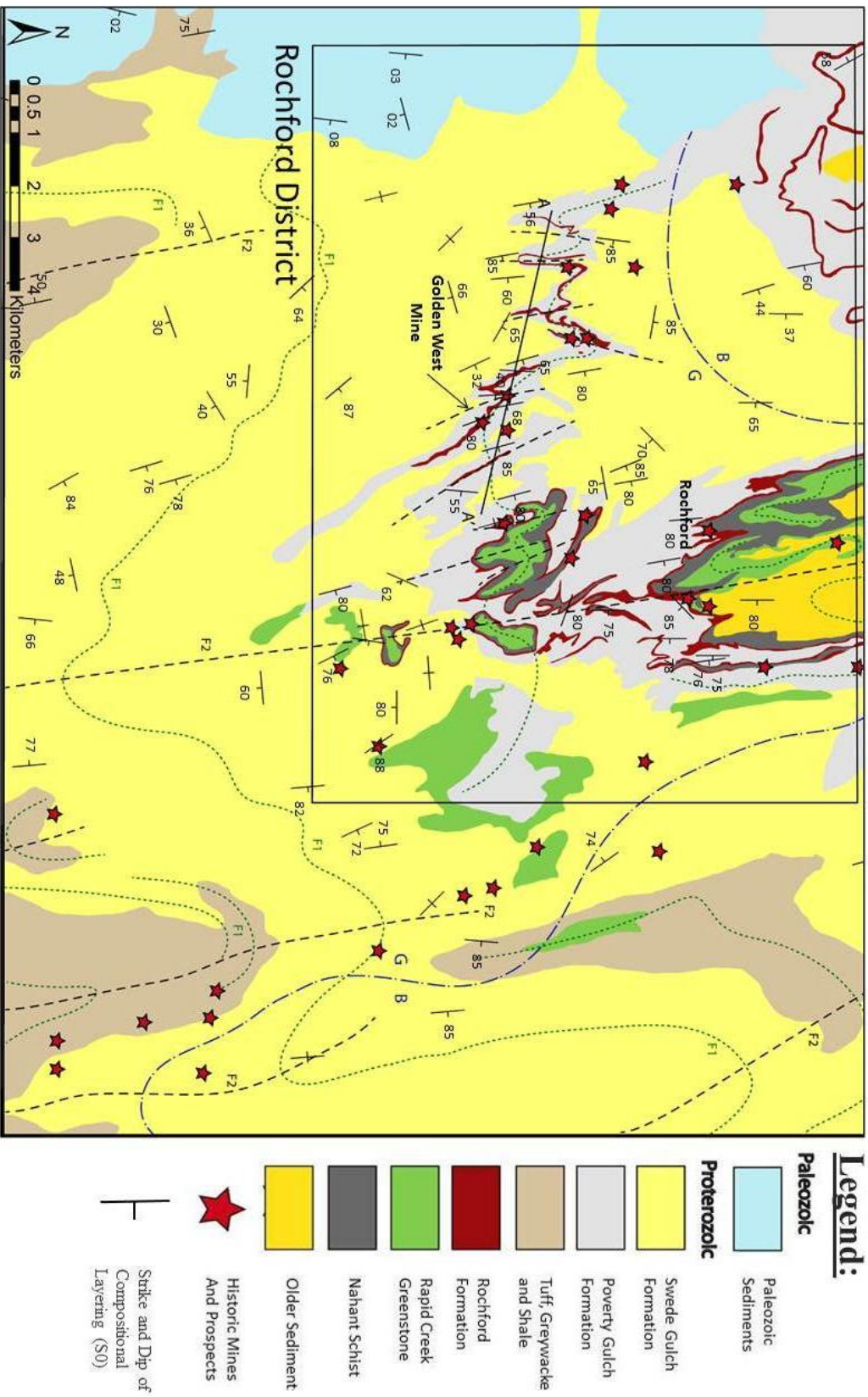
Appendix A-2: Figure 2 with measurements for compositional layering (S0). Geologic map of the Rochford district and surrounding areas with major unit distributions, fold axes, the garnet-in isograd, and locations of historic mines. Map compilation from Bayley (1972), Redden and Dewitt (2008), and Martin et al. (2004), and new data.
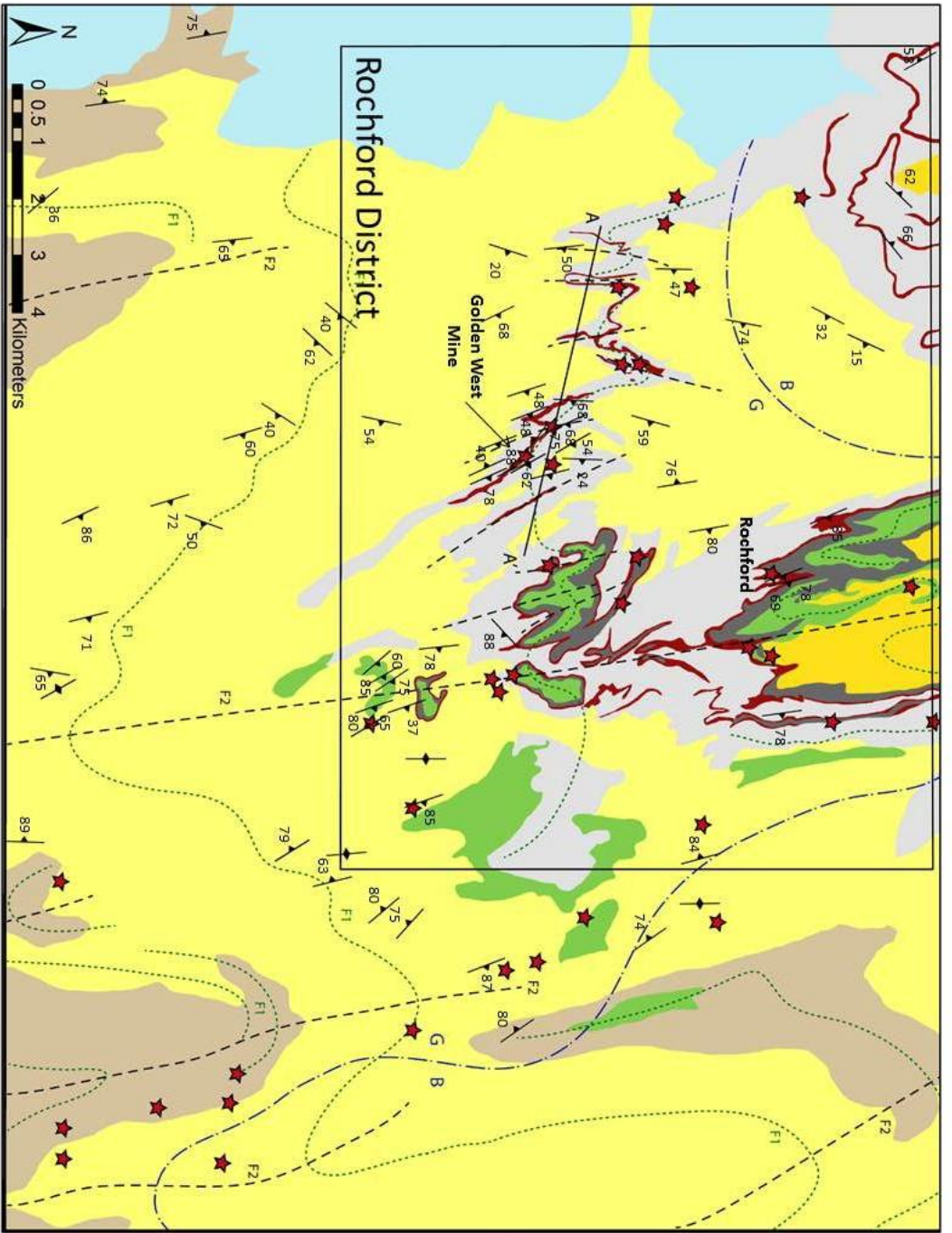
Appendix A-3: Figure 2 with measurements for the S2 fabric. Geologic map of the Rochford district and surrounding areas with major unit distributions, fold axes, the garnet-in isograd, and locations of historic mines. Map compilation from Bayley (1972), Redden and Dewitt (2008), and Martin et al. (2004), and new data.

58
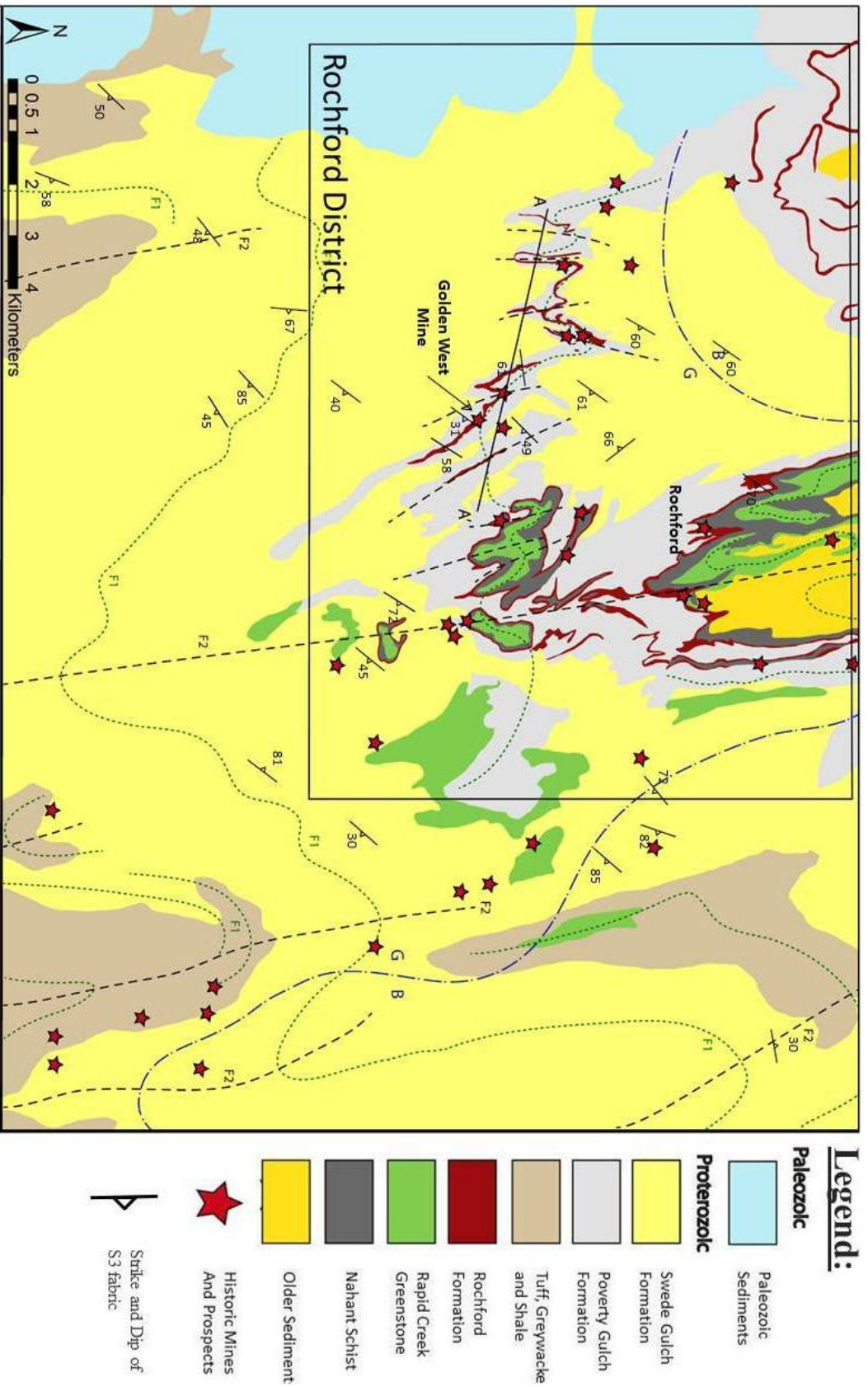
Appendix A-4: Figure 2 with measurements for the S3 fabric. Geologic map of the Rochford district and surrounding areas with major unit distributions, fold axes, the garnet-in isograd, and locations of historic mines. Map compilation from Bayley (1972), Redden and Dewitt (2008), and Martin et al. (2004), and new data.

Appendix B: Garnet and Biotite Compositons (see Appendix A-1 for sample locations)

Composition data collected via electron microprobe (EPMA) at UCSB.

Table 1: Compositions of Garnet from pelites											
Sample	Garnet	SiO_2	TiO_2	Al_2O_3	Cr_2O_3	FeO	MnO	MgO	CaO	Na_2O	K_2O	Sum
5045	1	55.766	0.663	19.099	0.004	11.171	0.214	1.542	0.013	0.076	7.171	95.718
5045	1	99.282	0.017	0.113	-0.015	0.488	0.116	-0.002	-0.006	-0.005	0.019	100.005
5045	1	36.402	0.162	20.114	0.037	25.614	15.046	0.345	1.739	0.016	0.002	99.478
5045	1	36.432	0.117	20.278	0.039	24.646	15.862	0.388	1.909	-0.001	-0.006	99.665
5045	1	99.555	-0.019	0.019	-0.003	0.393	0.193	-0.005	0.011	-0.004	-0.006	100.133
5045	1	92.449	0.008	2.479	-0.006	2.409	1.851	0.015	0.198	-0.006	0.003	99.400
5045	1	36.149	0.123	20.356	0.029	22.890	18.055	0.386	1.742	0.011	0.003	99.744
5045	1	36.223	0.144	20.327	0.026	22.387	18.249	0.374	1.937	0.000	0.007	99.675
5045	1	36.117	0.143	20.280	0.024	22.338	18.493	0.377	1.871	0.001	0.001	99.645
5045	1	99.464	0.004	0.110	-0.002	0.616	0.439	-0.012	0.010	-0.011	0.003	100.621
5045	1	59.304	0.046	11.504	0.007	14.369	11.677	0.141	1.334	0.006	-0.004	98.383
5045	1	36.076	0.089	20.203	0.015	22.244	18.215	0.390	1.699	0.024	-0.003	98.952
5045	1	99.707	0.006	0.019	0.007	0.432	0.271	-0.004	-0.004	-0.005	0.003	100.431
5045	1	36.078	0.095	20.190	0.025	22.943	18.089	0.386	1.486	0.003	-0.006	99.288
5045	1	36.007	0.095	20.210	0.028	23.388	17.663	0.383	1.556	0.005	-0.002	99.331
5045	1	78.498	0.015	3.180	-0.004	5.761	2.951	0.035	0.254	0.005	0.012	90.706
5045	1	44.020	0.056	16.528	0.015	21.889	13.767	0.298	1.374	0.014	0.003	97.962
5045	2	36.158	0.046	20.168	0.029	24.826	16.063	0.419	1.754	0.003	-0.005	99.460
5045	2	36.307	0.050	20.382	0.024	24.718	16.140	0.396	1.818	-0.001	0.001	99.835
5045	2	33.868	0.809	18.000	0.022	27.212	4.419	3.072	0.473	0.030	7.340	95.244
5045	2	91.878	0.001	3.384	0.003	3.534	2.919	0.056	0.308	-0.011	-0.001	102.071
5045	2	36.138	0.046	20.132	0.033	23.977	17.061	0.393	1.697	-0.003	-0.001	99.473
5045	2	36.195	0.064	20.418	0.016	23.740	17.266	0.395	1.712	0.005	0.001	99.812
5045	2	100.020	-0.010	0.060	-0.007	0.657	0.407	-0.003	0.005	-0.005	-0.006	101.118
5045	2	36.148	0.089	20.384	0.027	23.613	17.229	0.394	1.748	0.003	0.002	99.637
5045	2	36.235	0.078	20.365	0.031	23.359	17.366	0.408	1.720	0.002	-0.002	99.562
5045	2	35.916	0.068	20.356	0.021	23.507	17.674	0.382	1.522	0.006	0.002	99.455
5045	2	36.213	0.077	20.353	0.033	23.259	17.665	0.370	1.670	-0.002	0.002	99.640
5045	2	29.780	0.104	14.712	0.009	18.356	13.954	0.256	1.914	0.051	0.039	79.174
5045	2	36.458	0.084	20.631	0.043	23.661	17.803	0.368	1.406	-0.002	0.004	100.456
5045	2	86.946	0.006	2.366	0.000	3.038	2.466	0.036	0.242	-0.004	0.008	95.105
5045	2	35.011	0.112	19.592	0.032	23.757	16.912	0.377	1.605	0.009	0.014	97.422
5045	2	26.696	0.083	14.572	0.015	20.488	15.799	0.508	1.441	0.093	0.014	79.708
5045	2	34.743	0.131	19.458	0.033	22.894	17.630	0.415	1.601	0.017	0.000	96.922
5045	2	28.693	0.061	12.538	0.004	14.929	11.681	0.193	1.113	-0.025	0.019	69.207
5045	2	35.916	0.089	19.844	0.034	23.127	17.715	0.380	1.563	-0.002	0.000	98.666
5045	2	36.091	0.106	20.057	0.032	23.616	17.759	0.406	1.592	0.001	-0.001	99.660
5045	2	36.125	0.123	20.189	0.032	23.384	17.521	0.399	1.589	0.002	0.004	99.367
5045	2	36.112	0.170	20.207	0.017	23.755	17.084	0.379	1.725	0.010	-0.001	99.458
5045	2	36.084	0.150	20.145	0.009	24.309	16.830	0.433	1.694	0.009	0.001	99.663
5045	2	36.182	0.170	20.220	0.024	24.647	16.277	0.397	1.769	-0.001	0.003	99.687

Table 1: Compositions of Garnet from pelites											
Sample	Garnet	SiO_2	TiO_2	Al_2O_3	Cr_2O_3	FeO	MnO	MgO	CaO	Na_2O	K_2O	Sum
5045	2	92.242	0.001	1.724	-0.009	3.628	0.424	0.509	0.021	-0.005	0.347	98.882
5045	2	36.359	0.082	20.420	0.008	25.531	15.100	0.385	1.801	0.000	0.002	99.689
5045	2	36.304	0.127	20.324	0.011	25.655	14.517	0.405	2.328	0.006	0.003	99.679
5045	2	19.866	0.021	7.781	-0.034	6.889	2.508	-0.097	0.729	-0.090	1.364	38.937
5045	2	41.094	-0.005	1.065	-0.024	3.760	1.407	0.140	0.303	0.094	0.124	47.957
6025	1	35.976	0.048	20.230	0.026	25.545	13.344	0.964	2.434	0.027	0.011	98.605
6025	1	36.250	0.091	20.299	0.017	25.498	12.659	1.043	2.560	0.040	0.005	98.463
6025	1	40.352	0.084	19.805	0.044	25.345	12.473	0.878	2.540	0.019	0.005	101.54
6025	1	37.166	0.086	20.182	0.034	26.126	12.822	1.052	2.121	0.010	0.004	99.603
6025	1	36.279	0.239	20.366	0.019	25.759	12.717	1.074	2.602	0.037	0.000	99.091
6025	1	36.832	0.167	20.510	0.008	25.823	12.697	1.041	2.747	0.030	-0.003	99.851
6025	1	100.123	0.007	0.282	-0.007	0.635	0.270	0.004	0.025	-0.008	0.003	101.33
6025	1	98.718	0.002	0.428	0.004	0.743	0.347	-0.002	0.050	-0.009	-0.003	100.28
6025	1	63.271	0.048	10.821	-0.003	16.028	7.188	0.522	1.519	0.019	0.000	99.414
6025	1	66.588	-0.004	8.292	-0.002	12.577	5.736	0.341	1.234	0.005	-0.001	94.765
6025	1	97.994	-0.008	0.262	0.001	0.710	0.290	0.002	0.029	-0.010	0.004	99.273
6025	1	38.944	0.062	19.945	0.013	25.504	12.638	1.010	2.254	0.058	0.006	100.43
6025	1	36.384	0.084	20.528	0.025	26.151	12.615	1.072	2.454	0.025	0.002	99.339
6025	1	36.226	0.078	20.573	0.022	25.828	12.831	1.087	2.118	0.077	0.002	98.842
6025	1	36.534	0.063	20.546	0.003	26.134	12.914	1.058	2.050	0.039	-0.003	99.337
6025	1	50.510	0.034	15.920	-0.014	20.825	9.822	0.703	1.822	-0.003	0.008	99.628
6025	1	36.327	0.118	20.516	0.016	25.673	13.187	1.001	2.187	0.042	-0.002	99.064
6025	1	36.534	0.083	20.519	0.010	25.684	12.976	0.985	2.319	0.050	0.000	99.161
6025	1	100.807	-0.002	0.048	-0.013	0.494	0.187	-0.008	0.002	-0.015	0.003	101.5
6025	1	100.723	-0.009	0.013	-0.011	0.345	0.120	-0.008	0.004	-0.012	0.009	101.17
6025	2	36.709	0.103	20.672	0.002	25.804	12.920	1.002	2.585	0.010	-0.001	99.806
6025	2	36.485	0.148	20.698	0.000	25.576	12.710	1.096	2.596	0.042	0.004	99.354
6025	2	93.484	0.011	2.432	0.001	2.378	1.148	0.057	0.264	-0.005	0.005	99.774
6025	2	37.546	0.330	20.329	0.000	25.721	12.664	1.069	2.241	0.035	0.002	99.936
6025	2	36.505	0.169	20.670	0.007	25.771	12.942	1.130	2.474	0.042	0.005	99.716
6025	2	36.400	0.166	20.624	0.013	25.782	12.861	1.105	2.536	0.039	-0.003	99.523
6025	2	58.473	0.071	12.413	0.014	17.832	8.174	0.632	1.645	0.023	0.001	99.277
6025	2	37.263	0.052	20.557	0.019	25.803	12.909	1.112	2.171	0.046	-0.004	99.928
6025	2	96.976	0.000	0.882	-0.004	1.249	0.535	0.038	0.113	-0.007	0.007	99.79
6025	2	99.817	-0.021	0.032	0.001	0.568	0.212	-0.010	-0.001	-0.012	0.001	100.59
6025	2	36.467	0.094	20.578	0.025	26.039	12.724	1.126	2.420	0.050	0.001	99.524
6025	2	72.963	0.014	7.243	0.008	9.820	4.766	0.389	0.914	0.001	-0.003	96.115
6025	2	36.402	0.073	20.696	0.018	25.802	12.785	1.068	2.470	0.063	0.002	99.378
6025	2	36.223	0.063	20.348	0.023	25.445	12.957	1.032	2.478	0.039	0.002	98.61
6025	2	37.649	0.026	19.904	0.004	24.452	14.310	0.771	2.150	0.022	0.026	99.315
6025	3	35.330	1.043	22.513	0.026	16.145	0.242	6.524	0.156	0.138	7.479	89.595
6025	3	3.782	0.006	2.126	-0.019	2.155	1.432	0.036	46.403	0.019	0.053	55.993
6025	3	27.087	12.598	15.172	-0.003	29.892	10.786	0.795	1.774	0.027	0.012	98.14

Table 1: Compositions of Garnet from pelites												
Sample	Garnet	SiO$_2$	TiO$_2$	Al$_2$O$_3$	Cr$_2$O$_3$	FeO	MnO	MgO	CaO	Na$_2$O	K$_2$O	Sum
6025	3	36.386	0.070	20.380	0.023	25.438	12.934	0.973	2.519	0.046	0.000	98.768
6025	3	69.812	0.014	8.154	0.012	13.564	5.512	0.392	1.178	0.013	0.002	98.653
6025	3	36.480	0.128	20.590	0.000	25.754	12.609	1.042	2.494	0.024	0.001	99.122
6025	3	52.771	0.035	16.928	0.006	21.013	10.473	0.748	2.124	0.007	-0.001	104.11
6025	3	47.529	0.049	18.259	0.015	23.152	11.165	0.849	2.103	0.019	0.004	103.14
6025	3	37.345	0.092	20.614	0.013	26.047	12.627	1.063	2.458	0.011	-0.005	100.27
6025	3	37.205	0.095	20.358	0.029	25.776	12.687	1.046	2.416	0.031	0.003	99.646
6025	3	36.403	0.100	20.525	0.010	25.942	12.606	1.087	2.142	0.049	0.002	98.865
6025	3	36.442	0.190	20.324	0.025	25.960	12.725	1.066	2.442	0.015	-0.005	99.183
6025	3	88.529	0.005	2.759	0.013	3.966	1.557	0.122	0.366	0.009	0.005	97.332
6025	3	36.380	0.120	20.504	0.022	25.576	12.870	1.044	2.465	0.070	0.008	99.059
6025	3	36.483	0.040	20.515	0.010	25.663	13.564	0.908	2.145	0.006	0.004	99.335
6025	3	36.422	0.053	20.404	0.009	25.251	13.272	0.935	2.274	0.044	0.009	98.673
BH075	1	36.305	0.02268	20.4063	0.00598	30.873	9.9307	0.4573	1.7532	0.00925	0.009	99.773
BH075	1	36.174	0.05467	20.4462	0.00796	29.626	11.567	0.4432	1.403	-0.0054	7E-05	99.716
BH075	1	36.29	0.04592	20.3758	-0.0012	28.674	12.48	0.4445	1.5107	0.00738	0.002	99.83
BH075	1	36.244	0.06294	20.4501	0.01287	27.905	13.339	0.4103	1.4619	-0.0072	-0.004	99.875
BH075	1	36.272	0.06576	20.495	0.00961	27.152	13.967	0.4124	1.5989	0.01	-0.003	99.98
BH075	1	36.261	0.05351	20.5302	0.00415	26.5	14.556	0.4098	1.6156	0.00266	0.004	99.937
BH075	1	36.236	0.09377	20.4999	0.00323	26.335	14.792	0.402	1.5889	-0.0005	-0.005	99.944
BH075	1	36.219	0.05746	20.4902	0.00058	25.948	15.378	0.3822	1.472	-0.0096	-9E-04	99.937
BH075	1	36.143	0.08208	20.3797	0.02293	25.855	15.411	0.368	1.5387	4.2E-05	0.003	99.804
BH075	1	36.265	0.06483	20.4727	0.02234	25.705	15.88	0.3874	1.4678	0.0013	-0.005	100.26
BH075	1	84.034	-0.0127	3.46646	-0.0181	2.5414	3.0956	0.0425	0.2769	-0.0155	-0.003	93.407
BH075	1	36.229	0.06639	20.581	0.01144	25.311	16.068	0.3972	1.5178	0.00163	-0.003	100.18
BH075	1	36.216	0.05275	20.518	0.00889	25.161	16.033	0.4002	1.5876	-0.0011	0.009	99.984
BH075	1	36.173	0.06101	20.4834	0.01285	24.907	16.138	0.3969	1.6748	0.00105	0.002	99.849
BH075	1	39.908	0.05368	19.1119	0.01572	23.773	15.427	0.3625	1.5995	-0.0034	-0.003	100.25
BH075	1	36.128	0.06939	20.5276	0.01564	24.799	15.981	0.3821	1.8325	0.00401	4E-05	99.739
BH075	1	85.28	0.01116	3.43064	-0.0103	4.0262	2.3042	0.0497	0.327	-0.0048	0.011	95.426
BH075	1	35.974	0.05394	20.5164	0.01604	24.331	15.825	0.4162	2.074	0.00888	-3E-04	99.215
BH075	1	36.08	0.03202	20.4012	0.01819	24.211	15.974	0.4084	2.0588	0.0275	0.002	99.213
BH075	1	36.515	0.06855	20.5879	0.01117	24.206	16.001	0.4009	2.0759	0.01448	-0.003	99.877
BH075	1	36.06	0.06081	20.3887	0.00913	24.27	15.857	0.4094	2.0838	0.02059	-0.005	99.153
BH075	1	36.073	0.07193	20.4392	0.00417	23.954	15.919	0.4307	2.1613	0.02002	-0.002	99.071
BH075	1	36.066	0.08507	20.483	0.0195	23.878	15.747	0.4223	2.1641	0.02279	-0.002	98.886
BH075	1	36.116	0.06501	20.3845	0.01097	24.205	15.846	0.4251	2.1382	0.01004	-0.001	99.199
BH075	1	36.053	0.07794	20.508	0.02085	24.276	15.869	0.4164	2.065	0.00526	-0.007	99.285
BH075	1	35.989	0.04882	20.3749	0.01305	24.323	16.041	0.4098	1.8939	0.01109	-0.004	99.1
BH075	1	36.039	0.08376	20.4035	0.01435	24.675	16.043	0.3862	1.8363	-0.0013	-0.003	99.477
BH075	1	36.43	0.08655	20.1167	0.0313	24.757	15.783	0.3828	1.6665	0.00192	0.001	99.257
BH075	1	36.105	0.07474	20.3483	0.02243	24.869	15.978	0.3905	1.6081	0.01269	-0.001	99.408
BH075	1	55.871	0.01504	12.0953	0.01285	17.01	10.497	0.1813	0.9828	0.01421	0.004	96.683

Table 1: Compositions of Garnet from pelites											
Sample	Garnet	SiO$_2$	TiO$_2$	Al$_2$O$_3$	Cr$_2$O$_3$	FeO	MnO	MgO	CaO	Na$_2$O	K$_2$O	Sum
BH075	1	45.121	0.03503	16.7954	0.02041	22.357	14.136	0.2685	1.2124	0.02356	-0.003	99.966
BH075	1	36.641	0.0809	21.8484	0.01288	24.597	14.945	0.6238	1.3047	0.26146	-6E-04	100.32
BH075	1	36.33	0.05348	20.369	0.01063	25.698	15.508	0.3956	1.4656	0.01016	-0.004	99.836
BH075	1	36.508	0.08076	20.1293	0.0389	26.07	15.136	0.4171	1.4424	0.00637	-7E-04	99.828
BH075	1	36.005	0.0669	20.3028	0.01583	26.349	14.867	0.4198	1.5068	-0.0026	-0.004	99.526
BH075	1	35.952	0.06964	20.2377	0.02263	26.845	14.292	0.4302	1.4898	-0.0023	-0.002	99.335
BH075	1	36.017	0.07312	20.3413	0.01237	27.373	13.845	0.4383	1.4959	-5E-05	-0.003	99.593
BH075	1	35.942	0.0772	20.3774	0.01182	28.106	13.144	0.4525	1.5296	-0.0037	0.001	99.638
BH075	1	35.932	0.04915	20.1828	0.01129	28.784	12.445	0.4534	1.5155	-0.0038	-0.006	99.363
BH075	1	36.185	0.05461	20.1601	0.00109	29.176	11.962	0.3975	1.3826	0.00858	0.002	99.33
BH075	1	36.106	0.04233	20.1295	0.01207	30.389	10.653	0.462	1.5177	0.00382	1E-04	99.316
BH075	1	36.135	0.02191	20.2299	0.00963	31.298	9.7488	0.4406	1.4767	0.00501	7E-04	99.365
BH075	2	36.527	0.04926	20.4679	0.01061	30.072	11.087	0.4426	1.3919	0.00057	0.006	100.05
BH075	2	36.465	0.03836	20.2217	0.00517	28.633	12.588	0.4324	1.4223	-0.0046	0.004	99.805
BH075	2	36.287	0.06707	20.3074	0.01161	27.774	13.419	0.4195	1.4803	0.00731	4E-04	99.774
BH075	2	36.239	0.06299	20.3131	0.01602	26.901	14.228	0.4103	1.4533	0.00642	0.004	99.634
BH075	2	36.267	0.04449	20.4108	0.03659	26.694	14.58	0.4111	1.4091	0.00142	-1E-03	99.854
BH075	2	36.301	0.06917	20.3323	0.01486	26.388	14.655	0.4155	1.3922	0.00173	-0.007	99.562
BH075	2	36.37	0.06365	20.3274	0.02168	26.184	15.012	0.4149	1.4133	-0.0005	-0.001	99.804
BH075	2	36.21	0.07857	20.2062	0.0215	26.334	14.875	0.4322	1.4136	0.00503	-0.001	99.574
BH075	2	36.077	0.07109	20.3516	0.02673	26.156	14.973	0.4318	1.4353	0.00185	-0.002	99.522
BH075	2	36.072	0.05258	20.2757	0.01332	26.073	15.205	0.4164	1.3701	-0.0013	0.003	99.479
BH075	2	36.099	0.05874	20.2487	0.00948	26.111	15.144	0.423	1.3371	0.00239	0.004	99.437
BH075	2	36.099	0.0498	20.3892	0.01238	26.2	15.271	0.4094	1.4237	-0.0071	-0.003	99.844
BH075	2	36.13	0.09096	20.3791	0.02256	25.87	15.228	0.423	1.4144	0.01212	-0.001	99.569
BH075	2	37.292	0.06269	20.2329	0.01243	25.851	15.115	0.4136	1.3708	0.00551	-8E-04	100.36
BH075	2	35.885	0.08596	20.3051	0.01623	26.02	15.296	0.4183	1.3851	-0.0035	0.002	99.411
BH075	2	35.987	0.07498	20.2429	0.00713	26.153	15.266	0.3768	1.351	0.0072	3E-05	99.466
BH075	2	36.008	0.04838	20.2918	0.02262	26.173	15.204	0.4136	1.3319	0.0017	0.004	99.499
BH075	2	35.351	0.08585	20.0637	0.01043	26.227	14.851	0.5104	1.4297	0.00421	-0.002	98.531
BH075	2	35.882	0.03813	20.186	0.01352	26.513	14.838	0.4157	1.4339	0.00291	-0.005	99.318
BH075	2	75.028	-0.0041	4.01571	-0.0075	5.4648	2.8908	0.0769	0.3057	-0.0075	8E-04	87.764
BH075	2	35.891	0.07526	20.2542	0.01168	26.703	14.209	0.4298	1.4728	-0.0044	2E-04	99.042
BH075	2	36.002	0.04028	20.3326	0.02177	27.06	14.16	0.3629	1.491	0.01405	0.02	99.506
BH075	2	35.888	0.05177	20.319	0.00822	28.185	13.243	0.4509	1.4701	0.00449	0.002	99.622
BH075	2	35.951	0.05855	20.1533	0.01236	28.819	12.653	0.4612	1.4215	0.0019	0.002	99.533
BH075	2	35.796	0.05589	20.1257	0.01493	29.667	11.398	0.4604	1.4561	0.01261	0.001	98.988
BH075	3	36.154	0.00868	20.4988	-0.0021	30.734	10.718	0.41	1.1562	0.00904	0.009	99.695
BH075	3	36.259	0.05394	20.6146	0.00915	29.878	11.681	0.4722	1.4644	0.01541	-0.001	100.45
BH075	3	36.159	0.06004	20.5636	0.0202	29.151	12.42	0.4546	1.477	-0.0033	0.005	100.31
BH075	3	36.088	0.07324	20.5709	0.01334	28.193	12.935	0.4622	1.4343	-0.0025	-0.003	99.765
BH075	3	36.115	0.0601	20.472	0.00723	27.8	13.418	0.4512	1.3373	0.00111	-0.007	99.655
BH075	3	36.232	0.0768	20.6734	0.01833	27.445	13.536	0.4581	1.4565	0.00507	-3E-04	99.902

Table 1: Compositions of Garnet from pelites											
Sample	Garnet	SiO$_2$	TiO$_2$	Al$_2$O$_3$	Cr$_2$O$_3$	FeO	MnO	MgO	CaO	Na$_2$O	K$_2$O	Sum
BH075	3	50.028	0.04798	15.8341	-0.0057	21.998	10.875	0.3313	1.0881	-0.0056	0.003	100.19
BH075	3	36.091	0.06306	20.5651	0.01655	27.065	13.881	0.4454	1.4776	0.00736	0.003	99.615
BH075	3	36.044	0.07331	20.6498	0.01656	27.031	13.872	0.4427	1.4759	0.00468	-0.001	99.608
BH075	3	36.087	0.09445	20.5528	0.01523	26.899	14.001	0.4734	1.5329	0.00396	0.001	99.661
BH075	3	35.985	0.08483	20.5916	0.02281	27.172	13.997	0.4698	1.5233	0.01235	3E-04	99.859
BH075	3	36.084	0.05411	20.5055	0.02757	27.153	13.923	0.4239	1.5199	0.00059	0.004	99.695
BH075	3	35.924	0.06492	20.4973	0.00129	27.234	13.951	0.4634	1.4613	0.00473	-0.004	99.598
BH075	3	36.074	0.06431	20.5588	0.0138	27.444	13.754	0.4665	1.3951	0.01091	-5E-04	99.78
BH075	3	36.013	0.05967	20.5843	0.01523	27.64	13.43	0.4568	1.3684	0.00337	0.002	99.572
BH075	3	36.072	0.08262	20.3607	0.00801	27.829	13.293	0.4628	1.5158	0.00387	6E-04	99.628
BH075	3	35.98	0.09759	20.3286	0.02236	28.464	12.86	0.4633	1.4506	-0.0008	-0.003	99.663
BH075	3	35.877	0.05545	20.2798	0.01622	28.794	12.065	0.4813	1.4249	0.00857	0.005	99.008
BH075	3	36.034	0.04921	20.241	0.0101	29.379	11.615	0.4772	1.3959	0.01391	-0.006	99.208
BH075	3	35.621	0.04074	20.0376	0.02226	27.076	14.02	0.2628	1.375	0.0201	0.018	98.494
BH075	3	35.91	0.04575	20.2573	0.00653	30.605	10.327	0.4086	1.4297	0.01769	0.021	99.03
6013	1	36.649	0.08124	20.7075	0.00422	17.301	20.312	0.7788	3.1055	0.05202	0.029	99.02
6013	1	36.428	0.08767	20.5867	0.01787	15.934	21.154	0.7897	3.441	0.07679	0.005	98.52
6013	1	36.524	0.08188	20.5931	0.02605	15.42	22.313	0.7516	3.3046	0.05893	0.004	99.077
6013	1	36.348	0.08641	20.6245	0.02853	15.035	22.9	0.7414	2.9439	0.06863	0.004	98.781
6013	1	36.137	0.08014	20.6139	0.02173	14.777	23.226	0.7157	2.9853	0.05528	-0.007	98.607
6013	1	36.338	0.08854	20.6705	0.01441	14.581	23.305	0.7085	2.9626	0.05038	-0.005	98.714
6013	1	36.144	0.1105	20.5615	0.00906	14.471	23.162	0.715	2.9741	0.08169	-0.003	98.225
6013	1	36.088	0.092	20.7318	0.01351	14.362	23.404	0.6963	3.1586	0.06382	3E-04	98.61
6013	1	36.08	0.10976	20.644	0.01477	14.503	23.281	0.7069	3.0129	0.07997	-1E-03	98.432
6013	1	36.068	0.0919	20.7945	0.00361	14.614	23.315	0.7107	2.9774	0.08227	-0.005	98.652
6013	1	36.135	0.07836	20.5784	0.0123	14.332	23.205	0.707	3.117	0.0778	0.001	98.244
6013	1	36.219	0.07124	20.6397	0.01384	14.454	23.502	0.7109	2.8402	0.08581	-0.002	98.535
6013	1	36.049	0.08352	20.5097	0.01059	14.537	23.392	0.7131	2.8367	0.05512	0.002	98.189
6013	1	36.169	0.08621	20.7335	0.00112	14.834	23.461	0.7136	2.9024	0.055	2E-04	98.956
6013	1	36.318	0.08859	20.6733	0.01309	14.807	23.019	0.7259	2.9776	0.05717	0.003	98.683
6013	1	36.24	0.08174	20.5484	0.00458	15.104	22.651	0.7608	3.0528	0.05545	0.001	98.5
6013	1	36.239	0.08197	20.6436	0.01458	15.439	21.999	0.7795	3.3259	0.06452	0.004	98.591
6013	1	36.28	0.07288	20.3861	0.01251	16.398	21.117	0.8006	3.2057	0.05877	0.01	98.342
6013	3	36.151	0.09423	20.3269	0.00503	16.273	21.105	0.8126	3.1317	0.08764	0.01	97.997
6013	3	36.404	0.0881	20.5224	0.00608	15.465	22.05	0.7646	3.1724	0.0533	-1E-03	98.525
6013	3	36.23	0.07847	20.632	0.0101	15.044	22.444	0.7547	3.2914	0.05032	-0.001	98.534
6013	3	36.198	0.08793	20.685	0.03044	14.984	22.767	0.7374	3.1212	0.06376	-3E-05	98.675
6013	3	36.292	0.0977	20.6166	0.011	14.724	23.056	0.7343	3.0758	0.05308	4E-04	98.661
6013	3	36.156	0.09023	20.5431	0.00104	14.76	23.394	0.727	2.8955	0.05604	0.003	98.625
6013	3	36.157	0.11943	20.5793	0.00636	14.603	23.225	0.7377	2.8842	0.06931	0.003	98.383
6013	3	36.158	0.10298	20.4528	0.00462	14.495	23.12	0.6991	2.9262	0.07906	-0.002	98.035
6013	3	36.165	0.09114	20.494	0.01912	14.699	23.146	0.7093	2.9356	0.07393	-0.002	98.331
6013	3	36.254	0.08985	20.6595	0.0108	14.69	23.187	0.7167	2.8204	0.07748	-4E-04	98.505
6013	3	36.268	0.0753	20.5503	0.02174	14.694	23.377	0.7126	2.7863	0.05403	0.001	98.54
6013	3	36.917	0.10797	20.4084	0.00394	14.65	23.131	0.7168	2.9399	0.05745	-0.001	98.931
6013	3	36.303	0.08397	20.6888	0.01102	14.829	22.777	0.7214	3.2403	0.04921	0.005	98.708
6013	3	36.311	0.13344	20.6842	0.0096	15.17	22.427	0.7581	3.2537	0.05225	0.002	98.801
6013	3	36.43	0.09724	20.5702	0.03067	15.92	21.474	0.7809	3.3695	0.07364	0.001	98.748
6013	3	36.621	0.06126	20.6716	0.01481	17.188	20.509	0.7548	3.1317	0.05611	0.013	99.021

Sample	Biotite	SiO$_2$	TiO$_2$	Al$_2$O$_3$	Cr$_2$O$_3$	FeO	MnO	MgO	CaO	Na$_2$O	K$_2$O	Sum	Location
												Table 2: Compositions of Biotite from pelites	
5045	1	31.096	1.187	17.449	0.019	26.325	0.312	4.259	0.166	0.079	7.011	87.904	adj. to G1
5045	1	31.337	1.218	16.047	0.022	27.088	0.354	4.199	0.110	0.084	7.007	87.466	adj. to G1
5045	2	98.945	0.021	0.769	-0.005	0.415	0.043	0.010	-0.006	-0.004	0.157	100.346	adj. to G1
5045	2	94.786	0.021	2.760	0.000	0.567	0.042	0.113	-0.007	0.005	0.804	99.090	adj. to G1
5045	2	45.224	0.189	32.804	0.039	3.588	0.056	0.773	0.013	0.163	10.715	93.564	adj. to G1
5045	3	31.043	1.243	17.641	0.017	28.123	0.399	3.653	0.189	0.068	6.731	89.109	adj. to G1
5045	3	47.298	0.195	33.994	0.048	3.225	0.039	0.813	0.011	0.142	10.380	96.145	adj. to G1
5045	3	97.948	-0.014	0.999	-0.015	0.401	0.020	0.040	-0.011	-0.002	0.258	99.624	adj. to G1
5045	4	32.253	1.638	16.753	0.036	26.788	0.491	3.697	0.041	0.050	9.579	91.325	adj. to G1
5045	4	35.562	1.681	17.045	0.033	27.039	0.504	4.018	0.021	0.038	9.647	95.588	adj. to G1
5045	4	39.451	0.515	17.759	-0.001	26.892	10.984	1.195	1.224	0.049	2.947	101.015	adj. to G1
5045	6	33.744	1.110	18.304	0.024	25.469	0.418	4.045	0.151	0.055	8.084	91.403	adj. to G2
5045	6	33.371	1.096	17.896	0.028	26.401	0.374	4.215	0.196	0.023	8.090	91.690	adj. to G2
5045	7	29.710	0.601	18.855	0.030	27.251	0.380	4.197	0.263	0.029	4.859	86.174	adj. to G2
5045	7	29.247	1.027	16.922	0.015	28.557	0.321	3.367	0.198	0.055	7.287	86.996	adj. to G2
5045	8	33.596	1.118	17.339	0.010	28.078	0.588	4.391	0.026	0.026	9.425	94.596	adj. to G2
5045	8	33.411	1.146	17.703	0.029	28.341	0.471	4.005	0.030	0.027	9.525	94.688	adj. to G2
5045	8	33.175	1.136	18.088	0.049	28.138	0.419	4.087	0.011	0.052	9.445	94.601	adj. to G2
5045	8	31.857	1.054	17.636	0.043	28.505	0.467	4.058	0.025	0.062	8.801	92.509	adj. to G2
5045	8	24.951	0.124	17.953	0.014	34.789	0.504	4.783	0.253	0.045	2.331	85.747	adj. to G2
6025	1	46.032	0.521	35.274	0.021	1.992	0.178	0.877	0.015	0.328	9.551	94.789	adj. to G1
6025	1	47.073	0.547	35.692	0.026	1.945	0.150	0.859	0.017	0.170	6.906	93.385	adj. to G1
6025	1	47.672	0.402	34.091	0.021	1.995	0.089	1.268	0.019	0.213	9.671	95.439	adj. to G1
6025	1	47.715	0.295	33.105	0.018	2.105	0.062	1.644	0.006	0.213	9.707	94.871	adj. to G1
6025	2	92.647	-0.009	2.461	-0.018	2.562	1.536	0.094	0.301	-0.008	0.003	99.570	adj. to G1
6025	2	35.933	0.060	20.397	0.025	25.512	13.281	0.995	2.289	0.035	0.009	98.536	adj. to G1
6025	2	39.840	0.018	20.191	-0.001	25.057	13.492	0.938	2.165	0.001	0.011	101.711	adj. to G1
6025	2	92.378	-0.006	0.059	-0.001	0.550	0.225	-0.005	0.003	-0.011	0.004	93.196	adj. to G1
6025	3	99.368	-0.008	0.025	0.004	0.188	0.018	-0.003	-0.009	-0.003	0.017	99.600	adj. to G1
6025	3	46.315	0.410	32.386	0.001	2.059	0.042	1.448	0.017	0.249	10.611	93.539	adj. to G1
6025	3	45.759	0.498	35.554	0.020	1.627	0.027	0.884	-0.002	0.352	10.466	95.186	adj. to G1
6025	3	98.806	0.002	0.134	-0.009	0.129	0.005	0.011	-0.004	0.002	0.035	99.112	adj. to G1
6025	4	46.984	0.391	32.794	0.025	1.694	0.024	0.877	0.067	1.324	8.670	92.849	adj. to G1
6025	4	42.489	0.918	29.039	0.021	9.216	0.139	3.684	0.032	0.178	9.899	95.615	adj. to G1
6025	5	46.626	0.492	36.075	0.016	1.744	0.101	0.843	0.017	0.375	9.936	96.224	adj. to G2
6025	5	46.659	0.469	35.978	0.011	1.657	0.088	0.837	0.025	0.402	9.877	96.003	adj. to G2
6025	5	79.134	0.153	14.219	0.008	0.777	0.009	0.383	0.006	0.135	4.130	98.952	adj. to G2
6025	5	90.127	0.018	0.771	-0.012	0.372	0.008	0.074	0.070	0.351	0.106	91.885	adj. to G2
6025	6	26.667	0.071	15.348	-0.019	17.891	11.819	0.748	1.671	0.041	0.848	75.086	adj. to G2
6025	6	44.714	0.346	36.315	0.030	1.673	0.060	0.552	0.023	0.437	9.448	93.597	adj. to G2
6025	6	44.447	0.331	33.454	0.018	2.095	0.042	0.822	0.045	0.279	8.428	89.960	adj. to G2
6025	7	36.974	1.670	20.203	0.015	20.281	0.401	7.245	0.044	0.076	9.390	96.298	adj. to G2
6025	7	7.118	0.086	3.466	-0.067	1.649	0.009	0.048	0.023	0.130	0.858	13.319	adj. to G2

Table 2: Compositions of Biotite from pelites													
Sample	Biotite	SiO$_2$	TiO$_2$	Al$_2$O$_3$	Cr$_2$O$_3$	FeO	MnO	MgO	CaO	Na$_2$O	K$_2$O	Sum	Location
6025	8	93.176	0.008	0.120	-0.010	0.224	0.034	0.002	2.078	-0.004	0.048	95.677	adj. to G2
6025	8	56.456	0.318	22.522	0.007	2.121	0.009	0.821	0.035	0.194	7.683	90.166	adj. to G2
6025	8	34.496	0.999	22.858	0.005	19.884	0.295	8.324	0.041	0.086	6.280	93.268	adj. to G2
6025	9	46.581	0.398	33.069	0.008	1.789	0.057	0.761	0.022	0.229	9.943	92.857	adj. to G2
6025	9	41.074	0.365	25.049	0.055	1.822	0.272	0.637	0.461	0.161	7.476	77.371	adj. to G2
6025	10	36.787	0.031	20.071	0.008	25.166	13.458	0.899	2.227	0.039	0.011	98.697	adj. to G3
6025	10	47.535	0.012	15.467	0.000	20.823	10.818	0.710	1.779	0.016	0.007	97.167	adj. to G3
6025	10	36.185	0.033	20.249	0.022	24.862	13.840	0.802	2.131	0.013	0.018	98.154	adj. to G3
6025	10	77.953	0.063	10.930	-0.004	1.516	0.058	0.146	0.116	0.035	2.814	93.628	adj. to G3
6025	10	71.407	0.002	0.512	-0.006	0.744	0.014	0.063	0.135	0.059	0.129	73.059	adj. to G3
6025	10	98.460	-0.001	0.017	-0.013	0.212	0.006	-0.004	-0.007	-0.010	0.012	98.670	adj. to G3
6025	11	98.664	-0.010	0.009	-0.010	0.210	0.042	-0.005	-0.008	-0.011	0.010	98.889	adj. to G3
6025	11	62.956	0.323	20.180	0.025	1.325	0.057	0.504	0.003	0.358	6.941	92.670	adj. to G3
6025	11	97.928	-0.003	0.038	-0.010	0.221	0.010	-0.006	-0.014	-0.005	0.019	98.178	adj. to G3
6025	11	84.440	0.081	3.302	0.000	0.844	0.038	0.489	0.020	0.056	1.075	90.345	adj. to G3
6025	12	91.757	0.023	1.412	-0.009	0.377	0.046	0.056	-0.003	0.016	0.385	94.061	adj. to G3
6025	12	60.227	0.344	21.320	0.004	1.292	0.026	0.559	0.020	0.248	6.912	90.952	adj. to G3
6025	12	34.840	1.710	18.163	0.006	21.088	0.297	8.490	0.027	0.082	9.348	94.050	adj. to G3
6025	12	98.477	0.034	0.093	-0.014	0.248	0.006	0.002	-0.001	-0.007	0.026	98.863	adj. to G3
6025	12	32.416	0.175	8.278	-0.003	7.392	0.029	0.442	1.022	0.068	0.171	49.991	adj. to G3
6025	13	36.172	0.062	20.214	0.006	25.530	13.099	1.002	2.274	0.064	0.003	98.426	adj. to G3
6025	13	32.646	0.049	16.424	-0.009	21.652	11.176	0.901	1.795	0.102	0.196	84.933	adj. to G3
6025	14	62.921	0.015	19.383	-0.004	0.204	-0.005	0.013	2.938	8.894	0.108	94.466	matrix
6025	14	46.020	0.327	30.856	0.058	2.561	0.024	1.587	0.072	0.268	9.471	91.244	matrix
6025	14	36.736	1.147	23.778	0.017	12.674	0.129	5.148	0.029	0.220	9.286	89.164	matrix
6025	15	93.674	0.005	0.945	0.001	0.198	-0.008	0.027	0.071	0.424	0.037	95.374	matrix
6025	15	98.075	0.002	0.019	0.009	0.189	-0.006	-0.008	-0.013	-0.008	0.012	98.270	matrix
6025	15	34.960	1.509	17.120	-0.004	19.788	0.251	7.872	0.041	1.074	8.406	91.018	matrix
6025	16	25.703	1.442	12.782	0.000	16.546	0.181	7.548	0.044	0.080	6.952	71.277	matrix
6025	16	43.905	0.509	33.146	0.020	2.638	0.028	1.288	0.036	0.287	9.484	91.340	matrix
6025	17	95.190	-0.005	0.402	-0.008	0.138	-0.010	0.018	-0.007	-0.006	0.098	95.810	matrix
6025	17	96.204	0.000	0.009	-0.002	0.132	-0.016	0.001	-0.003	-0.012	0.006	96.319	matrix
6025	18	33.238	1.713	17.159	0.007	20.486	0.259	8.640	0.019	0.094	9.161	90.778	matrix
6025	18	88.483	0.017	2.988	0.000	0.384	-0.013	0.140	0.027	0.016	0.759	92.802	matrix
BH075	1	34.323	1.251	18.725	0.037	28.200	0.346	3.303	0.084	0.022	9.355	95.647	Adj. to G1
BH075	1	32.669	1.066	18.211	0.021	28.580	0.296	3.786	0.140	0.017	8.459	93.246	Adj. to G1
BH075	1	32.530	1.077	17.924	0.031	28.681	0.286	3.844	0.156	0.026	8.188	92.742	Adj. to G1
BH075	2	32.265	0.976	17.647	0.018	29.118	0.344	4.155	0.178	0.032	6.936	91.668	Adj. to G1
BH075	2	32.736	1.222	17.255	0.024	28.177	0.322	3.800	0.401	0.041	7.369	91.348	Adj. to G1
BH075	2	29.601	0.463	18.824	0.019	31.198	0.431	4.141	0.206	0.034	4.138	89.056	Adj. to G1
BH075	3	33.671	0.969	18.180	0.028	27.815	0.367	3.787	0.078	0.016	9.143	94.053	Adj. to G1
BH075	3	33.337	0.934	18.428	0.025	28.511	0.327	3.780	0.033	0.017	9.660	95.052	Adj. to G1
BH075	3	31.721	0.767	17.846	0.042	30.642	0.331	3.846	0.209	0.029	7.290	92.723	Adj. to G1

Table 2: Compositions of Biotite from pelites												
Sample	Biotite	SiO$_2$	TiO$_2$	Al$_2$O$_3$	Cr$_2$O$_3$	FeO	MnO	MgO	CaO	Na$_2$O	K$_2$O	Sum	Location
BH075	4	28.740	0.637	18.552	0.025	32.282	0.467	4.662	0.130	0.013	4.903	90.410	Adj. to G1
BH075	4	27.132	0.349	18.746	0.006	33.380	0.465	4.867	0.167	0.023	2.733	87.867	Adj. to G1
BH075	4	27.674	0.502	17.752	0.015	31.390	0.349	4.522	0.250	0.039	3.867	86.359	Adj. to G1
BH075	5	34.598	1.021	17.630	0.005	27.017	0.237	4.014	0.313	0.065	8.460	93.359	Adj. to G1
BH075	5	33.299	1.053	17.738	0.011	26.909	0.229	3.717	0.322	0.036	7.770	91.083	Adj. to G1
BH075	5	33.571	1.107	17.345	0.010	27.581	0.221	3.913	0.244	0.046	8.708	92.747	Adj. to G1
BH075	6	33.916	1.194	17.684	0.034	28.232	0.406	3.778	0.020	0.016	9.371	94.651	Adj. to G2
BH075	6	33.522	1.264	17.955	0.049	28.634	0.399	3.743	0.059	0.018	9.080	94.723	Adj. to G2
BH075	6	32.930	1.225	17.939	0.037	28.324	0.341	3.759	0.090	0.031	8.841	93.518	Adj. to G2
BH075	7	36.003	1.104	17.028	0.026	26.117	0.354	3.468	0.218	0.025	8.478	92.821	Adj. to G2
BH075	7	33.325	1.195	17.962	0.034	27.560	0.340	3.947	0.265	0.050	8.475	93.154	Adj. to G2
BH075	7	33.265	1.203	18.434	0.028	28.005	0.351	3.778	0.107	0.029	9.002	94.202	Adj. to G2
BH075	8	32.795	1.157	17.343	0.004	27.222	0.327	3.944	0.179	0.049	8.900	91.921	Adj. to G2
BH075	8	31.918	1.170	17.238	0.007	27.903	0.338	4.123	0.426	0.047	7.837	91.006	Adj. to G2
BH075	8	27.362	0.819	16.441	0.014	34.553	0.254	3.549	0.265	0.024	6.638	89.918	Adj. to G2
BH075	8	31.931	1.187	17.419	0.033	27.975	0.269	3.718	0.086	0.014	9.159	91.791	Adj. to G2
BH075	8	33.034	1.268	18.048	0.024	28.679	0.244	3.749	0.027	0.016	9.541	94.629	Adj. to G2
BH075	9	31.546	1.058	17.199	0.010	28.978	0.307	3.663	0.664	0.024	6.922	90.371	Adj. to G2
BH075	9	33.306	1.103	17.532	0.033	26.807	0.264	3.952	0.189	0.047	8.765	91.996	Adj. to G2
BH075	10	32.286	1.130	17.652	0.017	28.946	0.346	3.883	0.318	0.060	7.561	92.200	Adj. to G3
BH075	10	32.802	1.293	17.361	0.012	28.485	0.322	3.958	0.235	0.057	8.420	92.944	Adj. to G3
BH075	11	33.029	1.256	17.155	0.025	28.137	0.411	4.107	0.336	0.045	8.120	92.621	Adj. to G3
BH075	11	32.952	1.313	17.475	0.039	28.291	0.368	4.101	0.275	0.036	8.716	93.565	Adj. to G3
BH075	12	32.932	1.259	17.964	0.025	28.553	0.362	3.856	0.145	0.027	8.938	94.061	Adj. to G3
BH075	12	32.809	1.210	18.296	0.017	28.171	0.322	3.692	0.161	0.023	9.164	93.865	Adj. to G3
BH075	12	32.340	1.184	18.068	0.023	27.848	0.297	3.769	0.238	0.034	8.534	92.335	Adj. to G3
BH075	12	32.718	1.242	18.132	0.010	27.756	0.261	3.754	0.188	0.032	9.038	93.131	Adj. to G3
BH075	13	32.275	1.336	16.788	0.012	26.890	0.207	3.825	0.355	0.044	7.603	89.336	matrix
BH075	13	31.822	1.303	16.444	0.013	26.830	0.221	3.731	0.322	0.043	7.826	88.554	matrix
BH075	14	31.410	1.205	17.283	0.033	28.027	0.256	4.068	0.344	0.046	6.819	89.491	matrix
BH075	14	29.467	0.636	17.908	0.028	30.298	0.285	4.200	0.265	0.037	4.669	87.793	matrix
BH075	15	31.819	1.198	17.379	0.034	28.801	0.215	3.778	0.163	0.034	8.630	92.051	matrix
BH075	15	33.230	1.249	17.746	0.018	28.165	0.229	3.710	0.265	0.049	8.780	93.441	matrix
BH075	16	31.209	1.023	18.465	0.024	29.194	0.280	4.269	0.127	0.030	6.899	91.520	matrix
BH075	16	33.503	1.294	18.147	0.026	28.386	0.239	3.649	0.115	0.068	9.083	94.509	matrix
6013	1	34.312	1.123	17.160	0.021	16.166	0.339	11.657	0.126	0.053	8.396	89.354	Adj. to G1
6013	1	35.522	1.118	18.405	0.019	16.554	0.440	12.619	0.032	0.056	8.983	93.748	Adj. to G1
6013	1	35.735	1.094	18.620	0.018	16.505	0.444	12.453	0.082	0.045	8.465	93.461	Adj. to G1
6013	2	35.897	1.434	18.047	0.026	16.611	0.355	12.088	0.025	0.069	9.547	94.098	Adj. to G1
6013	2	36.094	1.481	18.028	0.026	16.389	0.357	12.168	0.030	0.064	9.436	94.072	Adj. to G1
6013	2	35.702	1.469	17.505	0.019	16.353	0.326	12.156	0.095	0.050	8.905	92.582	Adj. to G1
6013	2	35.854	1.405	17.969	0.022	16.248	0.281	12.165	0.080	0.069	9.179	93.273	Adj. to G1
6013	2	35.466	1.308	18.192	0.025	16.897	0.312	12.425	0.040	0.062	8.722	93.449	Adj. to G1

Sample	Biotite	SiO_2	TiO_2	Al_2O_3	Cr_2O_3	FeO	MnO	MgO	CaO	Na_2O	K_2O	Sum	Location

Table 2: Compositions of Biotite from pelites

Sample	Biotite	SiO_2	TiO_2	Al_2O_3	Cr_2O_3	FeO	MnO	MgO	CaO	Na_2O	K_2O	Sum	Location
6013	3	36.346	1.407	17.875	0.039	16.275	0.295	12.179	0.004	0.061	9.768	94.249	Adj. to G3
6013	3	36.136	1.380	18.292	0.026	16.231	0.282	11.866	0.009	0.071	9.741	94.034	Adj. to G3
6013	3	35.598	1.375	18.092	0.024	17.020	0.260	11.647	0.030	0.051	9.206	93.303	Adj. to G3
6013	3	35.919	1.345	18.151	0.039	16.605	0.301	11.999	0.019	0.067	9.728	94.172	Adj. to G3
6013	3	36.082	1.400	18.181	0.035	16.684	0.302	11.865	0.018	0.067	9.745	94.379	Adj. to G3
6013	3	35.666	1.412	18.223	0.057	17.231	0.285	11.796	0.023	0.059	9.444	94.197	Adj. to G3
6013	3	36.935	1.317	17.681	0.041	16.367	0.280	10.816	0.167	0.051	8.618	92.272	Adj. to G3
6013	3	35.177	1.273	18.070	0.034	19.183	0.236	11.441	0.068	0.050	8.812	94.343	Adj. to G3
6013	4	26.870	0.413	19.439	0.022	21.903	0.457	13.980	0.074	0.012	2.290	85.460	matrix
6013	4	35.003	1.501	17.728	0.024	16.222	0.304	12.510	0.101	0.068	8.983	92.444	matrix
6013	4	35.374	1.449	17.545	0.045	17.334	0.271	11.861	0.062	0.055	8.958	92.954	matrix
6013	4	34.417	1.203	17.292	0.040	18.868	0.259	11.205	0.110	0.048	8.228	91.669	matrix
6013	5	29.886	1.064	14.994	0.020	28.326	0.265	9.629	0.189	0.063	7.078	91.515	matrix
6013	5	34.842	1.294	16.570	0.027	19.675	0.292	11.922	0.027	0.049	8.942	93.639	matrix
6013	5	33.346	1.057	18.026	0.023	18.841	0.344	12.581	0.086	0.034	6.976	91.313	matrix
6013	5	35.775	1.313	18.206	0.018	16.656	0.291	11.495	0.124	0.057	8.665	92.600	matrix
6013	5	24.442	0.058	22.228	0.009	22.988	0.640	15.300	0.003	0.001	0.019	85.687	matrix
6013	5	33.636	1.455	15.763	0.009	18.319	0.285	11.752	0.325	0.058	7.293	88.895	matrix
6013	5	31.866	1.241	18.329	0.020	18.451	0.382	12.968	0.137	0.046	5.716	89.155	matrix
6013	6	28.052	0.460	20.218	0.010	20.402	0.475	14.979	0.008	0.007	2.202	86.812	matrix
6013	6	33.133	1.258	18.315	0.005	18.145	0.374	13.317	0.013	0.033	6.588	91.180	matrix
6013	6	31.847	0.859	19.478	0.016	19.094	0.391	13.827	0.029	0.013	4.495	90.047	matrix
6013	6	36.367	1.611	17.246	0.026	16.246	0.271	12.243	0.010	0.054	9.610	93.683	matrix
6013	6	36.587	1.511	17.417	0.024	15.846	0.277	12.161	0.008	0.053	9.720	93.603	matrix
6013	6	36.231	1.483	17.677	0.032	15.887	0.303	12.038	0.005	0.066	9.699	93.420	matrix
6013	6	35.933	1.494	17.764	0.028	16.407	0.312	12.050	0.005	0.064	9.552	93.610	matrix

Table 3: Compositions of Garnet from Rochford Formation											
Sample	Garnet	SiO$_2$	TiO$_2$	Al$_2$O$_3$	Cr$_2$O$_3$	FeO	MnO	MgO	CaO	Na$_2$O	K$_2$O	Sum
5161	1	36.416	0.031	21.416	0.001	31.448	5.195	0.799	5.126	0.002	-0.003	100.432
5161	1	36.417	0.029	21.219	-0.008	31.421	5.072	0.880	5.469	-0.002	-0.006	100.491
5161	1	36.553	0.022	21.339	-0.001	31.265	4.950	0.876	5.531	0.009	-0.003	100.541
5161	1	36.380	0.038	21.277	-0.002	31.568	5.176	0.875	5.062	-0.002	-0.006	100.367
5161	1	36.492	0.058	21.209	0.003	31.839	5.185	0.867	4.491	-0.008	-0.002	100.134
5161	1	36.393	0.064	21.155	-0.001	32.300	5.314	0.891	4.317	0.002	-0.010	100.425
5161	1	36.468	0.038	21.363	0.000	32.333	5.371	0.861	4.126	-0.002	-0.003	100.555
5161	1	36.595	0.057	21.312	-0.002	32.044	5.296	0.885	4.539	0.007	-0.003	100.731
5161	1	36.863	0.063	21.161	-0.015	31.916	5.390	0.883	4.482	-0.001	-0.004	100.737
5161	1	36.294	0.066	21.172	0.008	31.834	5.410	0.862	4.401	0.002	0.003	100.053
5161	1	36.341	0.071	21.259	-0.001	31.912	5.392	0.835	4.581	0.003	-0.003	100.389
5161	1	36.732	0.054	21.269	0.015	31.584	5.259	0.819	4.803	-0.011	-0.004	100.518
5161	1	36.605	0.066	21.222	0.006	32.007	5.397	0.862	4.428	0.000	-0.004	100.587
5161	1	36.494	0.064	21.451	-0.006	31.962	5.340	0.903	4.530	-0.004	0.002	100.737
5161	1	36.643	0.062	21.402	0.000	31.771	5.198	0.886	4.718	0.001	0.000	100.681
5161	1	36.747	0.042	21.323	0.003	31.405	5.027	0.882	5.274	-0.001	-0.004	100.697
5161	1	36.663	0.043	21.493	-0.009	31.241	5.000	0.873	5.390	0.003	-0.001	100.694
5161	1	36.878	0.004	21.358	0.008	31.530	5.106	0.895	4.692	-0.003	0.003	100.471
5161	1	36.642	0.050	21.333	-0.015	31.124	4.995	0.862	5.542	0.005	-0.002	100.535
5161	1	36.774	0.038	21.461	-0.001	30.718	5.000	0.856	5.719	0.003	-0.003	100.565
5161	1	36.860	0.033	21.341	-0.019	30.935	4.991	0.845	5.839	-0.006	-0.004	100.816
5161	1	37.071	0.031	21.435	-0.003	31.262	5.084	0.788	5.440	0.005	0.001	101.112
5161	2	36.460	0.019	21.281	-0.004	31.535	5.102	0.856	5.225	-0.002	-0.002	100.470
5161	2	36.459	0.004	21.472	0.005	31.223	4.942	0.864	5.581	-0.006	-0.001	100.544
5161	2	36.496	0.042	21.388	-0.004	31.353	5.078	0.884	5.376	-0.003	-0.003	100.609
5161	2	36.494	0.017	21.385	-0.009	31.392	4.983	0.898	5.327	-0.007	0.000	100.479
5161	2	36.600	0.055	21.349	-0.006	31.305	4.928	0.864	5.578	-0.004	-0.003	100.667
5161	2	36.513	0.037	21.359	0.006	31.638	5.046	0.874	5.079	0.003	-0.003	100.551
5161	2	36.399	0.050	21.350	-0.007	32.006	5.207	0.796	4.499	-0.003	-0.006	100.292
5161	2	37.274	0.028	18.943	-0.008	32.704	5.056	1.743	4.110	0.012	-0.003	99.858
5161	2	36.473	0.089	21.293	0.014	31.545	5.131	0.861	5.117	0.001	0.003	100.526
5161	2	36.550	0.098	21.244	-0.033	31.500	5.152	0.781	5.292	0.003	-0.006	100.580
5161	2	36.372	0.083	21.223	-0.011	32.035	5.283	0.829	4.473	-0.002	-0.009	100.278
5161	2	36.319	0.058	21.195	-0.010	32.453	5.544	0.873	3.968	0.002	-0.004	100.397
5161	2	36.396	0.058	21.087	-0.003	31.846	5.506	0.840	4.532	-0.001	-0.008	100.253
5161	2	36.500	0.041	21.115	-0.011	31.410	5.419	0.829	5.019	-0.002	0.002	100.322
5161	2	36.468	0.017	21.258	-0.007	31.850	5.787	0.762	4.377	-0.011	-0.001	100.499
5161	2	36.492	0.045	21.274	-0.025	31.969	5.827	0.783	4.401	0.005	-0.005	100.764
5161	2	36.381	0.083	21.040	0.006	31.622	5.527	0.780	4.795	-0.002	-0.007	100.225
5161	2	36.509	0.096	21.084	0.005	31.911	5.561	0.776	4.506	0.001	-0.003	100.446
5161	2	36.432	0.069	21.235	0.009	31.730	5.532	0.791	4.602	0.005	-0.004	100.402
5161	2	36.363	0.090	21.246	-0.003	32.217	5.474	0.818	4.285	-0.004	0.001	100.485
5161	2	36.495	0.088	21.207	-0.005	32.378	5.499	0.856	4.159	-0.005	-0.005	100.667

Table 3: Compositions of Garnet from Rochford Formation											
Sample	Garnet	SiO$_2$	TiO$_2$	Al$_2$O$_3$	Cr$_2$O$_3$	FeO	MnO	MgO	CaO	Na$_2$O	K$_2$O	Sum
5161	2	36.624	0.065	21.075	-0.013	32.294	5.388	0.928	4.313	0.005	0.003	100.681
5161	2	51.502	-0.006	0.377	-0.018	33.364	0.815	10.558	0.371	0.031	-0.008	96.986
5161	2	36.357	0.071	21.277	0.005	31.872	5.171	0.833	4.731	-0.006	-0.002	100.308
5161	2	36.466	0.050	21.445	-0.008	32.281	5.331	0.856	4.526	-0.004	0.000	100.942
5161	2	36.462	0.078	21.377	0.010	31.772	5.121	0.878	4.712	0.001	0.001	100.413
5161	2	36.870	-0.004	20.641	-0.002	32.425	5.226	1.124	3.780	-0.005	0.006	100.060
5161	2	36.818	0.043	21.234	0.003	30.781	4.932	0.787	5.973	-0.009	-0.003	100.558
5161	2	36.518	0.070	21.383	-0.003	30.679	4.798	0.825	6.139	-0.003	0.002	100.407
5161	2	36.503	0.049	21.352	-0.018	31.139	4.960	0.835	5.579	0.002	-0.001	100.400
5161	2	36.743	0.037	21.457	-0.012	30.934	4.853	0.834	5.823	0.002	0.002	100.674
5161	2	36.575	0.038	21.380	-0.008	31.125	5.037	0.822	5.567	-0.003	0.000	100.533
5161	2	36.708	0.027	21.252	-0.003	30.832	5.013	0.801	5.883	-0.002	-0.003	100.507
5161	2	36.611	0.002	21.418	-0.005	31.881	5.117	0.816	4.848	-0.009	0.007	100.687
5161	4	36.564	0.030	21.466	0.004	31.553	4.664	0.841	5.766	-0.003	-0.002	100.884
5161	4	36.097	0.044	21.119	0.019	31.288	4.779	0.901	5.540	0.001	-0.002	99.786
5161	4	35.137	0.028	20.471	0.018	30.781	4.645	0.935	5.500	-0.001	0.000	97.514
5161	4	36.300	0.059	21.292	0.011	32.324	4.947	0.907	4.703	-0.005	-0.006	100.531
5161	4	36.144	0.050	21.260	-0.014	32.665	4.944	0.828	4.373	-0.006	0.001	100.247
5161	4	36.315	0.046	21.340	-0.019	32.472	5.017	0.798	4.436	-0.003	-0.005	100.398
5161	4	36.176	0.079	21.223	0.005	32.328	5.111	0.836	4.304	-0.003	-0.004	100.054
5161	4	37.592	0.025	15.530	-0.011	31.461	3.024	3.081	2.520	0.008	0.079	93.309
5161	4	34.966	0.084	19.883	-0.018	32.389	4.977	1.658	3.566	0.017	0.536	98.057
5161	4	36.275	0.048	21.248	0.010	32.511	5.252	0.789	4.311	-0.004	-0.008	100.432
5161	4	36.315	0.054	21.371	0.000	32.044	5.278	0.845	4.691	-0.006	-0.002	100.590
5161	4	36.331	0.068	21.309	-0.013	31.711	5.185	0.860	5.041	-0.001	-0.003	100.489
5161	4	36.382	0.084	21.273	0.008	31.758	5.369	0.867	4.611	0.004	-0.002	100.354
5161	4	36.269	0.094	21.107	-0.007	31.693	5.365	0.851	4.683	-0.003	-0.006	100.045
5161	4	37.497	0.032	20.475	0.001	32.324	5.379	1.352	3.845	-0.003	-0.005	100.897
5161	4	36.214	0.101	21.193	-0.003	32.213	5.300	0.799	4.434	0.002	-0.001	100.252
5161	4	14.173	0.052	7.494	-0.003	60.556	0.308	1.106	0.444	0.003	-0.012	84.122
5161	4	36.361	0.058	21.385	-0.003	32.332	5.226	0.836	4.428	-0.003	-0.008	100.613
5161	4	36.127	0.086	21.187	0.005	32.270	5.173	0.882	4.482	-0.003	-0.004	100.203
5161	4	36.153	0.055	21.091	0.010	32.496	5.112	0.829	4.649	0.000	-0.004	100.392
5161	4	36.514	0.074	21.220	-0.005	32.555	5.303	0.793	4.158	-0.002	0.001	100.612
5161	4	51.354	-0.031	0.215	-0.020	33.277	0.758	10.594	0.333	0.033	-0.003	96.508
5161	4	36.562	0.057	21.257	0.012	32.232	5.125	0.835	4.471	-0.014	-0.010	100.525
5161	4	40.179	0.026	19.645	-0.007	32.705	4.264	1.883	3.382	-0.004	0.008	102.081
5161	4	36.074	0.035	21.252	0.012	32.066	4.966	0.843	5.068	-0.001	0.012	100.326
5161	4	36.310	0.004	21.289	-0.003	32.064	4.795	0.876	4.792	-0.006	0.000	100.122
5161	4	36.452	0.036	21.314	-0.006	31.295	4.752	0.831	5.703	-0.005	-0.001	100.372
5161	4	36.507	0.046	21.236	0.002	31.327	4.664	0.845	5.617	-0.009	-0.008	100.227
5161	5	36.437	0.084	21.190	0.021	31.979	4.994	0.852	4.760	0.003	0.005	100.324
5161	5	36.059	0.055	21.427	0.011	32.343	5.212	0.866	4.304	-0.012	0.005	100.271

Sample	Garnet	SiO$_2$	TiO$_2$	Al$_2$O$_3$	Cr$_2$O$_3$	FeO	MnO	MgO	CaO	Na$_2$O	K$_2$O	Sum
5161	5	36.043	0.085	21.067	0.001	31.336	5.236	0.887	4.876	0.021	0.003	99.555
5161	5	36.464	0.059	21.299	-0.003	31.817	5.638	0.865	4.435	0.004	0.001	100.580
5161	5	24.371	-0.012	16.307	-0.027	18.554	0.243	3.603	0.461	0.012	0.448	63.959
5161	5	35.360	0.102	20.742	-0.005	31.539	5.655	0.667	4.905	0.006	0.025	98.997
5161	5	36.947	0.090	20.887	0.000	31.022	6.026	0.704	4.679	0.008	0.000	100.364
5161	5	17.326	0.124	13.398	-0.022	50.399	0.434	0.918	0.423	0.024	0.759	83.781
5161	5	37.268	0.084	21.927	0.017	30.609	5.800	0.574	4.927	0.004	0.034	101.245
5161	5	17.822	0.001	6.092	-0.019	55.788	0.183	0.118	0.187	0.015	-0.005	80.180
5161	5	36.420	0.064	21.176	-0.007	31.099	6.049	0.706	5.008	-0.007	0.000	100.508
5161	5	36.478	0.057	21.289	0.001	30.880	6.061	0.795	4.881	-0.006	0.002	100.437
5161	5	35.787	0.074	20.995	-0.011	31.465	5.827	0.637	4.350	0.003	0.001	99.127
5161	5	35.663	0.247	20.698	0.000	31.025	6.180	0.822	3.729	0.016	-0.008	98.371
5161	5	34.685	0.015	20.274	0.001	30.710	5.915	0.801	3.906	0.038	0.001	96.345
5161	5	32.737	0.047	18.002	-0.004	35.754	5.501	0.653	3.740	0.016	0.001	96.446
5161	5	25.748	0.069	19.389	-0.007	32.481	0.274	7.622	0.064	0.004	1.263	86.907
5161	5	36.296	0.090	20.778	0.001	31.413	5.816	0.591	5.059	0.007	0.073	100.124
5161	5	36.344	0.071	20.938	0.023	30.710	6.062	0.680	5.345	0.003	0.000	100.175
5161	5	36.401	0.083	21.067	0.007	30.655	5.906	0.783	5.194	0.007	0.002	100.103
5161	5	36.482	0.089	21.123	0.004	30.876	6.012	0.818	4.915	0.005	0.000	100.325
5161	5	36.702	0.121	20.965	-0.009	30.035	5.510	0.797	6.189	-0.009	-0.005	100.295
5161	5	36.664	0.105	21.090	0.009	30.283	5.514	0.789	5.821	-0.008	-0.001	100.267
5161	5	36.595	0.087	21.108	0.007	30.641	5.532	0.817	5.427	0.001	-0.006	100.208
5161	5	36.680	0.072	21.110	0.010	30.906	5.501	0.849	5.191	0.002	-0.005	100.316
5161	5	36.579	0.086	21.123	0.004	31.306	5.305	0.878	5.047	-0.002	-0.004	100.321
5161	5	36.681	0.094	21.125	0.020	31.567	5.188	0.909	4.708	-0.007	-0.001	100.284
5161	5	36.818	0.074	21.202	-0.003	31.716	4.950	0.912	4.879	0.001	0.002	100.550
5008	2	36.093	0.072	21.111	-0.001	30.678	4.092	0.528	6.982	-0.005	-0.004	99.545
5008	2	36.016	0.058	20.982	-0.003	32.222	4.268	0.561	5.892	0.003	-0.002	99.995
5008	2	36.078	0.073	21.046	0.007	32.314	4.341	0.553	5.606	0.000	0.000	100.018
5008	2	16.367	0.283	7.466	-0.011	53.234	0.301	0.196	0.447	0.041	0.170	78.493
5008	2	18.773	0.221	9.807	0.010	47.344	0.275	0.490	0.213	0.004	0.135	77.273
5008	2	35.701	0.058	21.002	0.007	33.891	4.544	0.614	4.130	-0.005	-0.004	99.938
5008	2	17.415	0.136	8.267	0.002	40.977	2.872	0.610	2.726	0.014	0.023	73.042
5008	2	17.194	0.117	9.423	-0.008	46.937	1.507	0.799	1.719	0.131	0.039	77.858
5008	2	35.882	0.128	20.790	-0.007	32.948	4.076	0.574	5.176	-0.004	-0.011	99.553
5008	2	23.242	0.041	9.704	-0.009	36.918	1.626	2.796	1.973	0.057	0.114	76.464
5008	2	3.388	0.005	1.283	-0.065	35.272	0.234	3.538	0.797	0.124	0.246	44.820
5008	2	19.686	0.047	10.253	-0.026	44.544	1.618	1.293	1.791	0.027	0.099	79.332
5008	2	36.622	0.076	21.180	-0.015	33.964	4.461	0.572	4.076	0.008	-0.007	100.938
5008	2	36.028	0.029	21.230	-0.005	34.311	4.461	0.570	4.024	0.001	-0.001	100.648
5008	2	36.103	0.082	20.935	-0.007	33.169	4.086	0.561	5.048	0.001	-0.003	99.974
5008	2	36.048	0.060	20.990	0.004	34.181	4.366	0.582	3.899	-0.004	-0.002	100.123
5008	2	36.128	0.069	20.919	0.005	33.219	4.062	0.563	4.951	0.013	0.005	99.935

Table 3: Compositions of Garnet from Rochford Formation

Sample	Garnet	SiO$_2$	TiO$_2$	Al$_2$O$_3$	Cr$_2$O$_3$	FeO	MnO	MgO	CaO	Na$_2$O	K$_2$O	Sum
					Table 3: Compositions of Garnet from Rochford Formation							
5008	2	36.064	0.076	20.879	0.016	33.919	4.244	0.588	4.238	-0.001	-0.008	100.016
5008	2	36.011	0.088	20.928	0.009	33.731	4.279	0.587	4.320	-0.004	-0.001	99.948
5008	2	35.992	0.067	20.860	-0.003	33.477	4.231	0.599	4.813	0.003	0.004	100.043
5008	2	36.175	0.023	21.043	-0.001	34.067	4.405	0.615	3.978	0.003	0.003	100.309
5008	2	36.398	0.069	21.234	0.007	33.433	4.412	0.592	4.438	0.006	0.003	100.594
5008	2	35.551	0.072	20.485	-0.007	32.376	4.904	0.472	4.435	0.010	0.004	98.302
5008	2	19.208	0.052	16.712	-0.002	38.360	0.355	4.368	0.768	0.010	0.028	79.860
5008	2	36.195	0.074	20.799	0.001	33.114	4.488	0.602	4.644	-0.002	-0.001	99.912
5008	2	36.213	0.065	21.069	0.003	34.018	4.555	0.622	3.927	0.005	-0.003	100.474
5008	2	36.443	0.055	21.292	-0.003	33.746	4.535	0.622	3.755	0.002	0.003	100.450
5008	2	36.101	0.040	21.009	0.002	34.406	4.649	0.645	3.619	0.002	-0.003	100.469
5008	2	36.383	0.053	20.974	-0.001	33.065	4.400	0.582	4.946	-0.007	-0.002	100.393
5008	2	36.276	0.076	20.939	0.009	32.481	4.471	0.578	5.191	-0.001	-0.004	100.016
5008	2	36.707	0.063	21.089	0.020	32.332	4.365	0.570	5.648	-0.002	-0.005	100.786
5008	2	36.226	0.059	21.110	0.012	32.911	4.635	0.556	4.669	0.007	-0.004	100.181
5008	2	36.703	0.079	21.040	0.006	30.964	4.033	0.525	7.175	0.002	-0.003	100.526
5135	1	35.693	0.102	20.894	0.015	28.239	9.803	0.603	4.356	0.003	0.000	99.707
5135	1	37.508	0.102	21.794	-0.007	26.942	11.239	0.476	4.282	-0.010	0.000	102.326
5135	1	35.854	0.088	20.812	-0.023	26.104	11.859	0.522	4.297	0.005	-0.004	99.515
5135	1	33.764	0.088	19.271	0.004	25.515	12.275	0.547	4.298	0.000	0.001	95.762
5135	1	36.072	0.140	20.789	-0.016	25.467	12.480	0.510	4.543	-0.004	-0.006	99.974
5135	1	34.754	0.092	19.855	0.003	25.713	12.346	0.564	4.060	-0.003	0.002	97.385
5135	1	35.789	-0.005	21.133	0.004	28.432	11.401	0.660	2.193	0.038	-0.004	99.639
5135	1	24.718	-0.024	15.039	0.001	21.203	7.458	0.503	14.433	0.027	-0.001	83.357
5135	1	30.972	-0.014	18.196	0.009	25.946	9.757	0.440	6.649	0.046	-0.010	91.990
5135	1	36.412	0.055	21.522	-0.002	28.794	10.347	0.533	2.849	0.030	0.003	100.544
5135	1	35.936	0.022	21.314	0.020	29.072	9.920	0.604	2.522	0.037	0.002	99.450
5135	1	35.286	0.049	20.501	-0.005	29.431	9.715	0.588	3.714	0.011	-0.003	99.289
5135	1	36.872	-0.010	22.177	-0.007	29.601	9.639	0.488	2.401	0.046	0.000	101.207
5135	1	35.506	-0.011	21.108	0.026	29.766	9.852	0.499	2.419	0.042	-0.008	99.198
5135	1	31.136	0.043	17.982	-0.026	28.446	9.339	0.981	5.263	0.032	-0.009	93.188
5135	1	33.780	-0.021	19.986	0.007	29.970	9.854	0.422	2.414	0.045	-0.009	96.447
5135	1	32.890	0.017	21.350	-0.017	30.452	0.462	5.479	0.130	2.466	0.002	93.231
5135	1	35.732	0.016	21.352	-0.002	29.844	10.114	0.324	2.307	0.035	-0.006	99.715
5135	1	19.158	-0.050	5.151	-0.024	15.940	4.924	2.769	13.751	0.014	-0.011	61.622
5135	1	35.651	0.028	21.153	0.008	29.652	9.862	0.493	2.459	0.060	-0.003	99.362
5135	1	35.471	0.033	21.067	-0.009	29.540	9.946	0.502	2.525	0.052	-0.006	99.120
5135	1	29.465	0.001	17.889	0.007	27.613	9.298	0.553	2.414	0.069	-0.002	87.307
5135	1	36.293	-0.019	20.987	0.007	28.750	10.688	0.545	2.332	0.052	-0.002	99.634
5135	1	35.944	0.057	20.954	-0.004	27.543	11.510	0.622	3.432	0.001	-0.003	100.056
5135	1	35.887	0.143	20.915	-0.002	26.018	12.205	0.537	4.157	0.000	-0.001	99.860
5135	1	10.667	0.016	6.136	-0.010	6.856	2.853	0.100	40.257	-0.005	-0.009	66.859
5135	2	36.166	0.086	21.167	0.018	28.595	9.899	0.586	3.997	0.004	-0.004	100.514

Table 3: Compositions of Garnet from Rochford Formation											
Sample	Garnet	SiO$_2$	TiO$_2$	Al$_2$O$_3$	Cr$_2$O$_3$	FeO	MnO	MgO	CaO	Na$_2$O	K$_2$O	Sum
5135	2	36.759	0.073	21.465	0.005	26.995	11.524	0.517	4.182	-0.010	-0.004	101.505
5135	2	35.831	0.091	20.853	0.001	26.160	11.955	0.515	4.324	-0.004	-0.003	99.722
5135	2	36.748	0.127	21.126	-0.001	25.982	12.891	0.491	3.888	-0.008	-0.006	101.237
5135	2	35.881	0.101	20.868	-0.018	26.353	12.452	0.547	4.011	0.001	-0.006	100.190
5135	2	0.224	-0.023	0.088	-0.032	0.866	0.409	0.003	53.534	0.007	-0.011	55.065
5135	2	35.105	0.004	20.546	-0.011	27.216	11.185	0.566	4.362	0.043	-0.003	99.012
5135	2	30.813	0.012	17.639	-0.020	26.490	10.218	0.534	6.682	0.056	-0.002	92.422
5135	2	36.038	0.066	20.927	-0.002	28.604	10.770	0.597	3.371	0.008	0.000	100.377
5135	2	35.894	0.080	20.888	-0.015	28.708	10.471	0.570	3.285	0.011	-0.004	99.889
5135	2	35.654	0.015	21.153	0.002	28.944	10.340	0.657	2.413	0.062	-0.003	99.238
5135	2	35.955	0.029	21.132	0.004	28.661	10.222	0.601	2.767	0.062	-0.004	99.428
5135	2	34.158	0.002	20.114	0.002	27.781	10.788	0.386	4.709	0.055	-0.001	97.994
5135	2	35.816	-0.005	20.994	-0.009	28.298	10.391	0.618	3.123	0.056	-0.001	99.281
5135	2	35.836	0.034	20.938	0.004	28.482	10.747	0.679	2.781	0.028	-0.001	99.528
5135	2	35.706	0.020	20.847	-0.014	28.487	10.901	0.669	2.876	0.027	-0.003	99.515
5135	2	32.747	-0.033	15.717	0.002	20.535	11.016	0.477	5.345	0.001	-0.001	85.806
5135	2	35.859	0.088	20.952	-0.010	26.239	12.286	0.564	3.807	-0.003	-0.005	99.777
5135	2	36.042	0.113	20.962	-0.007	25.813	12.728	0.515	3.994	0.006	-0.005	100.161
5135	2	35.973	0.098	20.989	-0.010	26.358	12.115	0.506	4.137	-0.009	0.000	100.155
5135	3	36.124	0.059	20.986	-0.007	29.286	8.995	0.616	4.081	-0.013	-0.002	100.125
5135	3	35.798	0.057	20.911	0.004	27.492	11.199	0.568	3.947	0.002	-0.002	99.977
5135	3	36.793	0.096	21.347	0.002	26.655	12.242	0.519	3.524	-0.001	-0.004	101.171
5135	3	1.978	0.001	1.267	-0.040	1.877	0.503	0.642	50.170	0.046	-0.006	56.438
5135	3	36.261	0.020	21.401	-0.006	28.217	11.585	0.469	2.428	0.042	-0.002	100.415
5135	3	35.603	-0.001	20.878	0.001	28.149	11.592	0.504	2.394	0.048	0.002	99.170
5135	3	35.458	-0.005	20.837	-0.004	28.121	11.335	0.547	2.410	0.064	-0.004	98.760
5135	3	34.876	0.047	20.399	-0.009	28.068	11.199	0.565	3.257	0.001	0.000	98.404
5135	3	35.759	0.032	21.135	-0.001	28.328	11.483	0.571	2.540	0.039	0.001	99.886
5135	3	35.594	0.092	20.805	-0.002	27.700	11.052	0.504	3.623	0.009	-0.004	99.371
5135	3	35.765	0.024	21.165	-0.005	27.985	11.805	0.517	2.287	0.046	-0.002	99.587
5135	3	35.864	0.088	20.796	-0.008	26.542	12.103	0.582	3.806	0.001	-0.002	99.772
5135	3	36.021	0.095	21.127	-0.010	26.458	11.533	0.546	4.342	-0.005	-0.006	100.099

Table 4: Compositions of Biotite from Rochford Formation												
Sample	Biotite	SiO$_2$	TiO$_2$	Al$_2$O$_3$	Cr$_2$O$_3$	FeO	MnO	MgO	CaO	Na$_2$O	K$_2$O	Sum	Location
5061	1	21.248	0.032	17.241	-0.004	29.647	0.188	8.392	0.231	0.003	0.017	76.995	matrix
5061	1	25.109	0.043	20.807	-0.016	32.272	0.214	8.710	0.508	0.021	0.026	87.695	matrix
5061	1	26.665	0.017	20.150	-0.013	30.567	0.191	8.509	0.608	0.040	0.044	86.776	matrix
5061	1	27.221	0.042	19.779	-0.006	29.685	0.185	8.430	0.683	0.051	0.041	86.111	matrix
5061	2	25.931	0.021	16.109	0.007	33.127	0.103	5.974	1.035	0.047	0.152	82.506	matrix
5061	2	22.833	0.059	19.112	0.000	33.118	0.192	8.172	0.147	0.035	0.010	83.679	matrix
5061	2	22.913	0.185	20.554	-0.002	34.365	0.230	8.233	0.001	-0.004	-0.001	86.473	matrix
5061	5	35.465	0.830	16.004	0.011	23.475	0.079	7.224	0.311	0.077	7.537	91.014	matrix
5061	5	30.894	0.835	13.952	0.015	24.581	0.066	6.278	0.647	0.055	6.032	83.355	matrix
5008	1	33.595	1.677	14.683	-0.015	27.466	0.082	5.681	0.331	0.046	8.564	92.111	matrix
5008	1	32.564	1.362	15.794	0.023	28.607	0.123	5.767	0.220	0.050	7.525	92.035	matrix
5008	1	33.326	1.602	14.557	0.001	26.383	0.055	5.327	0.490	0.050	7.830	89.620	matrix
5135	1	33.760	1.437	15.420	0.027	27.907	0.134	7.619	0.021	0.042	8.109	94.475	matrix
5135	1	34.511	1.593	15.017	0.045	26.960	0.152	7.318	0.006	0.044	9.408	95.054	matrix
5135	1	33.257	1.536	15.456	0.037	27.454	0.099	7.280	0.055	0.042	8.327	93.544	matrix
5135	1	34.564	1.480	15.289	0.085	26.646	0.115	7.384	0.017	0.054	9.104	94.739	matrix
5135	2	34.447	1.507	15.213	0.023	24.428	0.115	8.006	0.167	0.008	7.462	91.377	matrix
5135	2	33.648	1.442	15.370	0.069	24.464	0.121	7.920	0.233	0.013	6.442	89.722	matrix
5135	3	33.139	1.437	14.974	-0.010	24.435	0.134	8.413	0.723	0.059	6.162	89.465	matrix
5135	3	33.006	1.499	15.158	0.020	24.372	0.129	8.255	0.524	0.050	6.565	89.579	matrix
5135	3	33.436	1.536	15.393	0.015	24.661	0.117	8.479	0.923	0.065	5.325	89.949	matrix

Appendix C: Major and Trace Element Data (see Appendix A-1 for sample locations)

Sample	Rock Type	Au (ppm)	SiO_2	TiO_2	Al_2O_3	Fe_2O_3	MnO	MgO	CaO	Na_2O	K_2O	P_2O_5	Sum
BH6025	Swede Gulch Phyllite	0	91.82	0.12	4.17	2.45	0.32	0.78	0.69	0.66	0.81	0.17	102.11
BH6013	Swede Gulch Phyllite	0	75.19	0.4	9.32	4.27	0.09	1.58	0.35	1.45	2.07	0.15	95.10
BH075	Poverty Gulch Phyllite	N/A	57.09	0.55	13.91	17.18	0.75	1.78	0.22	1.07	4.3	0.08	97.10
BH5045	Poverty Gulch Phyllite	N/A	53.27	0.6	14.68	13.75	0.43	1.71	0.13	0.01	5.9	0.09	90.74
BH113	Rapid Creek Greenstone	1.781	56.03	2.12	12.02	12.4	0.12	5.49	2.77	0.69	3.37	0.29	95.52
BH114	Rapid Creek Greenstone	0	42.28	2.62	14.71	14.83	0.2	2.95	8.4	3.25	2.46	0.42	92.36
BH6104	Moonshine Gulch Quartzite	0.172	74.71	0.57	12.91	4.82	0.02	0.84	0.04	0.31	3.5	0.04	97.95
AQA33346	Rochford Formation	0	90.63	0.17	4.17	3.54	0.01	0.36	0.02	-0.07	1.46	0.06	100.48
BH091	Rochford Formation	0	60.25	0.24	6.45	27.47	0.89	4.84	0.92	0	0.43	0.05	101.64
AQA33351	Rochford Formation	0	94.87	0.01	0	2.41	0.01	0.1	0	0	0	0	97.48
AQA10418	Rochford Formation	0.137	60.23	0.28	6.07	23.55	0.95	3.51	0.92	0.14	0.77	0.05	96.58
BH096 BE	Rochford Formation	0.171	68.21	0.33	8.88	11.63	0.5	3.19	0.17	0	3.48	0.03	96.57
GWPXCC	Rochford Formation	17.285	60.57	0.13	3.6	22.46	0.28	3.76	0.52	0.01	1.1	0.05	92.58
GWPXDD	Rochford Formation	11.507	45.98	0.25	5.25	28.85	0.79	5.35	1.59	0.13	1.37	0.1	89.78

Table 1: Major Element Geochemistry Data: Whole-rock major element measurement via x-ray fluorescence (XRF) spectrometry, using a Pan Alytical Axios wavelength-dispersive system with standard crystals and duplex detector at Cal Poly Pomona. Methods for instrument calibration followed those used by the Washington State University Geoanalytical Laboratory.

Sample	Rock Type	Au (ppm)	La	Ce	Pr	Nd	Sm	Eu	Gd	Tb	Dy	Ho	Er	Tm	Yb	Lu	Y
BH6025	Swede Gulch Phyllite	0	1.282	5.5	0.35	1.387	0.909	0.3	1.332	0.131	0.775	0.1555	0.496	0.0648	0.509	0.084	7
BH6013	Swede Gulch Phyllite	0	17.01	34	3.86	14.27	5.34	0.946	4.99	0.389	2.59	0.542	1.56	0.255	1.69	0.243	22
BH075	Poverty Gulch Phyllite	N/A	27.8	58.1	6.42	24.7	10.34	2.385	9.28	0.727	4.29	0.843	2.3	0.345	2.52	0.36	26
BH5045	Poverty Gulch Phyllite	N/A	16.38	45.7	3.84	14.38	5.69	1.355	5.5	0.41	2.8	0.567	1.62	0.26	1.74	0.271	21
BH113	Rapid Creek Greenstone	1.781	21.83	47.5	6.08	25.76	10.96	3.384	10.5	0.814	4.74	0.99	2.86	0.421	2.87	0.433	25
BH114	Rapid Creek Greenstone	0	27.66	59.8	7.75	32.43	14.21	4.977	12.97	0.958	5.7	1.201	3.32	0.463	3.18	0.491	36
BH6104	Moonshine Gulch Quartzite	0.172	5.49	10.7	1.119	3.88	1.333	0.348	1.255	0.093	0.557	0.12	0.344	0.0547	0.391	0.057	19
AQA33346	Rochford Formation	0	1.25	1.76	0.156	0.563	0.211	0.043	0.209	0.019	0.108	0.0198	0.0556	0.0084	0.054	0.008	5
BH091	Rochford Formation	0	17.2	28.8	3.558	13.82	5.01	1.309	5.23	0.408	2.66	0.6	1.896	0.282	2.019	0.298	19
AQA33351	Rochford Formation	0	29.93	58.7	7.49	29.97	11.79	3.88	10.46	0.736	4.38	0.868	2.587	0.379	2.65	0.399	25
AQA10418	Rochford Formation	0.137	13.38	29.7	3.054	11.84	4.89	1.261	4.626	0.419	2.9	0.703	2.22	0.337	2.26	0.328	20
BH096 BE	Rochford Formation	0.171	14.53	34.8	3.47	13.43	5.23	1.1	4.84	0.398	2.59	0.529	1.493	0.222	1.56	0.246	20
GWPXCC	Rochford Formation	17.285	22.14	36.4	4.49	17.23	6.24	1.374	5.57	0.404	2.52	0.565	1.684	0.25	1.68	0.245	17
GWPXDD	Rochford Formation	11.507	14.96	26.1	3.612	15.12	6.83	1.873	7.97	0.656	3.92	0.863	2.38	0.366	2.34	0.333	26

Table 2: Trace Element Geochemistry Data: Data collected by LA-ICP-MS. One line scans (50 μm wide by 250 μm long at 4 μm/second for ~2 minutes) were performed per sample. USGS whole-rock reference materials (Atho-G, BHVO-2, AGV-2, ML3B, StHs 6/80, BCR-2, GOR132, and T-1) were measured at the beginning and end of the analyses, with Atho-G and AGV-2 measured between every 9 unknowns. Data were reducing using "Trace Elements IS" in Iolite v2.5 (Paton et al., 2011), using the calcium content measured by XRF (see above) as the internal standard.